Er was eens....

September 2003. Een telefoontje van d'unief. Of ik nog steeds interesse had om onderzoek te doen. Natuurlijk!
Enkele dagen later: op sollicitatiegesprek bij prof. Dewettinck. Een project rond chocolade? Interessant. En vooral lekker.
Weer een paar dagen later: opnieuw een telefoontje. Ik had de job!
Aldus begon mijn verhaal.....

Het chocolade-project was echter van kortere duur dan mijn zin voor onderzoek. Een IWT-specialisatiebeurs kon soelaas bieden. De winstkansen waren niet bijster hoog (net iets hoger dan de lotto), maar hoera!, het lukte (de lotto winnen voorlopig nog niet). Januari 2005: de overstap van chocolade naar palmolie was een feit!

Januari 2009: wat je nu in je handen hebt, is het resultaat van vier jaar inspiratie en vooral transpiratie, van euforie en frustratie, van uitdagingen en nieuwe inzichten. Dit alles zou natuurlijk niet mogelijk geweest zijn zonder de steun van vele mensen, die het allen verdienen om hier in de bloemetjes gezet te worden.

Eerst en vooral wil ik mijn promotor prof. Koen Dewettinck bedanken.
Koen, bedankt voor alle kansen en steun je mij gegeven heb. Ik kijk er naar uit om ook in de toekomst mijn wetenschappelijk steentje te kunnen bijdragen.

Dank aan het Instituut voor de aanmoediging van Innovatie door Wetenschap en Technologie in Vlaanderen (IWT-Vlaanderen) voor de financiële steun.

De leden van de lees- en examencommissie (Prof. dr. G. Mazzanti, Prof. dr. B. Goderis, Prof. P. Van der Meeren, Prof. dr. ir. R. Verh, Prof. dr. ir. B. De Meulenaer, Prof. dr. P. Van Oostveldt, Dr. L. Wiking en Dr. F. Arnaut) wens ik te bedanken voor hun inspanningen. Jullie opmerkingen en suggesties zijn de kwaliteit van dit werk zeker ten goede gekomen.

Verder wens ik ook een woordje van dank te richten tot prof. Imogen Foubert, prof. Peter

Van Puyvelde en prof. Bart Goderis van de KULeuven.
Imogen, op wetenschappelijk gebied heb ik veel van je geleerd. Mijn schrijfwerk heeft zeer zeker baat gehad bij je niet altijd even genuanceerde opmerkingen.
Bart, Peter, het was en is zeer fijn met jullie samen te werken. Eén bepaalde Grenoble uitstap zal me altijd bijblijven : −). *Het is duidelijk dat interactie tussen de 'polymeren' en de 'vetten' een veelbelovende aanpak is. Ik hoop in de toekomst nog regelmatig bij jullie binnen te stappen.*

Natuurlijk mogen ook de collega's niet ontbreken. FTE is een hechte, toffe, gezellige groep en dat komt door jullie allemaal. Bedankt voor de toffe sfeer, de aangename koffiepauzes, de gezellige babbels. *Jullie verdienen allen een afzonderlijk bedankje, maar ik zal het kort houden: Jullie zijn stuk voor stuk super! Bedankt voor alles!*

De kers op de taart was voor mij mijn verblijf in Viborg. Op het Deense platteland mocht ik een maand lang vertrouw raken met een tot dan toe voor mij onbekende techniek: confocale microscopie. Ettelijke uurtjes in die donkere kamer hebben geleid tot prachtige foto's van vekristalnetwerken en extra mogelijkheden voor verder onderzoek. Dit was niet mogelijk geweest zonder de steun en inzet van dr. Lars Wiking en Marianne Rasmussen.
Lars, I got to know you first as an office-mate when you were staying in Ghent. You came up with the suggestion that I could visit Denmark to do CSLM experiments. Thanks for taking such good care of me when I was in Denmark. You arranged everything from housing to transportation to and from the faculty. I really enjoyed my stay in the Kollegium.
Marianne, you tought me about the confocal microscope with a very broad smile and I will remember the time we spent laughing at 'funny twisting things'. Never knew that fat crystals could be so amusing.

Dank ook aan de beide thesisstudentes die een academiejaar lang hard gewerkt hebben en aldus hun steentje bijgedragen hebben tot dit proefschrift. *Lien, Priscilla, thank you both!*

Aan mijn studententijd als bio-ingenieur heb ik een aantal goede vrienden overgehouden. *Isabelle en Joeri, Karen, Lieselot, Anja, Lieven, Dominik en Sven: bedankt voor alle fijne momenten, het ene al zotter en hilarischer dan het andere. Dat er zo nog vele mogen volgen.*

Intussen heb ik in ontdekt dat er in Leuven ook een hele boel super gezellige en toffe mensen wonen en hun enthousiasme is nog maar eens duidelijk geworden tijdens onze verhuis enkele weken geleden. *Iris en Joris, Wim, Jan en Lore, en alle anderen: een dikke merci en de house-warming is op komst!!*

Steun van het thuisfront is onontbeerlijk.
Mama en papa, bedankt voor jullie onvoorwaardelijke steun en jullie nooit aflatende geloof in mij, ook als ik het allemaal wat somberder inzag. Jullie hebben altijd gezorgd voor een warm nest en dat koester ik.

En tot slot een heel speciaal bedankje voor mijn lieve schat.
Joaquin, er zijn geen woorden voor wat jij voor me betekent... Het klikte tussen ons vanaf die eerste ontmoeting en vanaf dat moment is ons verhaal alleen maar mooier geworden. Uit het diepst van mijn hart dankjewel voor alles: van het nalezen van teksten, het oplossen van mijn latex problemen tot het smeren van mijn boterhammen als ik weer eens supergehaast naar het station vertrok, je was er altijd voor mij en je liefde en steun is onbetaalbaar. Nu is het mijn beurt om jou te steunen bij het schrijfwerk. Hoteldebotel van jou xxx.

Een welgemeende merci aan jullie allen!

Veerle

Contents

Samenvatting

Inzicht in de microstructuur gevormd door gekristalliseerd vet is cruciaal in de productie van levensmiddelen. Vele sensorische eigenschappen worden immers in sterke mate bepaald door de mechanische sterkte van het onderliggende vetkristalnetwerk. Dit onderzoek tracht dan ook meer inzicht te verwerven in deze microstructuur, die afhankelijk is van zowel de chemische samenstelling (triacylglycerolen en minorcomponenten) van het kristalliserende vet als van de procescondities (tijd, temperatuur, afschuiving). Palmolie, één van de meest geproduceerde plantaardige oliën wereldwijd, werd geselecteerd als substraat voor deze studie.

Een eerste luik spitst zich toe op de isotherme, statische (= niet-geroerde) kristallisatie van palmolie. Hoewel hier al een duidelijk beeld kan verkregen worden van de microstructuur, spelen tijdens een industrieel productieproces ook andere parameters naast temperatuur een rol. Eén van de belangrijkste is afschuiving. Denk maar aan roeren om kristallisatiewarmte af te voeren, verpompen door leidingen en dergelijke meer. Een tweede luik richt zich dus op de invloed van afschuiving op de microstructurele ontwikkeling. Zowel het effect van continue afschuiving als van een korte afschuifstap gevolgd door statische kristallisatie op de microstructurele ontwikkeling wordt nagegaan. In een derde luik wordt tot slot dieper ingegaan op de rol van transvetzuren in het verkrijgen van de gewenste producteigenschappen. Omwille van de negatieve gezondheidsimplicaties dienen deze transvetzuren immers vervangen te worden door gezondere alternatieven zonder dat daarbij de gewenste productfunctionaliteit verloren gaat.

De verschillende fasen in het kristallisatieproces, namelijk primaire kristallisatie, microstructurele ontwikkeling en macroscopische eigenschappen, worden toegelicht in hoofdstuk 1. Vooreerst wordt aandacht besteed aan de basisprincipes van primaire kristallisatie

(nucleatie en kristalgroei). Aggregatie vangt aan zodra enkele kristallen gevormd zijn, wat uiteindelijk resulteert in een driedimensionale netwerkstructuur. Speciale aandacht wordt gegeven aan deze microstructurele opbouw en de beïnvloedende factoren. De microstructuur bepaalt immers in grote mate de macroscopische eigenschappen van het eindproduct. Hoofdstuk 1 geeft tot slot ook een overzicht van veelvuldig gebruikte experimentele technieken om kristallisatiegedrag te karakteriseren.

Hoofdstuk 2 behandelt de productie, verwerking en fractionatie van palmolie, alsook de specifieke chemische en fysische eigenschappen. De specifieke chemische en fysische eigenschappen maken palmolie uitermate geschikt voor fractionatie. Via fractionatie kan een breed gamma palmoliefracties bekomen worden, ieder met zijn specifieke samenstelling en karakteristieke eigenschappen. Tot slot wordt ook aandacht besteed aan de toepassingsmogelijkheden van palmolie en palmoliefracties in levensmiddelen.

Hoofdstuk 3 en 4 hebben betrekking tot het statische kristallisatiegedrag van palmolie. In hoofdstuk 3 wordt oscillatorische reologie vergeleken met differentiële scanning calorimetrie (DSC) en gepulseerde nucleare magnetische resonantie (pNMR) met betrekking tot het opvolgen van het kristallisatieproces. Oscillatorische reologie bleek een waardevolle aanvulling te vormen op DSC en pNMR om primaire kristallisatie onder statische condities te evalueren. Net zoals met DSC en pNMR kon aan de hand van oscillatorische reologie een onderscheid gemaakt worden tussen een éénstaps en een tweestaps kristallisatieproces. Bovendien leverde oscillatorische reologie ook informatie op met betrekking tot de microstructurele ontwikkeling (en dus ook de macroscopische eigenschappen) daar waar DSC en pNMR beperkt zijn tot het opvolgen van de primaire kristallisatie.

In hoofdstuk 4 wordt het kristallisatieproces van palmolie bij 18, 20, 22 and 25°C geëvalueerd aan de hand van verschillende experimentele technieken. Primaire kristallisatie werd opgevolgd via pNMR en DSC. Hoofdstuk 3 had al aangetoond dat oscillatorische reologie niet alleen informatie verschaft met betrekking tot de primaire kristallisatie maar ook over de microstructurele ontwikkeling. Gepolariseerd licht microscopie (PLM) en confocale scanning laser microscopie (CSLM) tonen aan dat naast het vast vet gehalte ook microstructurele verschillen in rekening gebracht moeten worden om de verschillen in netwerkrigiditeit te verklaren. Bij lagere temperaturen nucleeert het vet snel, wat aanleid-

ing geeft tot een groot aantal kleine kristallen. Wanneer deze kristallen aggregeren wordt een zeer compacte netwerkstructuur gevormd, wat resulteert in hoge dynamische moduli. Bij hogere temperaturen daarentegen worden een kleinere hoeveelheid grotere kristallen gevormd. Deze kristallen groeien trager en vormen een lossere netwerkstructuur, wat zich vertaalt in een lagere complexe modulus. CSLM toont bovendien ook aan dat bij lagere kristallisatietemperaturen meer filamenten gevormd worden die bruggen vormen tussen de kristalaggregaten doorheen het resterende vloeibaar vet.

De microstructuur wordt niet alleen beïnvloed door de kristallisatietemperatuur en de samenstelling van het vet. Andere procescondities zoals afschuiving kunnen eveneens een grote invloed uitoefenen. Hoofdstuk 5 en hoofdstuk 6 hebben dan ook tot doel inzicht te krijgen in het effect van afschuiving op het kristallisatieproces. Hoofdstuk 5 bestudeert het effect van continue afschuiving op de isotherme kristallisatie van palmolie. In hoofdstuk 3 werd aangetoond dat oscillatorische reologie kan gebruikt worden om zowel de primaire kristallisatie als de microstructurele ontwikkeling op te volgen tijdens statische kristallisatie. Dit inzicht wordt vervolgens toegepast in de ontwikkeling van een reologische methode om kristallisatie op te volgen onder continue afschuiving. Schijnbare viscositeit, complexe modulus en fase hoek werden geëvalueerd in functie van de isotherme tijd tijdens de kristallisatie van palmolie bij 18°C en verschillende afschuifsnelheden (1, 10 and $100 s^{-1}$). Deze reologische data werden vervolgens vergeleken met kristallisatie data verkregen via tijdsgeresolveerde x-stralen analyse (XRD) en PLM. Daar waar XRD alleen informatie geeft over de hoeveelheid en het type kristallen, biedt de ontwikkelde reologische methode tevens informatie over de evolutie van de microstructuur onder continue afschuiving.

Aansluitend op hoofdstuk 5 behandelt het eerste deel van hoofdstuk 6 het effect van lage afschuifsnelheden op het polymorfe gedrag van palmolie bij 18, 20, 22, 25°C zoals gemeten met tijdsgeresolveerde XRD. Afschuiving blijkt geen effect te hebben op de inductietijd voor de vorming van α kristallen, maar de omzetting naar de stabielere β' polymorf wordt wel versneld door toenemende afschuifsnelheden. Bij de onderzochte afschuifsnelheden wordt geen effect waargenomen op de inductietijd voor de vorming van β' kristallen bij 25°C. Het tweede deel van hoofdstuk 6 focust op het effect van een afschuifstap voorafgaand aan statische kristallisatie op de microstructurele opbouw. Deze afschuifstap vangt aan in de koelfase en omvat tevens een deel van de isotherme periode (1, 15, 30 min).

Kristallisatie wordt opgevolgd aan de hand van oscillatorische reologie en PLM. De afschuifstap beïnvloedt de microstructurele organisatie tijdens de daaropvolgende statische kristallisatie. De grootte van het effect wordt bepaald door de afschuifsnelheid, de duur van de afschuifstap en de kristallisatietemperatuur.

In hoofdstuk 7 tot slot wordt een case study uitgewerkt waarin het kristallisatiegedrag en de textuur van transvrije en transbevattende palmgebaseerde vetten, gebruikt in zoetwaren, geëvalueerd wordt aan de hand van DSC, pNMR, PLM, oscillatorische reologie en penetrometrie. Deze studie heeft als doel meer inzicht te verwerven in de rol van transvetzuren in de kristallisatie van palmgebaseerde zoetwarenvetten. De aanwezigheid van transvetzuren reduceert tot op zekere hoogte het effect van variaties in samenstelling. Voor de transvrije vetten vertaalt het verschil in chemische samenstelling zich zowel in het kristallisatiemechanisme als in de textuur. Het vervangen van transbevattende vetten door hun transvrije alternatieven moet dus met grote zorg gebeuren daar variaties in chemische samenstelling een groot effect kunnen hebben op de uiteindelijke productkwaliteit.

Summary

In the production of fat containing food products, insight in the properties of the fat crystal network is of utmost importance to obtain the desired product functionality and product quality. After all, many sensorial properties such as texture and spreadability strongly depend on the mechanical strength of the underlying microstructure. This research aims at gaining more insight into this microstructure that is influenced by the chemical composition (triacylglycerols and minor components) of the crystallizing fat as well as the processing conditions (time, temperature, shear). Palm oil, one of the largest vegetable oils worldwide, was selected as a substrate for this study.

A first part of the research deals with the isothermal, static (= non-stirred) crystallization of palm oil. This can already provide a good view of the microstructure. However, other parameters besides temperature also play a role in an industrial production process, one of the most important being shear. The fat is subjected to shear for instance by stirring to remove crystallization heat or during pumping from one vessel to another. Therefore, the second part in this study aims at understanding the effect of shear on the microstructural development. Both continuous shear during crystallization as well a time limited shear step prior to static crystallization are considered. In conclusion, the third part consists of a case study investigating the role of trans fatty acids in obtaining the desired product properties.

The different stages in fat crystallization, namely primary crystallization, microstructural development and final macroscopic properties are reviewed in chapter 1. Firstly, the basic principles of primary crystallization, including nucleation and crystal growth, are considered. Secondly, microstructural development is discussed. Special attention is given to the factors influencing this process as it will greatly affect the macrostructural properties of the final product. Primary crystallization and microstructural development cannot be

completely separated as aggregation can already start as soon as some crystals are formed, which will eventually lead to a three dimensional network structure, while nucleation and crystal growth still go on. Finally, Chapter 1 also presents the principles of different experimental techniques commonly applied to obtain crystallization data.

Chapter 2 describes the production, refining and fractionation of palm oil as well as its physicochemical properties. Due to its specific chemical and physical properties, palm oil is very suitable for fractionation, which leads to the production of several high added value palm oil fractions, each having their specific composition and characteristic properties. In addition, the applications of palm oil and palm oil fractions in food applications are highlighted.

Chapter 3 and 4 deal with the static isothermal crystallization of palm oil. In chapter 3, oscillatory rheology is compared with differential scanning calorimetry (DSC) and pulsed nuclear magnetic resonance(pNMR)in monitoring the crystallization process. It was shown that oscillatory rheology is a valuable complementary tool in studying static primary crystallization. Like DSC and pNMR, oscillatory rheology proved to be capable of differentiation between a single-step and a two-step crystallization process. However, DSC and pNMR, which are widely used techniques, do not provide any information on the formation of the fat crystal network. In contrast, oscillatory rheology offers the advantage of being able to evaluate the three stages of the crystallization process, namely primary crystallization, microstructural development and macroscopic properties, by one single analysis.

In chapter 4, a multi-methodological approach is used to study the isothermal crystallization of palm oil at four crystallization temperatures (18, 20, 22 and 25°C). Differential scanning calorimetry (DSC) and pulsed nuclear magnetic resonance (pNMR) were used to gain insight in the primary crystallization, while oscillatory rheology provided information on both primary crystallization and microstructural crystal network development and strength. Polarized light microscopy (PLM) and confocal scanning laser microscopy (CSLM) revealed that differences in microstructure have to be taken into account besides the amount of solid fat to explain the higher network stiffness for samples that crystallized at a lower temperature. At lower temperatures the fat nucleates quickly, leading to

a large number of small crystals. When these crystals start to aggregate, a very compact network structure is formed, giving rise to high dynamic moduli. At higher crystallization temperatures, fewer but larger crystals are generated that grow more slowly. As a result, a looser network structure is formed, leading to a lower complex modulus. In addition, CSLM reveals that at lower crystallization temperatures, more protruding crystalline filaments exists that bridge the crystalline aggregates through the remaining liquid fraction.

However, the fat crystal network is not only influenced by the crystallization temperature and the composition of the crystallizing fat. Other processing factors such as shear also play an important role. The influence of continuous shear on isothermal palm oil crystallization is the topic of chapter 5. It was demonstrated in chapter 3 that oscillatory rheology can be applied to monitor not only primary crystallization but also the microstructural development of fats crystallizing under static conditions. This insight was used to develop a rheological method to evaluate fats crystallizing under shear. Apparent viscosity, complex modulus, loss modulus, storage modulus and phase angle are monitored as a function of isothermal time during the isothermal crystallization of palm oil at 18°C and various shear rates (1, 10 and 100s^{-1}). The thus obtained results are compared with crystallization data obtained via time resolved XRD and PLM. The proposed method is capable of measuring moduli and phase angle , thus gaining information on primary crystallization and microstructural development under shear. In contrast, XRD only provides information on the amount and type of crystals.

In addition to chapter 5, the first part of chapter 6 studies the effect of low shear rates on palm oil crystallization at four temperatures (18, 20, 22, 25°C) by time-resolved X-ray analysis. No effect on the induction time for the formation of α crystals is observed. However, the applied shear rate causes an earlier polymorphic transformation from the α to the β' polymorph at 18, 20 and 22°C. In contrast, no effect of the applied shear rates on the induction time for the formation of β' crystals was noted at 25°C. In a second part, the influence of a shear step, starting during the cooling phase and comprising the first part of the isothermal period (1, 15, 30 min) on the microstructural development, is studied by rheology and PLM. The shear step is shown to affect the subsequent static crystallization by altering the microstructural arrangement. The extent of the effect of the shear step is determined by both the duration and the applied shear rate but also by the crystallization

temperature.

In conclusion, chapter 7 describes a case study in which 3 trans containing and 3 trans free palm oil based confectionery fats were analyzed with several techniques to asses their crystallization behavior and texture at 10°C with DSC, pNMR, PLM, oscillatory rheology and penetrometry. The aim of this study is thus to gain more insight into the role of trans fatty acids on crystallization and texture of palm oil based confectionery fats. Although the trans fat-series differ in chemical composition, this difference is not reflected in major variations in SFC, or in network formation. The presence of trans fat seems to reduce the influence of compositional variations to some degree. The trans free palm oil based confectionery fats show more differences in chemical composition, which greatly influence the solid fat content, network formation and hardness as well as the mechanism of primary crystallization. These results indicate that, when replacing trans containing fats with trans free alternatives, variations in chemical composition of these alternatives can have a tremendous effect on the final product quality, which makes the formulation of a suitable alternative not straightforward.

Outline of the research

In the production of fat containing food products, insight in the properties of the fat crystal network is of utmost importance to obtain the desired product functionality and product quality. After all, many sensorial properties such as texture and spreadability strongly depend on the mechanical strength of the underlying microstructure. This research aims at gaining more insight into this microstructure that is influenced by the chemical composition (triacylglycerols and minor components) of the crystallizing fat as well as the processing conditions (time, temperature, shear flow). Palm oil, one of the largest vegetable oils worldwide, was selected as a substrate for this study of which the outline is presented in Figure 1.

The first two chapters provide a literature review of fat crystallization and of the substrate palm oil. The first part of the research deals with isothermal crystallization without shear. Chapter 3 and 4 deal with the static isothermal crystallization of palm oil. In chapter 3 oscillatory rheology is applied to monitor the crystallization process and is compared with more conventionally used techniques such as DSC and pNMR. In chapter 4, a multi-methodological approach is used to study the isothermal crystallization of palm oil at four crystallization temperatures (18, 20, 22 and 25°C). In addition to pNMR, DSC, PLM and oscillatory rheology, CSLM was used to visualize the network structure.

The second part of the research focusses on the effect of shear on the microstructural development of isothermally crystallizing palm oil. In chapter 5 a rheological method is developed to evaluate fats crystallizing under continuous shear. In chapter 6 the effect of low shear rates on palm oil crystallization at four temperatures (18, 20, 22, 25°C) was evaluated by time-resolved X-ray analysis. In addition, the influence of a shear step, starting during the cooling phase and comprising the first part of the isothermal period (1, 15, 30 min) on the microstructural development, is studied by rheology and PLM.

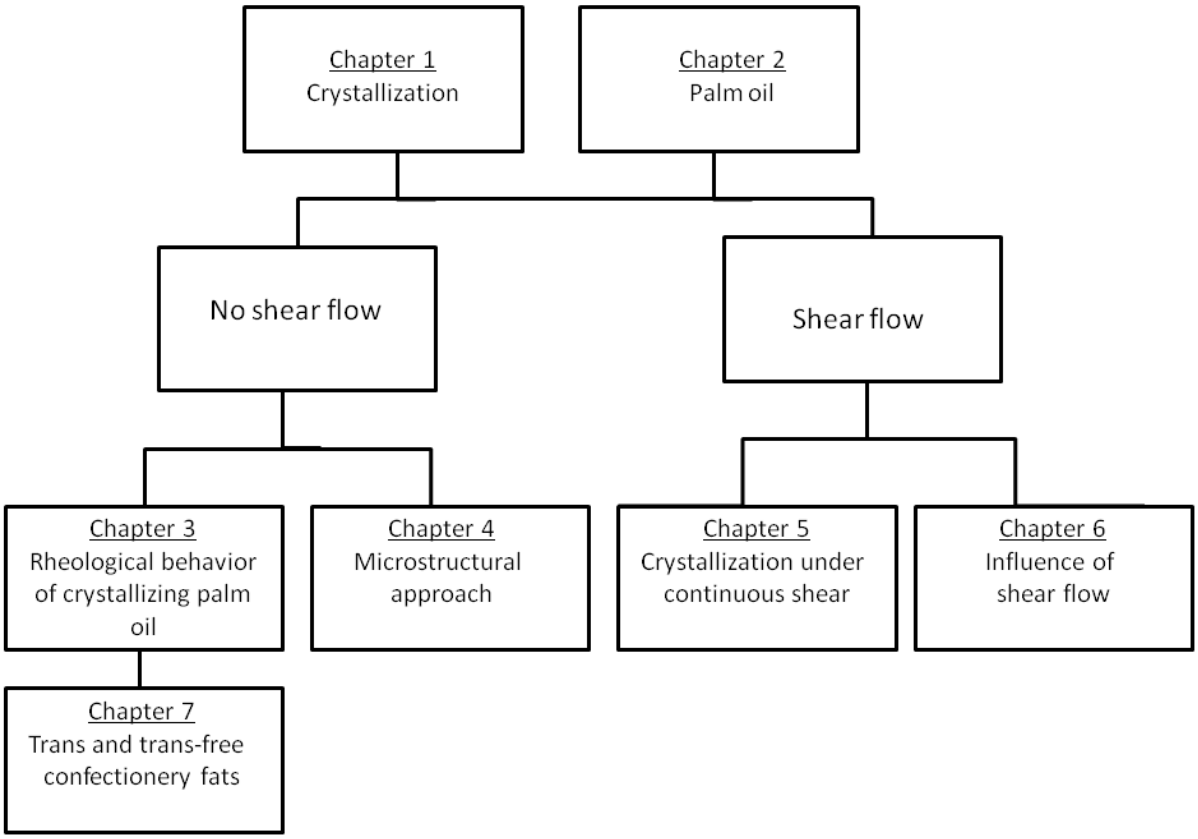

Figure 1: General outline of the research

The fat crystal network and consequently the macroscopic properties are not only influenced by processing conditions such as crystallization temperature and shear rate, but also by the chemical composition of the crystallizing fat. This is taken into account in the final chapter of this research. In chapter 7 the crystallization behavior and texture of trans containing and trans free palm oil based confectionery fats are investigated, using the insight obtained in chapter 3.

Chapter 1

Fat Crystallization

It's a dangerous business going out your front door.
Lord of the rings - J.R.R. Tolkien (1982-1973)

1.1 Introduction

Numerous food products contain a substantial amount of fat, of which a significant part is present in the crystallized form. Many of the sensory attributes such as spreadability, mouth feel, snap of chocolate, texture etc. are dependent on the mechanical strength of the underlying fat crystal network (Narine and Marangoni 1999c; Narine and Marangoni 1999e; Foubert 2003). The processes involved in the crystallization and storage of fats are schematically shown in Figure 1.1.

The chemical composition (triacylglycerols and minor components) and the processing conditions (combination of time, temperature and shear flow) influence the primary crystallization behavior of fats. This primary crystallization behavior does not only include when and to what extent the fat crystallizes, but also polymorphism, polymorphic transitions and the morphology of the crystals. The fat crystal network is formed by the aggregation of fat crystals through van der Waals attraction (Walstra et al. 2001; Kloek 1998). Fat crystals already start to aggregate at low volume fractions of crystallized fat, forming voluminous aggregates, while nucleation and crystal growth still go on (Walstra et al. 2001). A consequence of simultaneous crystallization and aggregation is that at a low fraction of crystallized fat already a continuous network is formed, while a substantial amount of fat still has to crystallize. This generally leads to sintering, i.e. the formation of solid bridges between aggregated crystals and aggregates (Kloek 1998). The number, size and shape of the particles and large clusters will define the microstructure, which will in turn determine the mechanical properties of the fat (Marangoni 2002a).

In this chapter, attention will be paid to principles of fat crystallization. This section is constructed according to the different stages presented in Figure 1.1, namely primary crystallization (nucleation and crystal growth), microstructural development and final macroscopic properties. A second section then covers the experimental techniques to monitor fat crystallization. Widely know techniques such as DSC and pNMR are only briefly touched. The emphasis of this section is placed on small deformation rheology.

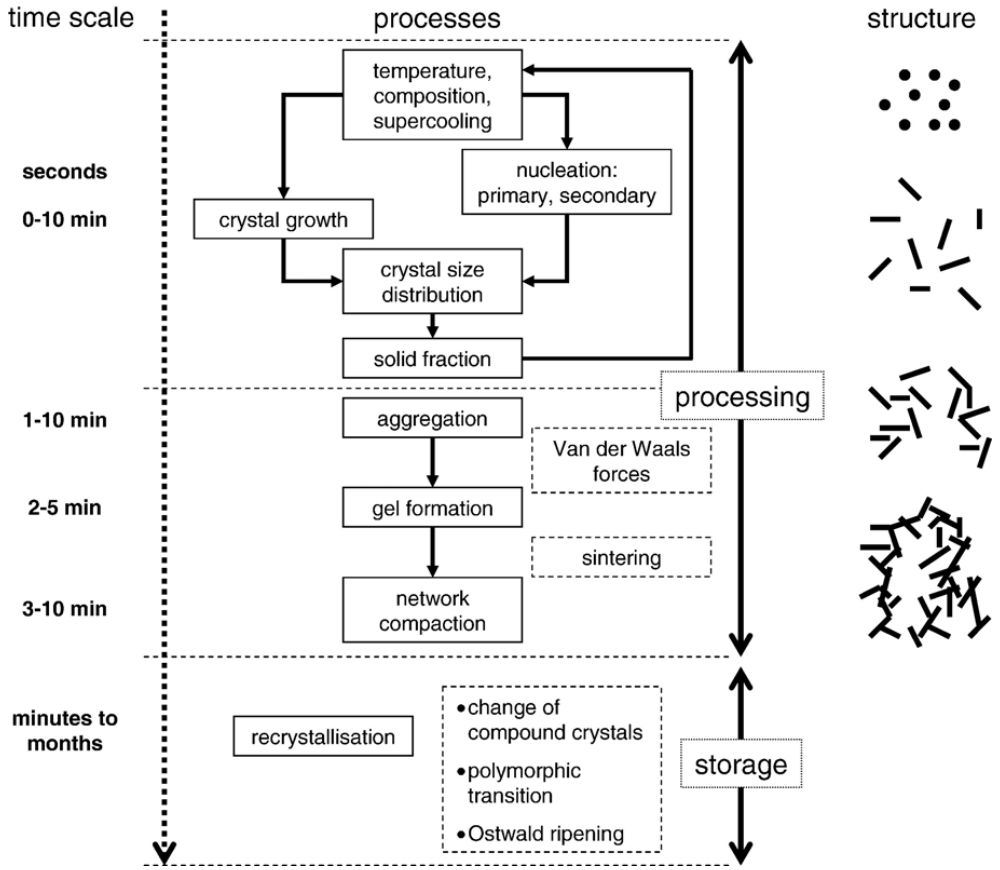

Figure 1.1: Schematic presentation of processes involved in crystallization and storage of fats (Walstra et al. 2001)

1.2 Primary crystallization

Crystals can be formed from the vapor phase, the melt or from solution. No specific theories have been developed to treat each of these different phase changes, but general theories have been adapted to apply to specific cases (Garside 1987). Primary crystallization can be divided into several steps, the first being the generation of sufficient thermodynamic driving force. Once this has been attained, nucleation can occur, whereby crystals are generated as a result of bringing growth units together so that a crystal lattice can be formed. From then on, proper crystal growth can proceed (Foubert et al. 2007). Although it is convenient to treat nucleation and crystal growth as consecutive events, these processes are not clearly separated in time: nucleation does not stop when crystal growth starts (Hartel 1992).

1.2.1 Thermodynamic driving force

The first step in crystallization is always the generation of sufficient driving force. The driving force for crystallization is a difference in chemical potential $\Delta\mu$ [J mole^{-1}], or partial molar Gibbs free energy, between the solution phase and the crystalline solid. The larger the chemical potential difference, the larger the driving force for crystallization. When a lipid system is considered to be a mixture of triacylglycerols, nucleation requires supersaturation of the system by achieving a concentration C [m^3 or equivalent] higher than the concentration at saturation C_s [m^3 or equivalent]. The difference in chemical potential can then be written as:

$$\Delta\mu = R_g \times T_K \times ln\frac{C}{C_s} \tag{1.1}$$

with R_g is the universal gas constant [8.314 $J\ mole^{-1}$] and T_K the absolute temperature [K]. The term $ln\frac{C}{C_s}$ is called the supersaturation $ln(\sigma)$ [-], while $\frac{C}{C_s}$ is the supersaturation ratio σ [-].

For nucleation from the melt, the thermodynamic driving force is proportional to the temperature difference between the crystallizing system and the melting point. The chemical potential difference can then be written as

$$\Delta\mu = \Delta H_m \times \frac{T_{Km} - T_K}{T_{Km}} = \Delta H_m \times \frac{\Delta T}{T_{Km}} \tag{1.2}$$

with ΔH_m the molar enthalpy variation in the system during crystallization [$J\ mole^{-1}$], T_{Km} the absolute melting temperature [K] and ΔT [K] the supercooling.

1.2.2 Nucleation

Several types of nucleation can be distinguished: primary nucleation, which can be either homogeneous or heterogeneous, and secondary nucleation (Garside 1987, Boistelle 1988, Hartel 1992). In primary nucleation, crystal nuclei are formed when molecules come together to form a stable cluster, whereas secondary nucleation occurs due to the presence of existing crystals in the desired form (Hartel 1992). Primary homogeneous nucleation occurs in the absence of foreign surfaces and requires supercooling up to 30 K (Kloek 1998). Heterogeneous nucleation on the other hand, takes place when foreign surfaces like

dust particles and different compound molecules are present. In this case, lower degrees of supercooling are needed (1-3 K) because of the affinity between the nucleus and the foreign surface (Garside 1987; Kloek 1998).

1.2.2.1 Primary homogeneous nucleation

When the thermodynamic driving force is sufficiently high, nucleation can take place. Nucleation occurs via bimolecular reactions leading to a distribution of clusters or embryos, which depends, among other parameters, on temperature and supersaturation. The Gibbs free energy change (ΔG [J]) for the formation of an embryo includes both a positive surface term (ΔG_s [J]), due to surface tension, and a negative volume term (ΔG_v [J]). ΔG [J] is also called the activation energy for nucleation and for a spherical embryo of size r [m] it is given by:

$$\Delta G = 4\pi r^2 \gamma - \frac{4\pi r^3 \Delta\mu}{3V_m} \tag{1.3}$$

Figure 1.2 illustrates the form of equation 1.3. The overall free energy change ΔG goes though a maximum at a critical size r* [m], which is in fact the embryo size for which $\delta G/\delta r = 0$ (equation 1.3). This critical embryo size is given by

$$r^* = \frac{2\gamma V_m}{\Delta\mu} \tag{1.4}$$

where γ [J m^{-2}] is the surface free energy per unit surface area and V_m [m^3 mole^{-1}] the molar volume.

All embryos will tend to change their size in such a way as to decrease their overall free energy. For those smaller than the critical size r^* this is achieved by dissolving, whereas embryos larger than r^* will continue to grow. Therefore, the critical embryo size r^* corresponds to the smallest embryo that can decrease its free energy by growing and is thus the minimum size of a stable nucleus. The critical activation energy for nucleation is then obtained by inserting r^* in Equation 1.3:

$$\Delta G^* = \frac{16\pi V_m \gamma^3}{3(\Delta\mu)^2} \tag{1.5}$$

The factor $16\pi/3$ results from the spherical shape of the nucleus and can in general be replaced by a dimensionless shape factor.

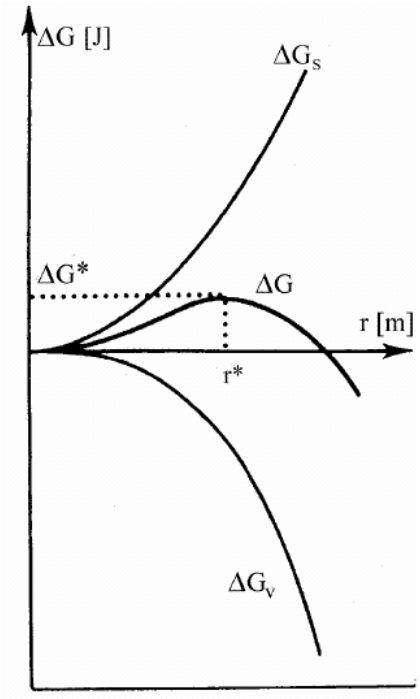

Figure 1.2: Gibbs free energy change ΔG [J] as a function of nucleus size r [m] (Garside 1987, Boistelle 1988)

The nucleation rate J [s^{-1} m^{-3}] is a problem of kinetics and is determined by the rate at which nuclei surmount the maximum in the free energy curve, which is the rate limiting step in the nucleation process. Assuming the nuclei follow a Boltzmann distribution as a function of their free energy, the nucleation rate can be written as

$$J = A_J \times e^{\frac{-\Delta G^*}{kT}} \tag{1.6}$$

with A_J [s^{-1} m^{-3}] the global kinetic coefficient and k the Boltzmann constant (1.380×10^{-23} J K^{-1}). A_J can also be written as

$$A_J = \frac{N \times k \times T}{h} \tag{1.7}$$

in which N [m^{-3}] is the number of molecules per unit volume that are formed and h Plank's constant ($6.626 \times 10^{-34} J$ s).

When nucleation occurs in a condensed phase (melt or solution), it is necessary to take into account the difficulty encountered by a molecule to cross the interface between the

solid and the liquid phase. This is especially valid for the melt or for solutions of high viscosity. In these cases, an additional critical free energy term for volume diffusion ΔG^*_{vd} [J] is added to Equation1.6, which is then rewritten as

$$J = A_J \times e^{\frac{-\Delta G^*}{kT}} \times e^{\frac{-\Delta G^*_{vd}}{kT}} \tag{1.8}$$

When temperature decreases, the volume diffusion term or transport term may become the rate-determining step of nucleation and growth. Equation 1.8 is know as the Fisher-Turnbull equation.

1.2.2.2 Primary heterogeneous nucleation

Heterogeneous nucleation takes place on solid particles for which the new phase has some chemical or physical affinity. The walls of the containing vessels, blades of impellers, emulsifiers, native mono-and di-acylglycerols, minor polar lipids, and even dust particles can provide catalytic nucleation surfaces. The activity of a foreign surface to nucleate a crystal depends on the match between the structure of the nucleating site and the crystal lattice and is generally related to the relative interfacial tensions between the three phases (crystal, solution and solid surface). The surface free energies involved are γ_0 [J m^{-2}] between mother phase and foreign surface, γ_1 [J m^{-2}] between mother phase and nucleus and γ_2 [J m^{-2}] between nucleus and foreign surface (1.3). A simple force balance leads to:

$$\gamma_0 = \gamma_2 + \gamma_1 cos\omega \tag{1.9}$$

with ω the contact or wetting angle between the nucleus and the surface. When the nucleus is in contact with the substrate, two excess energies have been expended for creating the new surfaces, whereas one has been gained in losing a fraction of the surface area. Therefore, the Gibbs free energy for nucleation can be expressed as the sum

$$\Delta G_{het} = -\Delta G_v + A_1\gamma_1 + A_2\gamma_2 - A_1\gamma_0 \tag{1.10}$$

For a cap-shaped embryo and taking into account Equation 1.9 ΔG_{het} can be written as

$$\Delta G_{het} = -\frac{\pi r^3 \Delta\mu(2 - 3cos\omega + cos^3\omega)}{3V_m} + 2\pi r^2\gamma_1(1 - cos\omega) + \pi r^2\gamma_1(1 - cos\omega)cos\omega \tag{1.11}$$

in which r [m] is the radius of the underlying sphere. The critical radius r^* for which ΔG_{het} is maximum is given by

$$r^*_{het} = \frac{2\gamma_1 V_m}{\Delta\mu} \tag{1.12}$$

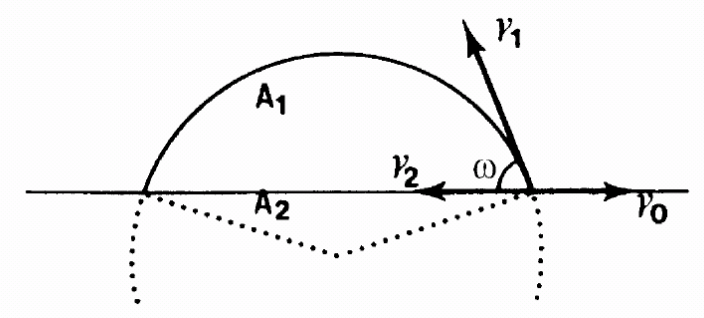

Figure 1.3: Cap-shaped nucleus model of heterogeneous nucleation. The surface free energies between the mother phase, the nucleus and the foreign surface are represented by arrows (Boistelle 1988)

The critical size of a nucleus for heterogeneous nucleation is thus the same as for homogeneous nucleation. However, since the spherical cap contains fewer molecules than the full sphere, the energy barrier is less for heterogeneous nucleation compared to homogeneous nucleation. Inserting Equation 1.12 into Equation 1.11 yields the critical activation energy for heterogeneous nucleation

$$\Delta G^*_{het} = \Delta G^* \times \left(\frac{1}{2} - \frac{3}{4} cos\omega + \frac{1}{4} cos^3\omega \right) \tag{1.13}$$

which is the sum of the critical activation energy for homogeneous nucleation ΔG^* and a term depending on the wetting angle ω. It can be easily understood that for a contact angle of 180° this term equals one and the catalyzing effect of the surface will be absent. Equally, in the case of perfect wetting of the surface, which would result in a contact angle of 0°, this term equals zero and no activation free energy would be needed for nucleation to take place.

1.2.2.3 Secondary nucleation

According to Kloek (1998) and Garside (1987) three types of secondary nucleation can be distinguished: true, apparent and contact. True secondary nucleation means that nuclei are formed in the vicinity of a crystal, not at the surface, resulting in enhanced nucleation. This can occur in the absence of agitation. In apparent secondary nucleation fragments of growing crystals act as new nuclei, while contact secondary nucleation results from collision of crystals with other crystals, the walls of the crystallizer, the impeller blades etc.

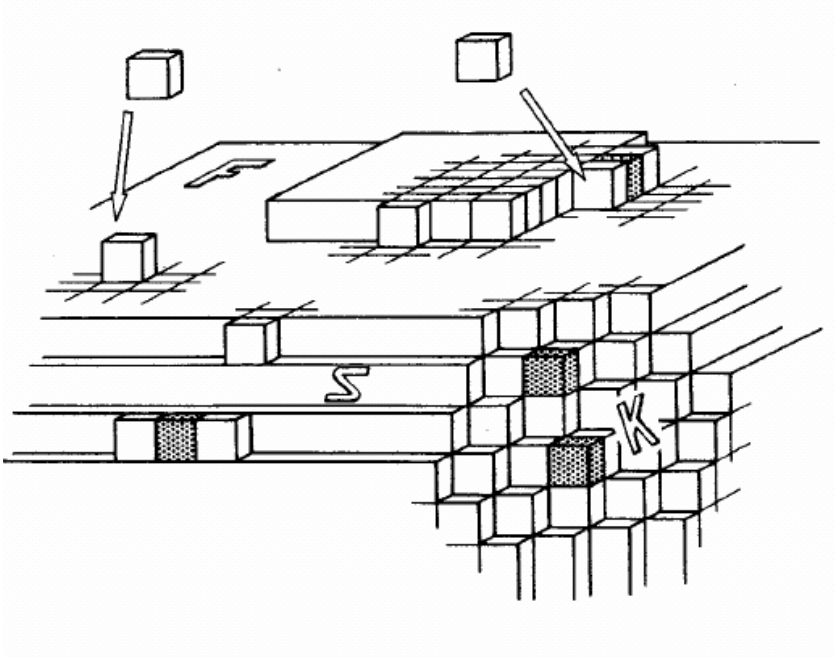

Figure 1.4: Schematic representation of three types of growth sites. Each cube depicts a growth unit (Aquilano and Squaldino 2001)

1.2.3 Crystal growth

Crystal growth occurs by attachment of molecules to a crystal surface. On the other hand, molecules will also become detached, thus resulting in a continuous transport of molecules across the crystal surface. Hence, growth rate is determined by the resultant of these two processes. Consequently, the crystal growth rate can vary by several orders of magnitude (Walstra 2003).

The solid-liquid interface, depending on both the crystal structure (internal) and the mother phase (external), plays a critical role in crystal growth (Boistelle 1988; Himawan et al. 2006). Generally, three distinct faces were described: kinked, stepped and flat as is illustrated in Figure 1.4. The highest growth rate is found at **kinked (K) faces**, which can be described as an infinite population of kink sites. Due to this infinite amount of kinks, each growth unit in a supersaturate state that reaches the crystal surface will be readily incorporated into the crystal lattice. Consequently, the growth rate of a kinked face is proportional to the supersaturation (Garside 1987; Aquilano and Sgualdino 2001).

A **stepped (S) face** contains less kinks per unit area compared to the K-face and consequently it will have a lower growth rate. From a kinetic viewpoint, the growth of a S-face is similar to the growth of a K-face. Therefore, the growth rate will also be proportional to the supersaturation. However, when crystal growth occurs from the melt, the growth kinetics are largely influenced by the activation free energy for self-diffusion of the molecules in the melt. The growth rate is then proportional to the supercooling and inversely proportional to the viscosity. If viscosity increases drastically with decreasing temperature, it can happen that at a certain temperature the growth rate passes through a maximum and subsequently start to decrease with increasing supercooling (Boistelle 1988).

Flat (F) faces exhibit a small number of kinks and the growth layers are added layer after layer, parallel to the surface (Boistelle 1988). F-faces can grow even at very low supersaturations by either a two-dimensional growth mechanism or by spiral growth (Aquilano and Sgualdino 2001). When no defects are present in the crystal surface, growth takes place via a two-dimensional growth mechanism. Sufficient molecules need to diffuse, encounter and coalescence to form a stable two-dimensional nucleus on the crystal surface. Once this is achieved, the edge of this nucleus forms an attachment point for other growth units, supplied by surface diffusion, and lateral growth can proceed on an otherwise flat surface. It is possible for several nuclei to exist on the surface simultaneously (Garside 1987). For this mechanism, the growth rate is proportional to the two-dimensional nucleation rate, which depends on an activation free energy, and is an exponential function of the supersaturation. This type of growth mechanism is rather rare (Boistelle 1988).

A more frequently occurring mechanism is the **spiral growth** mechanism. In this mechanism, a step is formed when a screw dislocation emerges on a face (defective surface). Molecules absorbing from the mother phase will first diffuse toward and along this step. As soon as they encounter a kink, they are trapped into the surface. The step advances by rotating around its origin of dislocation, and after a complete rotation, one or several layers of molecules have been added to the crystal (Aquilano and Sgualdino 2001). Several theoretical expressions exist for the growth rate and the general growth rate is very complex. In general, two growth rates can be distinguished. At low supersaturation, the growth rate of the face is a quadratic function of the supersaturation, while at high supersaturations it turns into a linear function of the supersaturation (Boistelle 1988).

In the last decades, some authors discussed growth rates based on two types of surfaces, namely **smooth and rough surfaces** (Ghotra et al. 2002; Walstra 2003). Smooth or faceted surfaces are characterized by an atomically abrupt change in the degree of crystalline order across the solid-liquid boundary, resembling 'terraces' separated by abrupt atomic-scale steps. In contrast, rough surfaces are structurally diffuse, with the degree of crystalline order varying continuously over the scale of a few atomic planes along the solid-liquid boundary (Asta et al. 2004). For a given supersaturation, the growth rate is distinctly faster at a rough surface then at a smooth surface. At a rough surface, attachment of a molecule can involve contacts with more than one molecule, thus greatly enhancing the 'sticking probability'. At smooth surfaces, growth occurs via surface nucleation, followed by two-dimensional growth, resulting in a lower growth rate compared to rough surfaces (Walstra 2003). Crystal growth rate is influenced by many factors besides the nature of the solid-liquid interface. Other factors such as viscosity, diffusive mass transfer, molecular conformation, surface defects, shear rates, impurities and the molecular diversity of the fats all play a role in influencing the rate of crystallization (Ghotra et al. 2002).

1.2.4 Polymorphism of triacylglycerols

Polymorphism is defined as the existence of several crystalline phases with the same chemical composition that have a different structure, but yield identical liquid phases upon melting. Two crystalline states are monotropic if one is stable and the other metastable under all conditions, regardless of temperature. Transformation will take place only in the direction of the more stable form. Crystalline forms which each have a definite range of stability are called enantiotropic. Either of the modifications may be the stable one and transformation can go in either direction, depending on temperature. Natural fats are invariably monotropic (Nawar 1996).

1.2.4.1 Basic polymorphs

In the middle of the previous century, Larsson (1966) used both powder X-ray diffraction and infrared spectroscopy to classify the basic polymorphs of triacylglycerols into three crystallographic types, namely α, β' and β, based on their hydrocarbon sub cell packing, which is the smallest spatial unit of repetition along the chain axis (Nawar 1996).

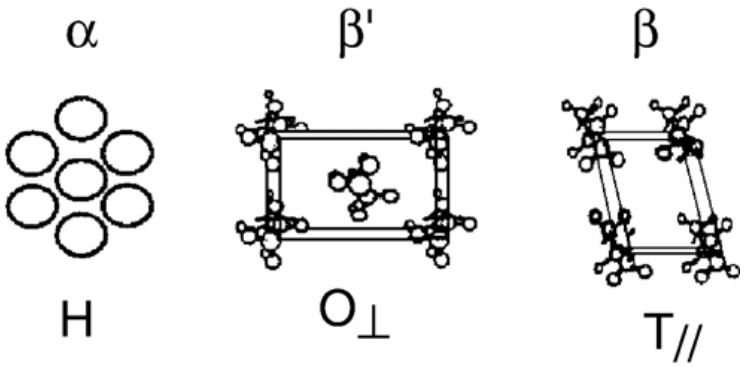

Figure 1.5: The sub cell structures of the three most common polymorphs in triacylglycerols (Sato 1999a)

Table 1.1: Classification of polymorphs based on WAXD (Hagemann 1988) s=strong line

polymorph	Unit cell	Short Spacing (nm)
α	hexagonal	0.415 (s)
β'	orthorombic	0.38 (s), 0.42 (s)
β	triclinic	0.455 (s), 0.36-0.39

Although polymorphism was initially much debated, and thus no uniform classifications existed, these basic crystallographic types are nowadays generally accepted as the basic polymorphs of simple triacylglycerols.

The α polymorph is characterized by a hexagonal sub cell packing in which the hydrocarbon chains are positioned perpendicular to the methyl end group plane and are assumed to oscillate with a high degree of freedom. The β' polymorph is associated with an orthorhombic perpendicular sub cell packing, where in the fatty acid chains are tilted with respect to the methyl end group plane and where adjacent zigzag fatty acid chains are in different planes. The chains have an angle of tilt between 50° and 70°. The β form is the densest polymorphic form having a triclinic chain packing, in which all zigzag fatty acid chains are in the same plane (parallel) and thus pack snugly together. The chains also have an angle of tilt between 50° and 40° (Sato et al. 1999; Himawan et al. 2006). These three basic polymorphs are schematically represented in Figure 1.5.

Each of the sub cell packings exhibits characteristic short spacings and thus each polymorph can be unambiguously identified by wide angle X-ray diffraction (WAXD). The characteristic short spacings for the 3 basic polymorphs are presented in Table 1.1. The α-polymorph is the least stable one, followed by the β' and the β polymorph. Melting point, melting enthalpy and density increase with increasing stability (Walstra 1987). According to Loisel et al. (1998) the growth rate increased with increasing stability, while Kellens (1991) stated that the growth rate of the stable polymorph was lower than that of the unstable polymorph.

The thickness of the layers formed by the side-by-side arrangement of the chains (long spacings) are measured by X-ray diffraction at small angles (SAXS). These long spacings depend on the length of the molecule, and the angle of tilt between the chain axis and the methyl end group plane. The triacylglycerols are arranged head to tail and form a chair-shaped structure with the fatty acid at the 2-position forming the back of the chair. This arrangement leads to two different packing modes, 2L or 3L, as is illustrated in Figure 1.6. The β' and β polymorph can exist as either double chain length or triple chain length structures. A double chain length structure normally occurs when the chemical nature of the three fatty acid moieties are the same or very similar. Consequently, if the fatty acid moieties are very different from each other, for example a mixed saturated-unsaturated triglyceride, a triple chain length structure is formed (Kloek 1998; Sato et al. 1999; Himawan et al. 2006). The α form is normally only found to exist in a double chain length structure (Himawan et al. 2006).

1.2.4.2 Other polymorphs

In addition to the three main polymorphic forms (α, β', β), the polymorphism of triacylglycerols has become more complicated with the discovery of multiple sub-modifications of these basic polymorphs. In saturated mono-acid triacylglycerols, at least two modifications of the β' have been recorded. Different sub-modifications are even more prevalent in mixed acid triacylglycerols (Kellens 1991; Sato et al. 1999). A fourth polymorphic form was revealed by low-temperature XRD. The sub-α polymorph, also called the γ polymorph, has an XRD pattern which is similar to that of the β' form (Hagemann 1988; Kellens 1991).

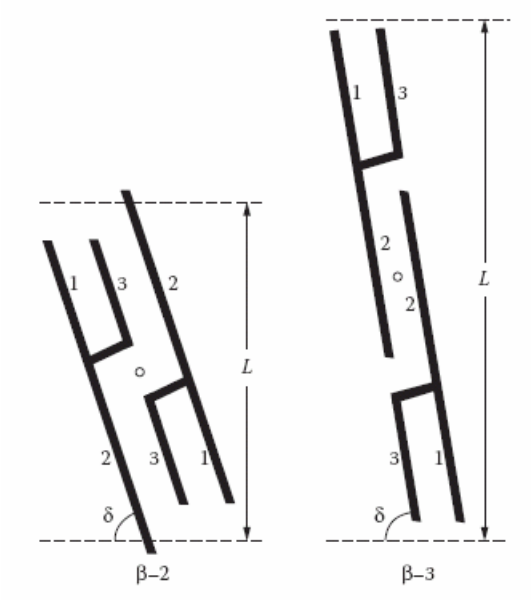

Figure 1.6: Arrangement of triacylglycerols in the crystalline phase: double and triple chair arrangements of the β form. L is the layer thickness and δ is the angle of tilt (Walstra 1987)

.

1.2.4.3 Phase transitions

The relative stability of two polymorphs and the driving force for phase transitions between them at a constant temperature are determined by their respective Gibbs free energies, with the most stable polymorph having the lowest Gibbs free energy (Himawan et al. 2006). Thermodynamically, the β polymorph is the most stable one, followed by the β' and the α polymorph. The thermodynamic stability relationships are shown in Figure 1.7a, where the Gibbs free energy values (G) are expressed as a function of temperature (T). The crossing point of the G-values and the liquid indicate the melting point (T_m) of each specific polymorph. Under proper conditions, all three polymorphs can be crystallized directly from the melt and any polymorph can be returned to the liquid phase by raising the temperature. However, transformations between polymorphs are always irreversible. The transformation pathways of the basic polymorphs are shown in Figure 1.7b.

Metastable crystals can change into a stable one through the rearrangement of its structural unities until a complete transformation occurs (solid-state phase transformation) or

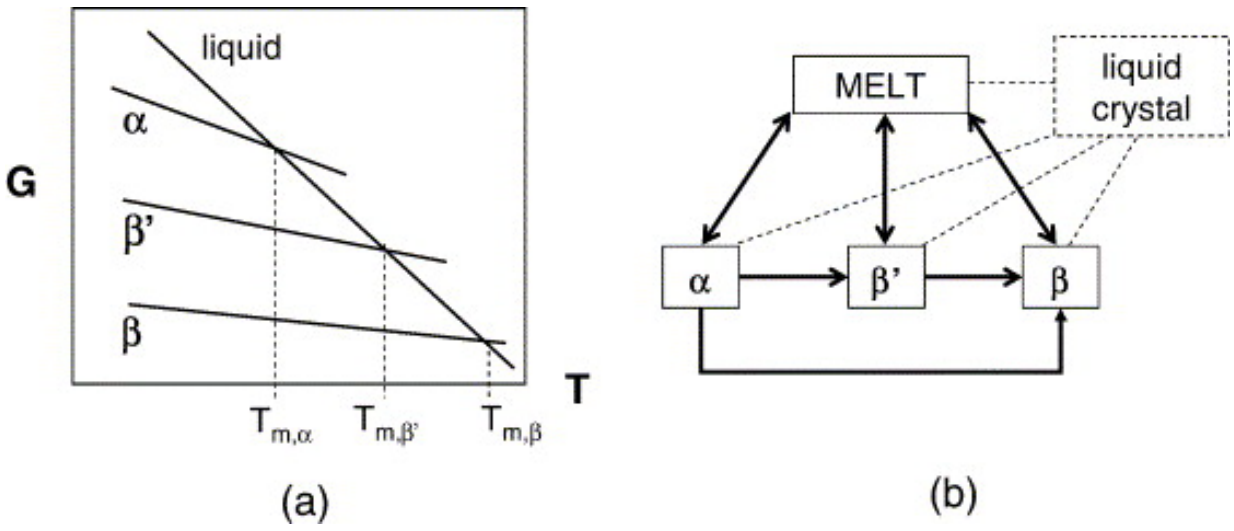

Figure 1.7: (a) Relation between Gibbs free energy and temperature for the three main polymorphs of triacylglycerols. (b) The polymorphic transformation pathways in fats involving the three main polymorphs (Sato 1999b)

by melting and recrystallization (melt-mediated phase transition)(Sato et al. 1999). In case a number of phase transitions from a less stable to more and more stable polymorphs are possible, the closest more stable phase is usually formed and not the most stable one. The kinetics of these phase transitions can vary greatly, ranging from almost instantaneously to extremely slow, for instance for some solid-state transitions (Aquilano and Sgualdino 2001). The transformations between liquid and crystalline states and between crystalline states are all first order transitions. Only the sub-α to α transition is assumed to be of the second order type and reversible. Second order transitions do not invoke large changes in crystal structure as they merely involve an increase in molecular movement. They can occur over a wide temperature range and do not involve heat exchange (Hagemann 1988; Kellens 1991).

1.2.5 Compound crystals

Compound or mixed crystals contain two or more different components (molecular species) and are more likely to be formed if the different molecular species are more similar in size, shape and properties. Triacylglycerol mixtures readily form compound crystals in the α-polymorph as this least dense packing mode has some freedom of movement, thus

allowing different molecules to fit into the same lattice. In the β'-polymorph, the compound crystal formation is restricted to groups of similar triacylglycerols due to the denser crystal lattice. Compound crystal formation in the β-polymorph will only occur for very similar triacylglycerols in restricted compositional ranges (Kloek 1998; Walstra 1987; Walstra 2003). Most compound fat crystals are not stable but tend to rearrange into purer crystals, which is often accompanied by a polymorphic transformation. Extensive compound crystal formation can have several consequences:

- The melting range is narrowed;
- The melting temperature at which most of the fats melts depends on the crystallization temperature;
- Slow cooling leads to less solid fat compared to quick cooling to the same final temperature;
- Unstable polymorphs tend to persist much longer.

1.3 Microstructure of fat crystal networks

1.3.1 Aggregation and network formation

The microstructural level of a fat crystal network can be defined as those structures that measure between 1 and 140μm. The lower range of the microstructural level is characterized by crystallites, while at the upper range clusters of crystals (aggregates) can be found (Narine and Marangoni 1999e). The different levels of microstructural development (aggregation, network formation and sintering) are illustrated in Figure 1.8.

As soon as fat crystals attain a certain minimum size (very roughly 0.1μm) they readily aggregate due to van der Waals' attraction (Walstra 1987; Johansson 1994; Kloek 1998). Virtually no repulsion exist between fat crystals, except hard core repulsion at very small distances between the crystals ($\leq$0.5nm) (Walstra et al. 2001). Random aggregation of fat particles which meet due to Brownian movement (perikinetic aggregation) and subsequently stick together results in the formation of fractal aggregates. A specific property of fractal objects is that they are on average self-similar, implying that they have, on average, the same structure when observed at different magnifications (Narine and Marangoni

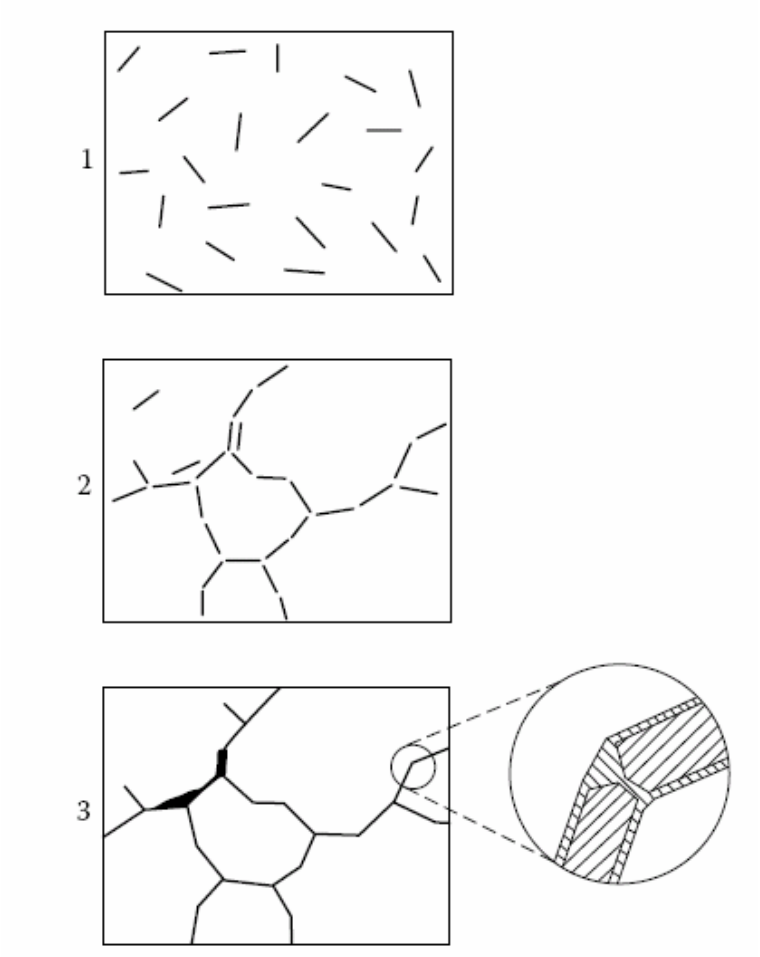

Figure 1.8: Various stages in microstructural development: aggregation, network formation and sintering of crystals (Walstra 1987)

1999e; Walstra et al. 2001; Marangoni 2002b). As soon as the volume fraction of the particles in a fractal aggregate approximates the volume fraction of primary crystals in the system, they start to impinge on each other, resulting in the formation of a continuous network. This network provides the fat with elastic properties, whereas a solution of fat crystals or non-touching aggregates will merely have a higher viscosity than that of the oil (Walstra et al. 2001).

Aggregation can already occur at very low volume fractions of crystallized fat (about 1%). Consequently, a substantial portion of the fat still has to crystallized while a primary network is already formed (Kloek 1998; Walstra et al. 2001). This additional crystalliza-

tion will lead to compaction of the aggregates that make up the primary network. Whether the fractal nature of the network is maintained at higher solid:liquid ratios is still a controversial point (Kloek 1998; Narine and Marangoni 1999e; Walstra et al. 2001). Additional crystallization after the formation of the primary network will also lead to sintering, which is the formation of solid bridges between aggregated crystals and aggregates. Two crystals will sinter when some triacylglycerol molecules are incorporated in both crystal lattices. This process is more likely to take place at crystal surfaces that have defects and may be related to the presences of compound crystals. Therefore, sintering is likely to occur in fats that contain a broad triacylglycerol composition (Kloek 1998; Johansson 1994). However, Johansson (1994) demonstrated that sintering can only proceed when the outer part of the crystals and the bridging material have the same polymorphic structure.

Kloek (1998), amongst others, demonstrated that the bonds constructing fat crystal networks can be split up in to primary bonds (crystal bridges) and secondary bonds (van der Waals forces). During mechanical treatment these primary bonds can be destroyed,resulting in softening of the fat. Firmness can subsequently increase again due to the reorganization of the fat crystals into a network stabilized by the weak van der Waals forces. In addition, slow (re-)crystallization leads to the formation of new primary bonds (Kloek 1998; Walstra et al. 2001).

1.3.2 Factors influencing the microstructure

The microstructural level has an enormous influence on the macroscopic properties of fat products as it is the closest level of structure to the macroscopic world. The nature of the fat crystal network, including its spatial distribution, and the number, size and shape of the constituting microstructural elements can be dramatically altered by changes in the crystallization conditions. The properties of a fat crystal network, and thus of the macroscopic properties of the final product, are easily changed with processing conditions. These processing conditions include the cooling rate, crystallization temperature, agitation speed and storage time (Heertje et al. 1988; Heertje et al. 1988; Shukla and Rizvi 1988; Litwinenko et al. 2002).

1.3.2.1 Crystallization temperature

The crystallization temperature has a pronounced effect on the crystal formation and thus also on the network development. At higher temperatures, and thus lower supercooling, fewer nuclei are formed and crystal growth is favored, resulting in fewer, larger crystals. On the other hand, lower temperatures (higher supercooling) numerous small crystals are formed as nucleation is favored over crystal growth (Herrera and Hartel 2000a; Wright and Marangoni 2003).

1.3.2.2 Cooling rate

As cooling rate increases, the driving force for crystallization is higher. Hence, crystallization will take place in a shorter period of time. Consequently, nucleation and crystal growth mechanisms are affected (Campos et al. 2002). The cooling rate affects which triacylglycerol molecules are incorporated in the crystal lattice, thus giving rise to distinct physical properties (Herrera and Hartel 2000a). As the system is crystallized rapidly, higher melting triacylglycerols will be rapidly supercooled and initially crystallized, developing a solid within the liquid phase (Toro-Vazquez et al. 2001). Moreover, different polymorphs can be formed during cooling, depending on the cooling rate.

Litwinenko et al. (2002) observed two distinct crystal morphologies when cooling a palm based shortening at different cooling rates. Slow cooling resulted in sperulitic crystals, while at fast cooling a larger amount of smaller needle like crystals was obtained. This difference in morphology could be attributed to the polymorphic form in which the sample crystallized upon reaching the final temperature, respectively β' at slow cooling and α at fast cooling. In addition, faster cooling rates resulted in more uniform morphologies, in contrast to slow cooling rates where two major crystal morphologies were observed (Litwinenko et al. 2002). Herrera and Hartel (2000a) and Campos et al. (2002) studied the effect of cooling rate on the microstructure of a milk fat model system and anhydrous milk fat and lard, respectively. Both studies reached the same conclusions as Litwineko et al. (2002) considering the crystal size. In addition, deMan (1964) reported that a slower crystallization process leads to a decrease in solid fat content and hardness, as well as the aggregation of small crystalline particles into larger ones. This was also observed by Campos et al. (2002). In contrast, Herrera and Hartel (2000a) measured the same solid

fat content for slow and fast crystallized samples, with fast cooled samples having less dens crystal structures and more defined solid and liquid zones. These inconsistent results illustrate that several factors play a role in determining the microstructure and that it is not an easy task to single out one specific factor.

1.3.2.3 Agitation

In industrial applications, crystallization of the fat blend usually takes place under shear since agitation speeds up the heat transfer and assists in producing a homogeneous product. Several products require proper mixing to obtain the desired product qualities. Examples are chocolate, where mixing and tempering is necessary to obtain the correct polymorphic form, and margarines and shortenings where agitation as well as other processing conditions are known to affect the consistency of the final product. Knowledge on the effect of shear rates on fat crystal structures formed under shear is still very limited. However, the last decade has seen an increase in publications considering this topic.

In 1985, Ziegleder (1985) acclaimed the accelerating effect of shearing on the crystallization of cocoa butter in form V, the desired polymorph in chocolate manufacturing. The results were later visualized by MacMillan et al. (2002), who studied the effect of shear on cocoa butter crystallization with time-resolved synchrotron XRD. Using the same technique, Mazzanti et al. (2004b) reported on the formation of a new crystalline phase in cocoa butter when applying low shear rates, which has not been observed under static conditions. Orientation of crystals and accelerated phase transitions induced by shear rates were demonstrated for cocoa butter, milk fat and palm oil using time-resolved synchrotron XRD (Mazzanti et al. 2004b). It was concluded that shear induces the crystallites formed from the melt and accelerates solid-phase transformations. These insights were used in a later study to model the phase transitions of palm oil during crystallization under shear (Mazzanti et al. 2005). Garbolino et al. (2000) designed a novel rheometer with incorporated ultrasonic sensors to study the effect of shear on the crystallization of a confectionery coating fat. Sonwai and Mackley (2006) combined small deformation rheology with time-resolved XRD en polarized light microscopy to investigate the effect of a shear step, varying in shear rate and duration, as well as continuous shear on cocoa butter crystallization. Both studies led to the conclusion that shear enhances the crystallization process.

Shear does not only affect the crystallization rate, but also has an effect on the crystal size. Herrera et al. (2000a) demonstrated that crystallization under high shear rates produce small crystals and a narrow particle size distribution. At low agitation, agglomeration can take place, whereas at high shear rates, smaller crystals are formed due to enhanced nucleation and breakdown of crystals and crystal aggregates by the shear forces of the impeller (Walstra et al. 2001). In addition, applying shear to dispersions of fat crystal aggregates leads to compaction of these aggregates (Kloek 1998).

1.3.2.4 Storage time

In semi-solid foods such as margarines and shortenings, several crystallization processes can take place during the storage period following production. These post-crystallization processes include (Johansson 1995; Kloek 1998): nucleation of new crystals followed by crystal growth, Ostwald ripening (which is defined as the dissolution of small crystals and growth of the bigger ones), polymorphic transformations, oil migration or migration of small crystals and sintering. In some cases, post-crystallization processes are desirable to produce a harder consistency in low-fat products. However, in most cases these processes lead to unwanted product properties. For instance, polymorphic transition from β' to β leads to grainy structures in margarine (deMan et al. 1989). Ostwald ripening can cause loss of consistency as larger crystals form a looser network structure. Sintering on the other hand will result in a firmer network structure as narrow gaps between fat crystals are filled by the formation of solid bridges.

Palm oil is frequently used in the production of margarines and shortenings (deMan 1998; Nor Aini and Miskandar 2000). However, the slow crystallization behavior as well as the post-hardening effects during storage are of major concern to the industry. Zaliha et al. (2005) demonstrated that during storage the crystal networks of hydrogenated palm oil and palm oil blends became more highly structured, resulting in an increase in hardness as measured by penetrometry. Kloek (1998) showed that a fat blend crystallized completely under shear obtained its final consistency after a few days, while the fat blend which had only partially crystallized under shear obtained its final consistency within a few hours. A fat blend completely crystallized under shear consists of a dispersion of aggregates that attract each other by Van der Waals forces. Slow recrystallization processes cause these

aggregates to sinter, leading to a slow increase in firmness.

1.4 Mechanical and macroscopic properties

The mechanical and macroscopic properties of the crystalline network structure are influenced by all levels of structure (individual triacylglycerols, crystalline units, agglomerates, microstructural network) defined during the formation of the network and each step in this structural hierarchy is influenced by both chemical composition and processing conditions (Narine and Marangoni 1999e; Narine and Marangoni 2005). Figure 1.9 depicts the structural hierarchy defined during the crystallization of a typical fat crystal network, the factors affecting it as well as some indicators commonly used to quantify the relationship between structure and macroscopic properties. The hardness of a fat, for instance, depends on the amount of fat crystals, among other factors, and lipid composition affects the molecular arrangement in crystals, which will in turn influence the strength of the interactions between the crystals (Juriaanse and Heertje 1988). However, differences in the crystalline structural characteristics can also be strongly influenced by the interactions between the crystals and the liquid oil in which they are dispersed, resulting in different crystalline structural characteristics at different structural levels (Shi et al. 2005).

1.4.1 Small and large deformations

Information about the network structure and the interaction forces between structural elements are obtained by small deformation experiments. Small-scale deformation behavior, which is mostly measured by oscillatory experiments, evaluates the network in terms of moduli (see also Section 1.5.5) which are a measurement of the stiffness (not the strength) of the system (Kloek 1998; Walstra et al. 2001). These rheological properties of fat crystal networks are largely determined by the fraction of crystallized material, the solid fat content (SFC). However, predicting the final hardness of a product based on SFC only has been shown to be unreliable (Narine and Humphrey 2004), indicating the importance of additional parameters such as the interactions between the crystals and the geometric arrangement of crystals and aggregates in the network structure (Kloek 1998; Marangoni 2000).

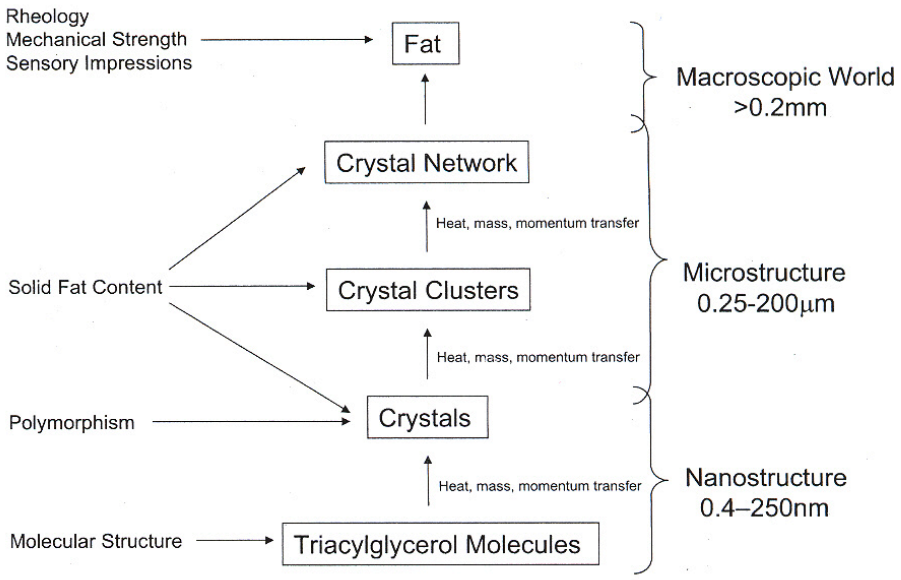

Figure 1.9: Schematic representation of the structural hierarchy defined the formation of a fat crystal network (Narine 2005)

The importance of large deformation (non-linear) behavior in food rheology should not be overlooked. Many processes, such as mastication and swallowing are only accomplished with very large deformations (Steffe 1996). Large deformation experiments yield information about important quality characteristics which are relevant to processing, handling and eating. For instance, when spreading margarine, the crystallized network is subjected to large deformations at high velocity gradients. Rearrangement of the crystal network will occur due to fracture of sintered bonds at certain length scales, which results in a softer product. This phenomena is called work softening and can be seen as a decrease of the elastic modulus (Kloek 1998; Walstra et al. 2001).

A major criticism of these large scale deformations is that it is difficult to correlate the measured parameters with fundamental properties of the material (Shellhammer et al. 1997; Kloek 1998). Large-scale deformation experiments can be done in various deformation modes, which tend to lead to different results. In addition, the results can be affected by several factors such as sample deformation during transfer into the measuring body or inhomogeneous deformation during the experiment (Walstra et al. 2001).

1.4.2 Mechanical network models

It has been stated above that the macroscopic properties are strongly influenced by the underlying fat crystal network. Several mathematical formulations have been developed in an attempt to describe the relationship between network structure and elastic properties (Marangoni 2000). Most of these equations can be written as the product of three factors: a numerical factor characteristic for the geometry of the network, a function due to the interaction forces involved and a function of the volume fraction of building blocks Φ.

1.4.2.1 Linear model

In 1961, van den Tempel was the first to propose a model to relate the rheological properties of fats to their microstructure. The linear chain model (van den Tempel 1961) suggests that the network structure of plastic fats is constructed of straight chains oriented in three dimensions, each direction perpendicular to the other. Each chain then consists of a linear array of particles held together by two types of bonds: irreversible primary bonds and reversible secondary bonds. The primary bonds are stronger than the secondary bonds and may consist of relatively strong van der Waals forces. Their contribution to the stiffness of the network is much higher than that of the secondary bonds. Furthermore, they do not reform easily upon disruption (Deman and Beers 1987).

The linear chain model predicts the shear modulus G to be proportional to the volume fraction of solids Φ and to the particle diameter a:

$$G = \frac{5A\Phi a^{0.5}}{24\pi H_0^{3.5}} \tag{1.14}$$

with A the Hamaker's constant and H_0 the inter particle distance. This model was developed for particles with a geometry between spheres and cubes. However, experimental

results have shown that the shear modulus does not vary linearly with the volume fraction solids as suggested by the linear model. This discrepancy is related to the assumption of straight chains, while in reality, the network is built from aggregates of fat particles (Vreeker et al. 1992; Kloek 1998; Tang and Marangoni 2006). van den Tempel (1961) also realized the need of an intermediate structure level and thus proposed an extended linear chain model in which the chains are constructed of crystal aggregates in stead of solid spherical fat particles (primary crystals). A correction factor was introduced and the shear modulus was recalculated as:

$$G = \frac{nd_a}{Na_a} \times G_{theory} \tag{1.15}$$

with G the corrected shear modulus, G_{theory} the shear modulus calculated from the linear chain model, n the number of connecting chains between two neighboring aggregates, N the average number of primary particles in an aggregate, d_a the average diameter of an aggregate and a_a the average primary particle diameter (Tang and Marangoni 2006). Although the extended model fitted the experimental results better then the original model, it has been not widely used due to the fact that the correction factor is almost impossible to calculate (Tang and Marangoni 2006).

1.4.2.2 Fractal models

Fractal geometry was introduced by Mandelbrot (1965) to quantify natural objects with a complex geometrical structure that could not be quantified by regular geometrical methods, i.e. Euclidean geometry. In Euclidean geometry, objects are characterized by integer dimensions (D): a line has D=1, a plane D=2 and a volume D=3. When enough kinks are placed in a line or a plane, the final structure will be between a line and a plane or between a plane and a cube, thus resulting in a fractal object: in stead of an Euclidean integer dimension it has a fractal non-integer dimension (Figure 1.10) (Narine and Marangoni 1999e; Marangoni 2002b).

Shih et al. (1990) developed a scaling theory for the flocculation of colloidal gels and identified two regimes, depending on the relative strength of the links between the clusters of a colloidal gel and the strength of the clusters themselves. In the **strong link regime**, the individual flocs or clusters grow large and each cluster acts as a weak spring. Consequently, the system is dominated by the elastic constant of the flocs an not of the

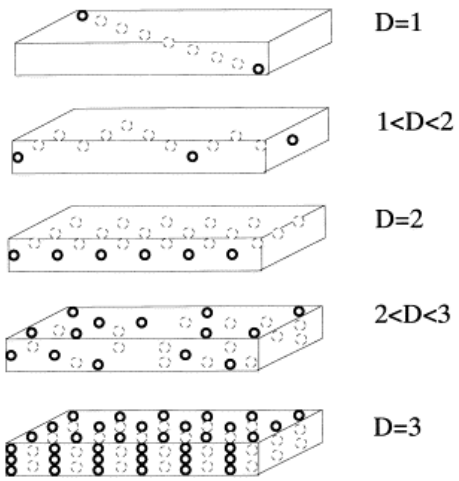

Figure 1.10: Spatial particle distribution and the corresponding dimension (Marangoni 2002)

elastic constant between the flocs. Shih et al. (1990) expressed the system as a function of the particle concentration Φ as follows:

$$K \propto \Phi^{((d+x)/(d-D)} \tag{1.16}$$

with K the elastic constant [N/m], d the euclidean dimension, x the chemical length exponent, and D the fractal dimension of the flocs. The chemical length exponent or 'back bone' fractal dimension x correspond to the spatial distribution of the microstructural elements, the tortuosity of the network. Usually it has a value below the fractal dimension of the system, but larger than 1 to provide a connected path (Narine and Marangoni 1999b).

The strong link regime is observed at low particle concentrations, while at high particle concentrations the microstructure can be described by the **weak link regime**. In the weak link regime, interfloc links are weak compared to the flocs and can be considered as small rigid springs. The elastic constant of the system will thus be dominated by the elastic constant of the interfloc links (Shih et al. 1990; Awad et al. 2004):

$$K \propto \Phi^{((d-2)/(d-D)} \tag{1.17}$$

Vreeker et al. (Vreeker et al. 1992) proposed that a network of tristearin crystals in paraffin oil resembled a colloidal gel. They suggested that fat networks had a fractal nature and demonstrated that the storage modulus G' of an aggregated fat network changed

with the particle concentration Φ according to a power law, similar to flocculated gel. Consequently, Marangoni and Rousseau (1996) applied the scaling theory of Shih et al. (1990) to fats at high Φ, thereby assuming the weak link regime. Various studies in the microstructure and rheological properties of a fat network have shown that the interfloc links of the network carry most of the stress loaded onto the system, whereby both the limit of linearity and the elastic constant increase with increasing particle concentration (Heertje 1993; Marangoni and Rousseau 1996; Narine and Marangoni 1999b; Marangoni 2000; Marangoni 2002b).

1.5 Experimental techniques to study fat crystallization

Several studies have reported on the isothermal and non-isothermal crystallization behavior of palm oil and palm oil fractions, using a variety of experimental techniques such as *Differential Scanning Calorimetry* (DSC) (Busfield and Proschogo 1990; Siew and Ng 1995b; Che Man et al. 1999; Siew and Ng 2000; Tan and Man 2002), *pulsed Nuclear Magnetic resonance* (pNMR), *X-ray Diffraction analysis* (XRD) (Mazzanti et al. 2003; Mazzanti et al. 2005), *polarized light microscopy* (PLM) to name a few. Often combinations of techniques are applied to gain more insight in the crystallization process. Numerous authors combined DSC and XRD to study the crystallization and polymorphism of palm oil and related products (Deroanne et al. 1977; Chong et al. 2007; Braipson-Danthine and Gibon 2007). Kawamura(1979, 1980), Che Man and Swe (1995) and Ng (1990) combined PLM and DSC. Jacobsberg and Oh (1976) also used pNMR next to XRD and DSC, while Zaliha et al. (2004) preferred PLM to complement their data obtained with DSC and pNMR. In addition to the widely used DSC and pNMR technique, Chen et al. (2002) monitored the viscosity during the crystallization of palm oil, while Toro-Vazquez et al. (2000) relied on the combination of DSC and diffusive light scattering.

1.5.1 Differential Scanning Calorimetry (DSC)

Differential scanning calorimetry (DSC) is a thermo-analytical technique to monitor changes in physical or chemical properties of materials as a function of temperature by detecting the heat changes associated with such processes. The measuring principle is to compare

the rate of heat flow to the sample and a reference material, usually air, which are subjected to a controlled time-temperature program. Any change in the evolution of heat causes a change in the differential heat flow, which is then recorded as a peak. The area under the peak is directly proportional to the enthalpy change and its direction indicates the nature of the event: endothermic in the case of melting and exothermic in the case of crystallization (Biliaderis 1983).

In an isothermal DSC experiment, the sample is first melted completely and subsequently cooled rapidly to the crystallization temperature. The exothermal heat flow induced by the crystallization process is then measured as a function of isothermal time. The relative amount of material crystallized as a function of time can be obtained by integrating the isothermal DSC-curves. The area enclosed by a baseline and the exothermal peak corresponds to the heat of crystallization, ΔH [J g^{-1}]. The relative amount of crystallized material F [-] at a given time t [any time unit] is approximated by the ratio of the integration of the exothermal peak to the total area in accordance with 1.18 (Kawamura 1979):

$$F = \frac{\int_{t=0}^{t} \frac{d\Delta H(t)}{dt} dt}{\Delta H} \tag{1.18}$$

The advantages and disadvantages of DSC can be summarized as follows (Ziegleder 1990):

- Advantages:
  - the ability to strictly control temperature;
  - the small sample size which makes the presence of foreign nuclei so seldom that they hardly influence the crystallization;
  - the ability to measure free from mechanical effects.
- Disadvantages:
  - the rather low sensitivity;
  - the calculation necessary to obtain F

In general, oils and fats can exhibit extremely complex thermal behavior, which will be highly dependent on the chemical composition and the time-temperature protocol applied in the DSC experiment (Tan and Che Man 2000).

1.5.2 Pulsed Nuclear Magnetic Resonance (pNMR)

In a pulsed nuclear magnetic resonance the sample is placed in a magnetic field and subjected to a short (5 μs) radio frequency pulse, thus exiting the protons. Once the pulse has ended, the exited protons will relax and this decaying signal (FID= free induction decay) is registered by the receiver coil, wound around the sample. The decay rate is largely influenced by the phase of the protons: protons in the liquid phase decay in about 1 ms, while protons in the solid phase decay in a few tens of μs. Classically, two different methods are used to determine the solid fat content. In the direct method, the solid/liquid ratio is determined by measuring the signal amplitude at two different moments in time: immediately after and about 70 to 150 ms after the end of the pulse (Brosio et al. 1980). The indirect method uses only one measuring point after approximately 70 μs where it can be assumed that all magnetization of solid components has relaxed (Trezza et al. 2006). The direct method has become the most widespread method because of its ease of use and its high precision (Trezza et al. 2006). The pNMR technique is quite insensitive to detect nucleation. At times, small amounts of crystals are visible in the melt before any solids are detected. At this stage, well beyond the induction time for nucleation, pNMR is measuring crystal growth (Wright et al. 2000).

Since the introduction of these NMR methods in the 70s, the electronic and computational specifications of commercial bench top NMR equipment have improved dramatically. The direct and indirect method do not fully exploit this as they are based on a rather crude acquisition and data treatment of the FID (Trezza et al. 2006). However, recent studies have shown that detailed phase-compositional information on complex food systems can be obtained via NMR. Detailed analysis of the NMR decay curves has been used to assess semi-solid behavior of lipids (LeBotlan and Heliefourel 1995; LeBotlan and Ouguerram 1997) and lipid crystallization in complex food systems (Lucas et al. 2005; Mariette and Lucas 2005). In addition, a NMR based method has been developed to assess lipid polymorphism in a quantitative manner (Trezza et al. 2006).

1.5.3 X-ray diffraction

The X-ray region is that portion of the electromagnetic spectrum which is situated between ultraviolet and gamma radiation. X-rays are electromagnetic radiation with typical photon

energies in the range of 100 eV - 100 keV. Only short X-rays are used in diffraction applications. Their wavelength is comparable to the size of atoms, making them ideally suited for probing the structural arrangement of atoms and molecules in a wide range of materials (Materials Research Laboratory 2008). For single crystals, X-ray diffraction analysis allows for the determination of the atomic positions in the unit cell with high precision, from which in turn the molecular conformation can be derived. Most of the information obtained by X-ray diffraction on triacylglycerol crystals is, however, based on the study of polycrystalline materials using X-ray powder diffraction (Kellens 1991).

Diffraction analysis is based on Bragg's Law which describes the relationship between the incident angel θ [°] and the distance between the reflecting entities d [Å], depending on the wavelength λ [Å].

$$d = \frac{1}{s} = \frac{n\lambda}{2sin\theta} \tag{1.19}$$

with n the order of diffraction.

Equation 1.19 also shows that small distances scatter at large angles. Consequently, small angle X-ray scattering (SAXS) and wide angle X-ray diffraction (WAXD) can be differentiated, depending on the detection angle relative to the incoming beam (see also Section 1.2.4). Historically, SAXS curves are plotted as a function of the reciprocal distance s [$Å^{-1}$], while WAXD intensities are presented as a function of 2θ (Goderis and Reynaers 2002).

X-rays can be generated by either X-ray tubes or by synchrotron radiation. In an X-ray tube, which is the primary X-ray source in laboratory applications, X-rays are generated when a focused electron beam accelerated across a high voltage field bombards a stationary or rotating solid target (Materials Research Laboratory 2008). In fat crystallization, laboratory X-ray instruments are often not sufficient to obtain valuable information as events such as polymorphic transformation often take place at a shorter time scale as the time needed to record one diffraction pattern. However, this disadvantage is overcome by synchrotron radiation.

In recent years synchrotron facilities have become widely used as preferred sources for X-ray diffraction measurements. Synchrotron radiation is emitted by electrons or positrons

traveling at near light speed and are obliged to change direction. These powerful sources, which are thousands to millions of times more intense than laboratory X-ray tubes, allow the exposure time to be reduced to a few seconds or even less (Materials Research Laboratory 2008; Goderis and Reynaers 2002). Consequently, by using synchrotron radiation crystallization experiments can be monitored in 'real time'.

1.5.4 Microscopy

The microstructure of fats and fat containing products largely influences the sensorial properties such as texture, mouth feel and spreadability. Knowledge of this microstructure is essential to predict ad control the behavior of food materials during processing. Several imaging techniques can be applied to gain more insight in the microstructural organization.

1.5.4.1 Light Microscopy

Light microscopy (LM) is a widely used microscopic technique in food research. Light microscopy can operate in several modes, namely bright field, polarized and fluorescence microscopy. In conventional bright field microscopy, the light beam is transmitted sequentially trough a condenser, the specimen and the objective, which serves as the first magnification lens. From the objective, the light beam continues to an ocular lens which also magnifies the image before it finally reaches the eye. When studying non-highly colored samples the addition of specific dyes or stains can be necessary to introduce some contrast (Kalab et al. 1995). Although the resolution of LM is rather limited ($\geq$0.2μm), the attainable magnifications allow the study of many food products as long as thin samples can be prepared (Autio and Salmenkallio-Marttila 2001). However, it must be kept in mind that by preparing such thin samples the microstructure of the sample may be destroyed by the shear or compression forces applied (Blonk and van Aalst 1993; Kalab et al. 1995).

A bright field microscope can easily be transformed into a polarization microscope by inserting two polarizers in the light path. The first polarizer is inserted between the light source and the sample, thus producing light that vibrates only in one plane, perpendicular to the direction of the incident light. The second polarizer (the analyzer) is then placed between the sample and the objective and the viewer (Kalab et al. 1995). Polarized light

microscopy used the difference in refractive index of a beam of incident light polarized in two perpendicular directions (crossed polarizers). As a result, amorphous regions in the samples will appear black, whereas birefringent crystalline regions will light up against a dark background (Wright et al. 2000).

1.5.4.2 Fluorescent microscopy

In fluorescent microscopy, light of a specific wavelength is absorbed by specific molecules that are present in the sample and the energy is re-emitted as light of a longer wavelength and lower intensity (Kalab et al. 1995). Fluorescence measurements are rapid, accurate and require only very small quantities of sample. In general, fluorescence experiments are relatively easy to perform (Strasburger and Ludescher 1995). Structures of interest can be visualized by labeling with specific fluorescent probes. However, the number of fluorophores with an absorption wavelength close to the emission wavelength of the available lasers (as a rule of thumb acceptable difference taken $\pm$ 20nm) is quite limited (Ferrando and Spiess 2000). Like in light microscopy, imaging with fluorescent microscopy is limited to thin samples. Obtaining sharp images along the viewing axis of the sample is extremely difficult as secondary fluorescence, not belonging to the region of interest, can interfere with the visualization of the structures that are in focus. Tedious an possibly harmful preparation techniques thus remain necessary (Blonk and van Aalst 1993; Kalab et al. 1995).

1.5.4.3 Confocal scanning laser microscopy

The restriction to thin samples was overcome by the development of confocal laser scanning microscopy (CSLM). The main difference with a conventional microscope is that out-of-focus light is eliminated by a pinhole in front of the detector. This pinhole ensures that only light emitted by the in-focus region is transmitted to the detector, thus producing sharper images and allowing optical sectioning of thick samples (Blonk and van Aalst 1993; Vodovotz et al. 1996; Durrenberger et al. 2001). .

1.5.4.4 Electron microscopy

Although image formation in electron microscopy (EM) is similar to that in light microscopy (LM), EM achieves a significantly higher resolution. The main difference is situated in the illumination source: in EM electrons are focused with magnetic lenses whereas

in LM photons are focused by glass lenses. As electrons are absorbed by air, the sample should be placed in a vacuum chamber. Consequently, additional sample preparation is necessary to avoid release of volatile substances from the sample (Kalab et al. 1995).

Electron microscopy exists in two complementary modes: scanning electron microscopy (SEM) and transmission electron microscopy (TEM). SEM is used to examine surfaces while TEM can be used to visualize the internal structure of food samples. These methods mainly differ in the method of image formation (Kalab et al. 1995; Ferrando and Spiess 2000). TEM visualizes electrons passing through thin sample layers embedded in epoxy resin or platinum-carbon replicas of the sample. The passing electrons attenuate due to interaction with the sample, with the degree of attenuation resulting in the formation of an image, which is observed on a fluorescent screen or photographed on film (Kalab et al. 1995). SEM on the other hand uses electrons reflecting back from the sample to construct its image. The necessary absence of volatiles to preserve the vacuum of the SEM instrument requires that samples are either dried or frozen (cryo-SEM) before being placed in the microscope (Roman-Gutierrez et al. 2002). Non-conductive samples require a thin (5-20nm) metal (gold) coating to provide electric conductivity, necessary to prevent charge effects that would distort the electric fields in the electron microscope (Depypere 2005). SEM images display a great depth of focus and are easy to interpret (Kalab et al. 1995).

In addition to conventional SEM, environmental scanning electron microscopy (ESEM) has been developed. In contrast to SEM, ESEM does not require to work under vacuum or the coating of the samples with a conductive layer and allows for the visualization of dry, moist or oily samples in a gaseous atmosphere. The presence of water vapor in the ESEM sample chamber allows for the observation of dynamic changes of microstructure during hydration or dehydration (Roman-Gutierrez et al. 2002).

1.5.5 Rheology

Rheology is defined as the science of flow and deformation and describes how a material responds to applied stress or strain (Steffe 1996). Fundamental rheological properties of food products and many other materials are frequently determined by means of a rotational rheometry, which involves the shearing of the test material between rotating cylinders,

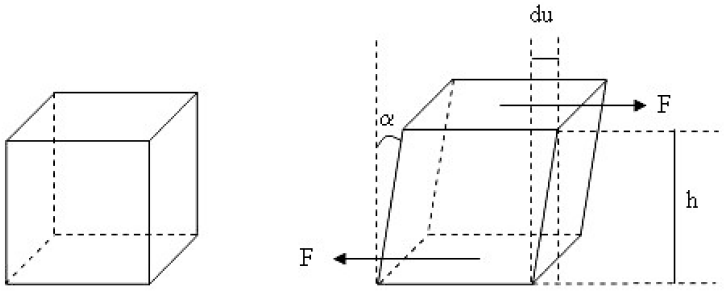

Figure 1.11: Deformation caused by shear force

cones or plates (Whorlow 1992). In comparison with other types of rheological equipment, rotational rheometers offer the advantage that the sample can be sheared for as long as desired, allowing the study of time-dependence, and that at the appropriate conditions the entire sample can be subjected to a uniform shear rate. The deformation that takes place upon subjecting a material to shear force is presented in Figure 1.11.

When shear stress (σ [Pa]) is applied to a solid, it will deform to a certain extent. Based on Figure 1.11 this deformation or strain (γ) can be expressed as:

$$\gamma = \frac{du}{h} = tg\alpha \tag{1.20}$$

For an ideal solid the resulting strain is proportional to the applied shear stress as is expressed by Hooke's law:

$$\sigma = G \times \gamma \tag{1.21}$$

where G is the shear modulus or modulus of rigidity [Pa]. Upon removal of the applied stress, the deformation will also disappear and the material will assume its initial shape and size, thus characterizing 'elastic' behavior. An ideal elastic solid is also called a Hookean solid.

An ideal fluid subjected to shear stress will continue to deform as long as the stress is applied. Upon removal of the stress, the material will not recover from its deformation (Gunasekaran and Ak 2000). This type of response is called 'viscous' and can be described by Newton's law, which constitutes a direct proportionality between the rate of deformation or shear rate ($\dot{\gamma} = d\gamma/dt$ [s^{-1}]):

$$\sigma = \eta \times \dot{\gamma} \tag{1.22}$$

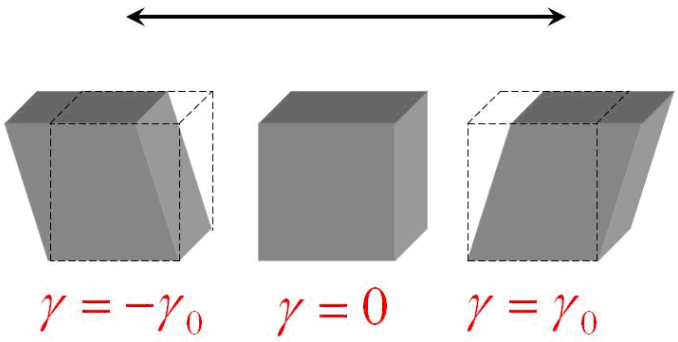

Figure 1.12: Material deformation during oscillatory test

where η is the viscosity [Pa.s]. An ideal viscous liquid is also called a Newtonian liquid.

The two above discussed types of deformation behavior are the two extremes: purely elastic and purely viscous. However, fat containing products usually display viscoelastic behavior as a result of the crystal network formed within these systems, indicating that their rheological behavior is intermediate between the two extremes. When such a material is subjected to shear stress, part of the deformation will be permanent upon removal of the stress due to viscous flow while the other part of the deformation will be reversible due to elasticity (Gunasekaran and Ak 2000; Rha 1979).

Dynamic or oscillatory tests are widely used for studying the viscoelastic behavior of food. In this type of test procedures the sample is subjected to small amplitude sinusoidal strains and the resulting stress is recorded (Figure 1.12).The results are very sensitive to chemical composition and physical structure what makes them very useful in a wide range of applications (Steffe 1996).

Two types of instruments exist to perform dynamic experiments. In a controlled rate rheometer the strain is fixed and the resulting stress is measured. Inversely, a controlled stress rheometer fixes the stress and records the resulting strain. In a controlled rate device the applied strain can be written as

$$\gamma = \gamma_0 \ sin(\omega t) \tag{1.23}$$

with γ_0 the maximum deformation or deformation amplitude and ω [rad s^{-1}] the oscillatory

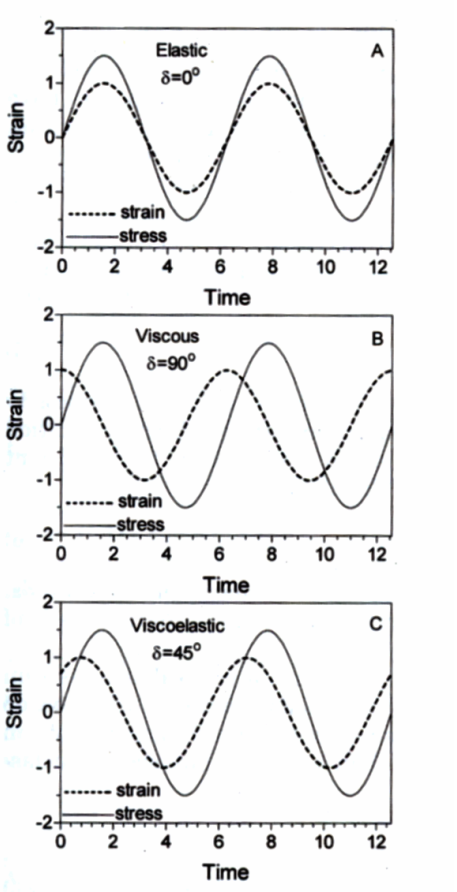

Figure 1.13: Dynamic response of an elastic, viscous, and viscoelastic material to oscillatory shear (Marangoni 2005)

frequency. Consequently, the deformation is given by

$$\dot{\gamma} = \frac{d\gamma}{dt} = \gamma_0 \omega \ cos(\omega t) \tag{1.24}$$

The resulting stress σ [Pa] is expressed as

$$\sigma = \sigma_0 \ sin(\omega t + \delta) \tag{1.25}$$

with σ_0 being the maximum stress or stress amplitude and δ [°] the phase shift, also called phase angle, relative to the applied strain. In an ideal solid, the stress will be in phase with the strain (δ=0) as all the energy is stored. For an ideal viscous material on the other hand, the stress will always be 90° out of phase as all energy is dissipated (Whorlow 1992; Marangoni 2005). A viscoelastic material will have a phase angle between 0° and

90°, depending on the relative elastic and viscous component of the material (Figure 1.13).

By applying trigonometry on equation 1.25 the resulting stress σ can be written as the sum of two components

$$\sigma = \sigma_0 \; cos\delta \; sin(\omega t) + \sigma_0 \; sin\delta \; cos(\omega t) \tag{1.26}$$

with the first being in phase and the second 90° out of phase with the applied strain.

Based on equation 1.26 two parameters can now be defined, namely G' and G''. G' [Pa] is denoted as the elastic, storage or in-phase modulus and is a measure of the energy that is stored and recovered per oscillation cycle The elastic modulus is defined as the in-phase stress divided by the strain:

$$G' = \frac{\sigma_0}{\gamma_0} \times cos\delta \tag{1.27}$$

The loss or viscous modulus G'' [Pa] is an estimate of the energy that is dissipated as heat per oscillation cycle and is defined as the out-phase stress divided by the strain:

$$G" = \frac{\sigma_0}{\gamma_0} \times sin\delta \tag{1.28}$$

Taking into account equation 1.27 and equation 1.28 the stress function (equation 1.26) can be re-written as:

$$\sigma = \gamma_0 \; (G' \; sin(\omega t) + G" \; cos(\omega t)) \tag{1.29}$$

The ratio of the loss and storage moduli is equal to the tangent of the phase angle, also referred to as the loss tangent:

$$tg\delta = \frac{G"}{G'} \tag{1.30}$$

Finally, the complex modulus G^* combines the in and out of phase component and can be written as:

$$G^* = G' + iG" \tag{1.31}$$

The modulus of the complex modulus $|G^*|$[Pa], which is regarded as a measure of the consistency of a material, is defined as the ratio of the stress amplitude to the strain amplitude:

$$|G^*| = \frac{\sigma_0}{\gamma_0} = \sqrt{(G')^2 + (G")^2} \tag{1.32}$$

Dynamic tests can be performed in several modes. In an **amplitude sweep** the frequency is kept constant and the sample is subjected to increasing stress or strain. This type of test is used to determine the linear viscoelastic region (LVR) in which stress and strain are linearly proportional to each other. Consequently, rheological variables are not stress or strain dependent within the LVR (Steffe 1996; Marangoni 2005). In addition to determining the limits of the LVR, amplitude sweeps are also used to differentiate between strong and weak gels as strong gels may have a larger LVR than weak gels (Steffe 1996).

The **frequency sweep** is a very popular mode of oscillatory testing because it shows how the viscous and elastic behavior of a material changes with the rate of application of stress or strain (Steffe 1996). In this test the frequency is increased while the amplitude of the input signal (stress or strain) is kept constant (Steffe 1996; Marangoni 2005). Frequency sweeps can be useful in comparing different food products or in comparing the effect of different ingredients or processing conditions (Steffe 1996). By varying the frequency of the oscillatory input it is possible to probe the numerous elements contributing to the structure, as the relaxation behavior of each interaction is different (Marangoni 2005).

To monitor time and temperature dependent changes such as crystallization, **time-temperature sweeps** can be performed. Here, frequency and amplitude are constant over time. It is of paramount importance that the applied stress or strain is chosen within the LVR to avoid structure breakdown of the material.

Chapter 2

Palm Oil

If more of us valued food and cheer and song above hoarded gold, it would be a merrier world.

Lord of the rings - J.R.R. Tolkien (1892-1973)

2.1 Introduction

Palm oil is one of the most important vegetable oils in the world. Due to the rapid increase of the palm oil production, palm oil has overtaken soy bean oil as the world 's leading vegetable oil and accounts now for almost 30% of the global vegetable oil output. In terms of its share in vegetable oil exports, palm oil is even more significant as it accounts for almost 60% of the global export (Carter et al. 2007). The success and expanding production of palm oil can be attributed to several factors. Palm oil has a high productivity of 4.5-5 tons per hectare and is economical to produce, providing a sustainable basis for its relatively low price. Due to its broad chemical composition and suitability for fractionation, palm oil and its fractions can be used in a wide range of applications. Moreover, palm oil has a high oxidative stability at elevated temperatures due to the presence of natural antioxidants and moderate content of polyunsaturated fatty acids, making it very suitable for frying applications (Berger 2001). In addition, manufacturers are confronted with increased pressure to ban trans fatty acids from food due to their negative health implications. To replace partially hydrogenated fats, the major source of trans fatty acids, they have to turn to alternatives such as palm oil and palm oil fractions. However, the prerogative is that these alternatives provide the same product functionality and structure as the original product containing the undesired trans fatty acids.

2.2 Extraction

Although the oil palm (*Elaeis guineensis*) originated from East Africa, it is nowadays also found in the tropical regions of Asia, Africa and the Americas, and is cultivated most extensively in Malaysia and Indonesia. Palm trees bear fruit in the third year after planting and continue producing for about 25 years. Fruit bunches of about 4 to 20 kg contain 200 to 2000 individual fruits and are harvested throughout the year (Gunstone and Harwood 2007; Fils 2000). Two types of oil can be obtained from the fruit of the oil palm: orange-red crude palm oil from the mesocarp and brownish-yellow crude palm kernel oil from the seeds. The crude palm oil (CPO) consists of mainly palmitic and oleic acids whereas the palm kernel oil is rich in lauric acid (Gee 2007).

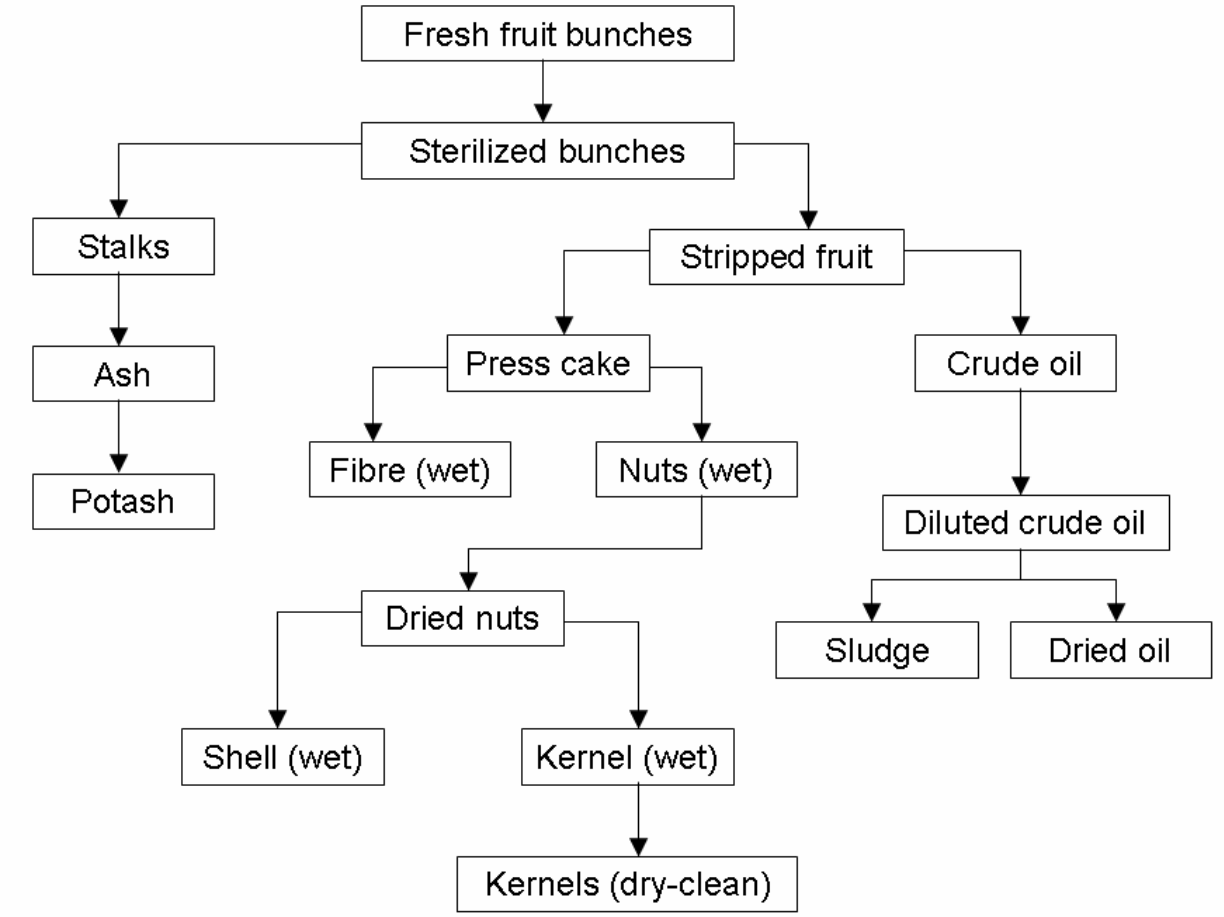

Figure 2.1: Processing of fresh fruit bunches (Fils 2000)

Palm oil processing does not start when the fresh fruit bunches reach the mill, but at the plantation itself. When harvesting the fruit bunches of the oil palm, it is of utmost importance that fresh fruit bunches are handled with great care as they may otherwise suffer from rapid deterioration. Upon harvesting, the level of free fatty acids (FFA) in unbruised fruit is low, generally 0-0.3% (Fils 2000). In bruised or over-ripe fruits the FFA level will be much higher due to a very active lipase (Fils 2000; Gibon et al. 2007).

The extraction of palm oil and palm kernel oil from the fresh fruit bunches requires several steps, as indicated in Fig. 2.1. Firstly, the fresh fruit bunches are sterilized. **Sterilization** stops the development of the lipolytic enzymes in the fruit bunches, eases the mechanical stripping and prepares the kernels for further processing. Furthermore, it prepares the nuts which will later on minimize the kernel breakage during the pressing and

nut cracking. Normally, sterilizing is a three-step process, in which different pressures and residence times are used. The cycle conditions are specific for each palm oil mill, according to the fruit processed. After sterilizing, the fruit bunches are stripped. The aim of the **stripping** process is to separate the sterilized fruit and the calyx leaves from the bunch stalks. This is done by feeding the sterilized bunches continuously to a beater arm stripper, for small palm oil mills, or a rotary drum stripper, for the larger mills, which strip and separate the fruit from the bunch stalks. The empty bunches are discharged and sent to the empty bunch hoppers for disposal or further processing (Fils 2000).

From the stripper the fruit is conveyed into a digester. The **digestion** process is of the utmost importance as it greatly affects the oil yield. The fruit is separated from the nut and the oil containing cells are caused to burst. Proper digestion ensures that most of the cells are ruptured, thus easing the task of the press, that will have to break a limited number of whole cells, and facilitating the oil extraction. The best digestion is attained by mixing the fruits at 90-100°C for about 20 min. Following the digestion, the mash of digested pulp and palm kernel nuts is transferred to continuous screw press, which separates the solids, including fibers and nuts, from the liquid oil, including water and oil. The mass is subjected to a variable pressure, thereby releasing the oil. An adequate digestion time will reduce the residual oil in the fibers to 5% while keeping the nut breakage rate below 15% (Fils 2000).

The **pressing** is the only part where the palm oil can be mixed with the palm kernel oil. Internationally, 5% admixture of both oils is accepted, but in practice the amount of admixture is unlikely to exceed 3%.At the end of the pressing, two products are obtained: a mixture of water, oil and solid impurities, and a press cake containing fibre and nuts (Fils 2000). The mixture of water, oil and impurities obtained by pressing is subsequently **clarified** in settling tanks. These continuous settling tanks to which the crude oil is transfered, use specific gravity differences to separate the palm oil from water and impurities. The oil leaving the settling tank (top oil) contains about 0.5% moisture and a small amount of impurities. The solids discharged from the settling tank still contain some oil. This stream can be recovered for further processing. Palm oil contains a very small portion of phosphatides or gums (Fils 2000).

If the oil is not **dried**, these gums hydrate slowly over time and subsequently, as these hydrated gums are insoluble, they can precipitate in the storage tanks. To remove the residual moisture from the oil two types of drying can be used: drying under atmospheric pressure and vacuum-drying. The main advantage of vacuum-drying is that it operates at lower temperatures compared to the atmospheric drying (80°C vs 100 - 115°C). The removal of the residual moisture will prevent the hydration and the subsequent precipitation of the gums. Furthermore, the dried oil will be less prone to hydrolysis, which would otherwise result in an increased amount of free fatty acids. Before transferring the dried oil to the storage tanks it is cooled down to 50°C to avoid oxidative damage, which would influence the bleaching process during the refining process (Fils 2000).

To **separate the nuts from the fibers**, the moisture of the press cake is first reduced from 40-45% to 30%. The compacted cake is also broken down in order to facilitate the fiber-nut separation. This separation is done in a separation unit which consists of a pneumatic separation column, which draws off the fibers by suction, and a polishing drum, which removes the residual fibres and other wast material from the nuts. Subsequently, the fresh nuts are dried to reduce the initial moisture content from 16% to 10-12% by blowing hot air (85°C) through the storage silo. This moisture reduction will facilitate the separation of the kernell from the shell (Fils 2000).

The **cracking** efficiency is determined by the adequacy of the earlier sterilization of the fresh fruit bunches. The nuts will break more easily at a high speed of the centrifugal or barrel crackers. However, if the speed is too high, the kernels will break into smaller particles, which leads to an increase in the free fatty acid content of the oil as well as kernel losses in the first stage of kernel separation. The cracked mixture consists of free kernels, shells, unbroken nuts, partly cracked nuts and dust. The separation of the kernels from the remaining fiber, shell and dirt is carried out by drawing air through a vertical column. The kernels and the shells can then be further separated by passing them through a clay bath, which uses the difference in specific gravity between the kernels and the shells to separate them, or by hydrocyclones. At the end of this process, the kernels contain about 20% moisture, and drying is thus essential. A moisture content of 7% is considered optimal to maintain stability and to prevent the formation of free fatty acids during storage. Finally, palm kernel oil can be obtained from the kernels by pressing or extraction (Fils 2000).

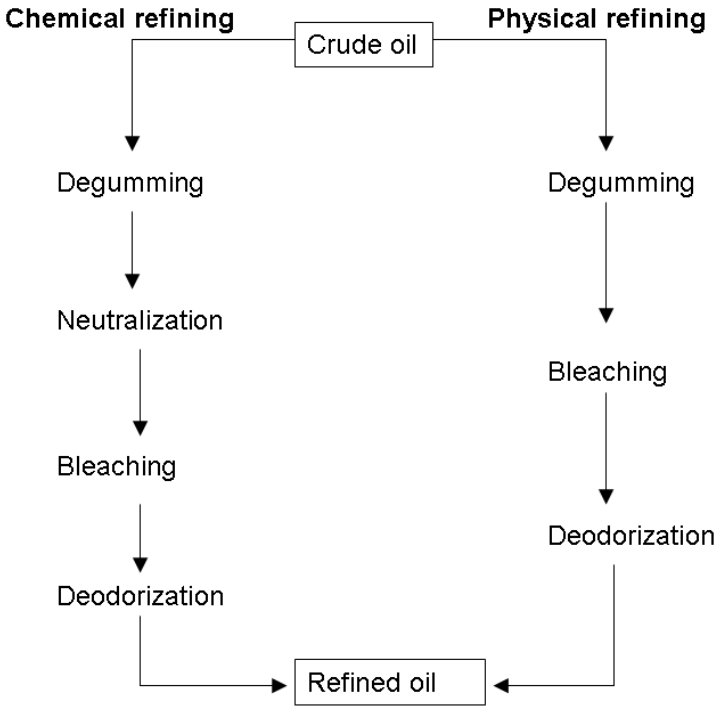

Figure 2.2: General overview of the chemical and physical refining processes (De Greyt and Kellens 2000)

2.3 Refining

The objective of the refining process is to remove those components which have a negative effect on the overall oil quality with the least possible damage to the triacylglycerols. At the same time, beneficial minor components such as pro-vitamins, vitamins and antioxidants should be retained as much as possible (Cmolik and Pokorny 2000; De Greyt and Kellens 2000; Gibon et al. 2007).

Industrially, two major processing routes are applied: physical refining or chemical refining. The main difference between those two approaches lies in the way the free fatty acids (FFA) are removed. In the physical refining process, the FFA are removed in the deodorization unit under carefully selected conditions of temperature, vacuum and steam. Before entering the deodorization unit, the oil must be carefully degummed and bleached, as distillation requires high temperatures. Conversely, during chemical refining the FFA

and gums are removed from the oil during the alkali-neutralization step and soap stocks are produced (Gibon et al. 2007). A schematic representation of both the chemical and physical refining is given in Fig.2.2.

2.3.1 Physical refining

The main advantages of physical refining can be found in the higher oil yield, the lower use of chemicals, the reduction of water and effluent and hence a reduction of the environmental impact. The disadvantage is the higher consumption of bleaching earth. Furthermore, physical refining depends more on the quality of the crude oil, as a wide range of undesirable products can be much more easily removed by alkali-neutralization than by degumming. Nowadays, more than 95% of the crude palm oil is refined through the physical refining route (De Greyt and Kellens 2000; Gibon et al. 2007). Physical refining can be split up into three steps: degumming, bleaching and deodorization and these steps are elucidated further in the next sections.

2.3.1.1 Degumming

The aim of degumming is the removal of phosphatides, also called 'gums', which is a necessary step in the refining process for multiple reasons. Firstly, phosphatides are excellent emulsifiers and therefore increase refining losses. Secondly, they lead to a reduced oxidative stability as they are connected to part of the metals, especially iron, which is the main cause of a reduced oxidative stability. Furthermore, they can cause color inversion and fixation in deodorized oils. In general, degumming consists in the fast or slow hydration of the phosphatides at lower or higher temperatures in order to reduce their solubility in the oil phase, thus facilitating their removal with the water phase. A sufficiently strong acid (phosphoric or citric acid) can be added to accelerate this process (De Greyt and Kellens 2000; Gibon et al. 2007).

2.3.1.2 Bleaching

During bleaching the coloring compounds, residual phosphatides, soaps, metals and oxidation products are removed from the crude oil. This is mostly established by their adsorption on a suitable material; however, some coloring pigments can also be destroyed during heat-treatment. This heat-bleaching effect is obtained during the deodorization step and is most

important for highly colored oils such as palm oil (De Greyt and Kellens 2000). A complete removal of pigments in the bleaching step is not necessary as carotenoids are mainly decomposed by the heat treatment during deodorization (Gibon et al. 2007).

The bleaching process is by far the most expensive process in refining considering utility costs. The relatively high cost of the bleaching clays as well as the oil-in earth losses and bleaching adsorbent disposal costs largely affect the operating cost of a bleaching plant. Nowadays, strong environmental regulations force the refiners to reduce the solid waste streams as they are difficult to treat. Therefore, efforts have been made to develop bleaching processes that consume less bleaching earth (De Greyt and Kellens 2000; Gibon et al. 2007).

2.3.1.3 Deodorization

Deodorization, usually the last step in edible oil refining, consists of three different processes (Gibon et al. 2007):

- distillation: stripping of volatile components such as FFA, tocopherols, tocotrienols, sterols and contaminants;
- actual deodorization: the removal of odiferous products;
- heating stage: thermal destruction of carotenoids.

Deodorization be be operated in batch or in continuous mode, depending on several factors such as oil quality requirements, number of feedstock changes, heat recovery and investment costs. Optimum deodorizing parameters (temperature, pressure, amount of stripping gas) are determined by the the type of oil, the selected refining process, chemical or physical, and the deodorizer design. At the end of the deodorization process a bland and colorless oil is obtained. Physical refining requires more stringent conditions compared to chemical refining due to the distillative removal of the FFA. This step is more critical in physical refining as the initial FFA levels are considerably higher (Gibon et al. 2007).

The composition of the distillate after deodorization depends not only on the oil type, but also on the applied refining technique (physical or chemical) and the operating conditions of the process. When palm oil is physically refined, the deodorizer distillate mainly

consists of FFA (83-88%) with only small amounts of unsaponifiable components (such as tocopherols and sterols) (2-4%) and neutral oil (8-13%)(Gibon et al. 2007).

2.3.2 Chemical refining

In the case of chemical refining, the non-hydratable phosphatides which remain in the oil after acid treatment are further removed during the neutralization step. In this step, the oil is treated with caustic soda, converting the non-hydratable phosphatides in sodium salts which are more easily removed as they are less oil soluble. In the neutralization step, the crude oil is treated with caustic soda and the free fatty acids, the phosphatides and a large portion of the pigments are removed from the oil by decantation or centrifugation. The high soap content in combination with intense water washing improves the removal of the phosphatides. The main disadvantage of neutralization is the production of soapstock which needs to be treated accordingly. Neutralized oil is separated from the soapstock by centrifugation. It is then washed with warm water to reduce the residual soaps and dried under vacuum before proceeding to bleaching and deodorization. The deodorizer distillate obtained via chemical refining is made up of 33-50% FFA, 25-3% unsaponifiable components and 25-33% neutral oil. Chemical refining is still used at a limited capacity and results in neutralized bleached and deodorized (NBD) palm oil (Gibon et al. 2007).

2.4 Chemical properties

2.4.1 Fatty acid composition

Palm oil has a balanced fatty acid composition in which almost equal levels of saturated and unsaturated fatty acids. Palmitic (44-45%) and oleic (39-40%) make up the major part of the fatty acids, along with linoleic acid (10-11%). Linoleic acid can only be found in trace amounts and linolenic acid is virtually absent, which renders palm oil relatively stable to oxidative deterioration (Siew 2002). Table 2.1 shows the mean fatty acid composition of over 200 refined palm oil samples originating from Malaysia (production 1990). No major variation was found between crude and refined palm oil (Berger 2001).

Table 2.1: Mean fatty acid composition (%) of refined palm oil (Berger 2001)

Fatty acid	C12:0	C14:0	C16:0	C16:1	C18:0	C18:1	C18:2	C18:3	C20:0
%	0.2	1.1	44.2	0.1	4.4	39.0	10.6	0.2	0.2

2.4.2 Triacylglycerol composition

Palm oil is a multicomponent fat which is made up of more than 12 different triacylglycerols (Ng and Oh 1994). The four main triglycerides are POP and POO together constituting about 55%, followed by POL with 9% and PPP with 6%. Some variability may exist depending on origin and extraction conditions (Busfield and Proschogo 1990; Che Man et al. 1999). Upon cooling from the melt below certain temperatures, the first crystals appear in the metastable α phase and have a high concentration of MMM, PPP, PPS, POS and POP (M=myristic acid, P=palmitic acid, O=oleic acid, S=stearic acid). When kept isothermal, palm oil undergoes a phase transition to form β' crystallites that are particularly stable over time, rather than forming β crystallites, while incorporating more of the lower melting component rich in POO, PLP and SOO. The liquid phase is mostly PLO, OOO, PLL and LOO (Busfield and Proschogo 1990; Kawamura 1979).

2.4.3 Minor components

2.4.3.1 Diacylglycerols

Palm oil is unique in its high content of diacylglycerols, which usually ranges between 4 and 7.5% (Jacobsberg and Oh 1976; Goh and Timms 1985; Siew and Ng 1995b), mainly consisting of palmitoyloleoyl glycerol (PO), dipalmitoyl glycerol (PP) and dioleoyl glycerol (OO) (Goh et al. 1985). The 1,3-isomers are found in higher proportions then the 1,2-isomers. In crude palm oil the 1,3- and 1,2-diacylglycerols are present in a ratio 7:3 (Siew and Ng 1999).

The high diacylglycerol concentration in palm oil affects its crystallization properties by inhibiting the nucleation process and retarding the crystal growth rate. Furthermore, the polymorphic transition of α to β' is also slowed down by the presence of diacylglycerols (Riiner 1970; Persmark et al. 1976; Okiy 1978; Okiy et al. 1978; Berger and Wright 1986; Siew and Ng 1999), with the extent of the inhibition depending on the nature and the

concentration of the diacylglycerols (Siew and Ng 1999; Siew and Ng 2000; Long et al. 2005). Siew and Ng (1999, 2000) demonstrated that the 1,2 isomers were more effective in depressing the melting point of palm oil than the 1,3-isomers. However, an excess of 1,3-PP elevated the melting point, thus enhancing crystallization.
Diacylglycerols are not removed from the palm oil during the refining process and can thus lead to several disadvantages during fractionation. They can form eutectic mixtures with triacylglycerols, resulting in an difficult separation and thus incomplete fractionation (Okiy 1978; Okiy et al. 1978; Berger and Wright 1986). High melting diacylglycerols, mainly 1,3-PP, are responsible for the cloudiness of olein fractions upon prolonged storage at room temperatures (Siew 2001).

2.4.3.2 Other minor components

Crude palm oil is rich in minor components such as tocopherols and tocotrienols, sterols, carotenes and squalene (Goh et al. 1985). It is the richest natural source of carotenoids and tocotrienols, which are potent fat-soluble antioxidants (Gee 2007). Crude palm oil has a rich orange-red color due to its high carotene content (700-800 ppm), of which 90% is present as α and β carotene (Goh et al. 1985). During refining, the carotenoids are removed by bleaching and deodorizing. The other minor components are diminished to varying extents, depending on the refining conditions (Berger 2001; Siew 2002). Crude palm oil contains about 0.02-0.06% of sterols. During each step of the refining process, the amount of sterols gradually decreases (Tan et al. 2007).

The vitamin E group is constructed of tocopherols and tocotrienols, which can each be present in four forms (α, β, γ, δ). Crude palm oil contains 600-1000 mg/kg tocols, of which 21-34% are present as tocopherols and 66-79% as tocotrienols. Palm oil is exeptional compared to other vegetable oils because the majority of its tocols is present as tocotrienols with 46% γ-tocotrienol, 22% α tocotrienol, 11% δ-tocotrienol and 1-2% β-tocotrienol. Furthermore, crude palm oil also contains 22% α-tocopherol)(Jacobsberg et al. 1978). Refining of the crude palm oil reduces the level of tocols to 378-890 mg/kg (Gapor 1990). Refined oils retain about 70% of their tocols, varying on refining conditions. Most of the losses occur during deodorization. Consequently, the deororizer distillate or palm fatty acid distillate (PFAD) contains five to ten times the amount of tocols in crude palm oil, which makes it a preferrable starting material for the recovery of vitamin E (Siew 2002).

2.5 Physical properties

2.5.1 Solid fat content

The solid fat content(SFC) of an oil determines its usage and applications. As palm oil contains saturated and unsaturated fatty acids in roughly equal proportions, solids exists from 50°C down to 10°C. The SFC of palm oil amounts to 50% at a temperature of 10°C, falling to half of this value at 20°C. The variations between different palm oil samples arise from differences in fatty acid composition and diacylglycerol levels (Siew 2002). An increase in free fatty acids and diglyceride content will decrease the solid fat content and increase the plasticity of palm oil up to free fatty acid contents of ca. 7% (Jacobsberg and Oh 1976).

2.5.2 Crystallization and melting

Palm oil is semi-solid at room temperature (28°C), the melting point range being from 32-40°C (Siew 2002). The appreciable amount of di-saturated and mono-saturated triacylglycerols in palm oil give rise to two distinct peaks in both the melting and the crystallization DSC thermograms. These two peaks are related to the melting/crystallization of a high melting (Hm) and low melting (Lm) fraction as is shown in Figure 2.3. The high melting fraction, or stearin fraction, mainly contains the saturated and disaturated triacylglycerols, while the low melting fraction, or olein fraction is rich in monosaturated and unsaturated triacylglycerols (Siew 2002).

Despite the wide range of triacylglycerols in palm oil, its DSC melting and crystallization thermograms are quite simple, illustrating the easy separation of stearin and olein. However, the isothermal crystallization behavior of palm oil is much more complex. Several studies demonstrated that the isothermal crystallization behavior of palm oil changes depending on the crystallization temperature (Kawamura 1980; Ng and Oh 1994; Chen et al. 2002). Above a certain cut-off temperature, palm oil is found to crystallize in two-steps, while below this cut-off temperature palm oil displays a single step crystallization. Kawamura (1980) found this cut-off temperature to be 24°C using DSC, while Ng and Oh (1994) reported a cut-off temperature of 25°C using DSC and pNMR. Chen et al. (2002) observed a cut-off temperature of 22C based on PLM and viscosimetry measurements.

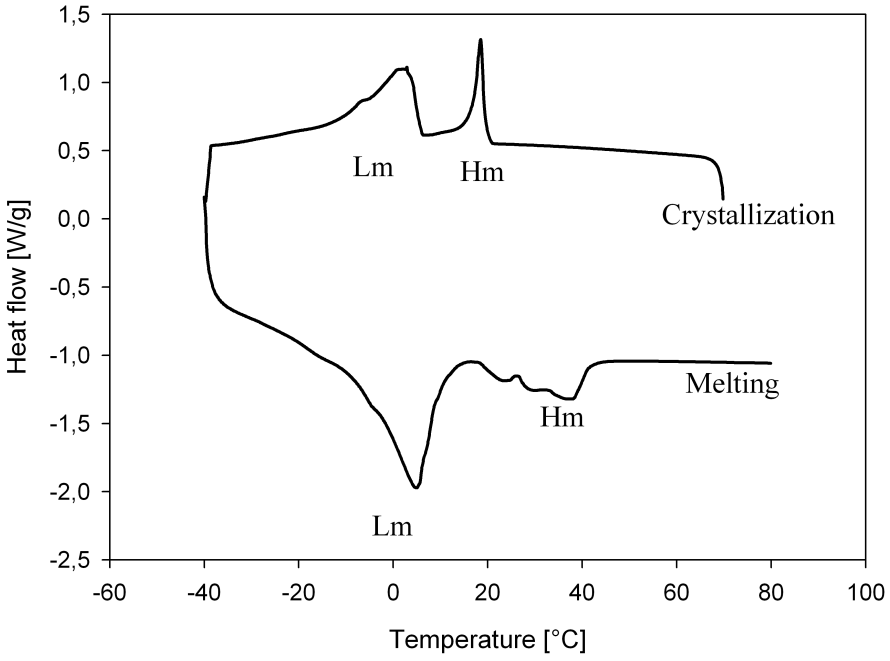

Figure 2.3: DSC melting and crystallization thermograms of palm oil

Kawamura (1980) and Chen et al. (2002) attributed this two-step crystallization behavior to the formation of α crystals followed by a polymorphic transition to β' crystals. At temperatures where a one-step crystallization was observed, palm oil crystallized directly from the melt in the β' polymorph.

2.6 Fractionation

Natural oils and fats usually have limited applications in their original form due to their specific chemical compositions. Therefore, oils often undergo modification processes to extend their applications range in food products. In the edible oil industry, three modification processes are widely used: hydrogenation, interesterification (enzymatic or chemical) and fractionation. Hydrogenation (reducing the degree of unsaturation of the acyl groups) and interesterification (redistributing the fatty acid chains on the glycerol backbone) are strictly based on a irreversible chemical change in the composition of the fats, whereas in fractionation the composition is modified by a selective physical separation of the different component groups, which makes it the only fully reversible modification process (Kellens et al. 2007)

Fractionation has its origin in the invention of margarine in 1869 (Anderson and Williams 1965). Freshly rendered tallow was carefully crystallized at 25-30°C and, subsequently, hydraulically pressed to separate the soft fraction (olein) and the solid fraction (stearin). In early 20th century, coconut oil was commonly fractionated to produce hardstock for margarine (Rossell 1985). However, as the then existing fractionation technology could not keep up with the ever growing demand, fractionation was replaced by hydrogenation. The rapid increase in palm oil production, particularly in Malaysia, invoked a revival of fractionation in the early 1960s (Illingworth 2002). Furthermore, the Malaysian government, aiming at rapidly developing its own industry, reduced the export taxes on palm oil in the early 1970s, providing the oil had been subjected to further processing. This policy naturally triggered a boom in the production of processed palm oil (Kellens et al. 2007).

Basically, fractionation is a thermo-mechanical separation in which a multi-component mixture is physically separated into two or more fractions with distinct physical and chemical properties. This separation can be based on differences in solidification, solubility, or volatility of the different compounds. Fractional crystallization refers to the separation process in which the fatty material is crystallized, after which the liquid phase is separated from the solid. This separation is based on the differences in solubility of the solid triacylglycerols in the liquid phase, depending on their molecular weight and degree of unsaturation (Kellens et al. 2007). Fractionation is usually applied to achieve one of the following objectives (Hamm 1995):

- removal of small quantities of high melting compounds, either triacylglycerols or non-glyceride material such as waxes, that would otherwise cause 'cloudiness' of the oil at refrigeration temperatures. This process is known as 'winterization' and is usually part of the refining process;
- enrichment of an oil with more unsaturated triacylglycerols in order to improve its application properties;
- recovery of a fraction with a narrower composition range and sharper melting properties that can be used in chocolate and confectionery applications.

On an industrial scale, three different fractionation techniques are in use: detergent fractionation, solvent fractionation and dry fractionation.

2.6.1 Detergent and solvent fractionation

The principle of **detergent fractionation** is to improve the separation of the crystallized phase from the remaining liquid by adding an aqueous detergent solution to the crystallized oil. The detergent, usually sodium lauryl sulfate, in combination with an electrolyte, in most cases magnesium sulfate, wets the surface of the crystals, which are consequently transferred to the aqueous phase. This mixture is then readily separated by centrifugation into a water phase and a liquid oil phase (olein fraction). In a next step, the water phase is heated and the melted stearin is recovered in a second centrifugation. The traces of detergent are removed from the olein and stearin fractions by washing and drying. This technique was patented by Lanza in 1905 and one form of this process is known as the Lipofrac process. Nowadays, detergent fractionation has become less appealing due to the high costs and contamination of the end product with the detergent (Illingworth 2002; Kellens et al. 2007).

In **solvent fractionation**, the fat is dissolved in acetone or hexane and the dilution is cooled to initiate the crystallization of the high melting triacylglycerols. The crystals are separated by filtration and the fractions are recovered by evaporation of the solvent. Acetone and hexane, consisting of molecules smaller than triacylglycerols, have very low melting points and are thus unlikely to crystallize. By adding these solvents, the solution is diluted, resulting in lower viscosities during the crystallization process. The reduced viscosity allows the triacylglycerol molecules to move around more freely, and as a result, they are more likely to attach to the growing crystal surface in the right configuration. Consequently, larger crystals with fewer dislocations are formed and a lesser tendency to form mixed crystals. Furthermore, the added solvent will also hinder oil inclusion in the solids. After evaporation of the solvent, a much lower quantity of liquid oil is found in the solid fraction. The process is characterized by short crystallization times and easy filterability. The high separation efficiency and hence improved yield and high purity of the end products are the main advantage of solvent fractionation. However, due to the high production costs and capital investments, as well as the possible fire hazards, solvent fractionation is becoming less interesting. Today, most of the plants in operation produce specialty fats with high added value, such as for example cocoa butter replacement fats (Illingworth 2002; Kellens et al. 2007).

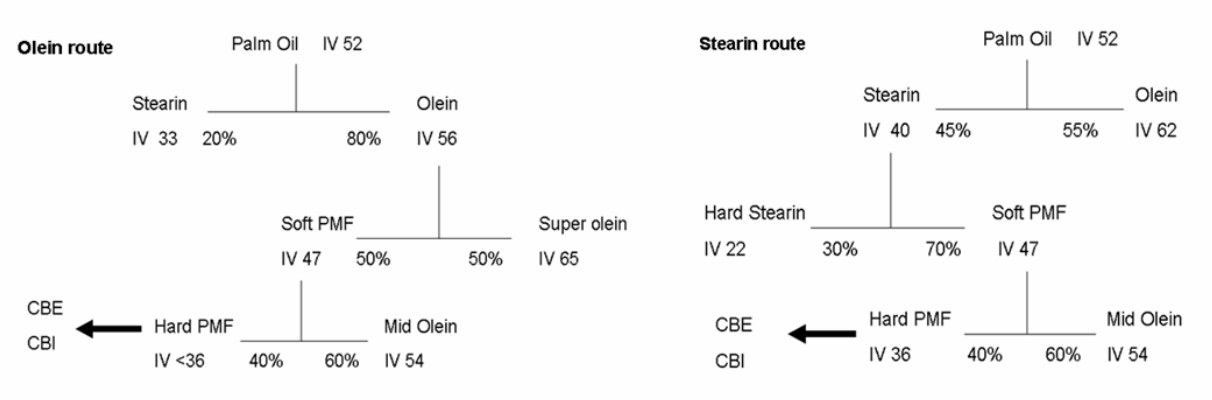

Figure 2.4: Dry fractionation routes of palm oil (IV=iodine value, PMF:palm mid fraction, CBE=cocoa butter equivalent, CBI=cocoa butter improver) (Kellens 2000)

2.6.2 Dry fractionation

Dry fractionation is the cheapest and simplest fractionation process. Unlike solvent and detergent fractionation, dry fractionation does not need an additional substance and thus no effluent is produced and no chemicals have to be removed from the final products (Illingworth 2002; Kellens et al. 2007). The very low operating costs together with the low operating costs and full reversibility of the process make it very attractive (Kellens 2000). Dry fractionation is based on the differences in melting points of the triacylglycerols and partial acylglycerols (Siew and Ng 1995a; Siew and Ng 1996) and consists of two steps: crystallization and separation. In the first step, solids are formed in the liquid phase by a controlled crystallization of the melted oil according to a specific cooling program. The second step separates the solids, the stearin fraction, from the liquid oil, the olein fraction. In dry fractionation, crystallization takes place in the bulk and, consequently, the degree of crystallization of the fat is limited by viscosity problems. Therefore, multi-step processes are applied, which have the advantage of resulting in a wide range of fractions suitable for multiple applications (Illingworth 2002; Kellens et al. 2007).

2.6.3 Palm oil fractions

Dry fractionation is usually applied when fractionating palm oil due to its low operating costs and limited impact on the environment. It usually results in a premium product with higher added value and a secondary product, sometimes with a market value below

that of the feedstock material and thus the profitability of the process depends on what the end-users are willing to pay. By applying multiple fractionation routes, a wide variety of palm oil fractions can be obtained (Kellens 2000) and a wide range of food products can be formulated by incorporating the most suitable fractions (Siew 2002). Figure 2.4 represents different pathways for the fractionation of palm oil. The olein route is generally used in South-East Asia while the stearin route is more commonly used in South America (Kellens 2000).

2.7 Food applications of palm oil products

Palm oil and palm oil fractions have become important raw materials in the food industry due to the unique composition of palm oil. Its balanced range of saturated and unsaturated fatty acids, allows the oil to be easily fractionated into products enriched in saturated or unsaturated triacylglycerols. A wide range in food products can be formulated by incorporating the most suitable fractions. The advantages of using palm oil and palm oil fractions include the cheap raw material, the ready availability and the low cost of processing. Due to its semi-solid character there is little need for hydrogenation. In addition, palm oil exhibits a high oxidative stability due to its low percentage of polyunsaturated fatty acids, but also due to its carotenoids and tocotrienols (Siew 2002). Almost 90% of the palm oil traded around the world is used in edible applications such as cooking and frying oils, margarines, shortenings and speciality fats (Siew 2002).

2.7.1 Shortening and margarines

Historically, shortenings were referred to as naturally occurring fats that were solid at room temperature and used to "shorten" baked products (O'Brien 1996). Nowadays, shortenings are defined as 100% fat products formulated with animal and/or vegetable oils that have been processed for functionality (Nor Aini and Miskandar 2000). In contrast, margarines are water-in-oil emulsions (80% fat) in which water droplets are kept separated by the fat crystals (Haighton 1976; Siew 2002).

Palm oil, being semi-solid at ambient temperatures, makes a very suitable component for the production of margarines and shortenings as these are both viscoelastic products in

which the liquid oil is entrapped in a crystal network structure. An important role of palm oil lies thus in providing consistency, texture and structure to these products. In addition, palm oil also provides oxidative stability due to its low content of polyunsaturated fatty acids coupled with the presence of tocopherols and tocotrienols (Nor Aini and Miskandar 2000). Because of its high percentage of palmitic acid (44%), palm oil is β' tending (Yap et al. 1989). Hence, palm oil promotes the formation of β' crystals. The relatively small β' crystals can incorporate large amounts of liquid oil in the crystal network, which is necessary to obtain a smooth, continuous and homogeneous product (deMan and deMan 1994; deMan 1998). In addition, β' crystals also attribute to good creaming properties as their small size helps incorporating air during the creaming process (Nawar 1996).

Palm stearin is widely used in the manufacturing of shortening as it is an economical feedstock that can be easily blended with soft oils such as sunflower, soybean, corn and canola oil. Palm stearin provides the solids required form plastic shortenings without the need for hydrogenation, which makes the obtained shortenings free of fatty acids (Nor Aini and Miskandar 2000). Shortenings influence the processing steps of many bakery products such as cakes, cookies, cream fillings and icings, laminated doughs and bread (Siew 2002; Nor Aini and Miskandar 2000).

Several types of margarines can be formulated with incorporating palm oil or its fractions. For tub margarines, the blend can contain up to 50% palm oil. This percentage can be raised to 60% when using palm olein (Siew 2002) . The high melting fraction of palm oil, palm stearin, makes an excellent hardstock for margarines formulated from liquid oils (Traitler and Dieffenbacher 1985).

2.7.2 Cooking and frying oils

An oil or fat has to fulfill several requirements to be considered as a good choice for frying applications, the most important being a high oxidative stability with respect to oxidation and polymerization. In order to provide the good oxidative stability the content of unsaturated fatty acids and in particular polyunsaturated fatty acids, has to be minimized. Palm oil, containing natural antioxidants like tocopherols and tocotrienols, meets these requirements and can thus be considered as an excellent choice for frying (Nor Aini and Miskandar

2000). Due to their high oxidative stability, palm oil and palm oil fractions are applied as frying oils for chips, crackers, cookies, pastries, dough nuts and instant noodles (Siew 2002).

Palm oil and palm olein are often blended with less stable vegetable oils, thus improving their oxidative stability by reducing the levels of linoleic and linolenic acids. Blending is more cost effective than partial hydrogenation and has the additional advantage that no undesired trans fatty acids are produced. In addition, the cloud points of most vegetable oils are raised slightly by blending with palm olein (Siew 2002; Nor Aini and Miskandar 2000)

2.7.3 Cocoa butter equivalents

The major characteristics of confectionery fats are a hard brittle texture at ambient temperature and a rapid meltdown at body temperature with no appreciable residue (Berger 2001). Palm mid fraction (PMF), obtained from palm oil via multi-stage fractionation, is used in the manufacturing of cocoa butter equivalents (CBE). CBE's have similar physical and chemical properties compared to cocoa butter and are compatible with cocoa butter in almost any proportions (Goh 2002; Siew 2002). PMF, which has a high content of POP, is easily blended with other fats such as shea, ilipe and sal stearin, to produce chocolate products (Berger 1981).Cocoa butter-like fats can also be formulated with interesterified oils. Suitable blends for cream filling in biscuits may be formulated from palm stearin/palm kernel olein (25:75) or palm stearin/palm kernel olein/palm kernel oil (25:37.5:37.35) (Noor Lida et al. 1997).

2.7.4 Other applications

In addition to the above described applications, palm oil is also used in snack foods, biscuits, ice-creams, salad dressings and so on. Fat plays an important role in all these food products and formulations based on palm oil and palm oil fractions can replace some of the oils used traditionally (Siew 2002).

Chapter 3

Rheological behavior of crystallizing palm oil[1]

In the beginning the Universe was created. This has made a lot of people very angry and been widely regarded as a bad move.
The hitchhicker's guide to the galaxy - Douglas Adams (1952-2001)

[1]This chapter has been published in:
De Graef, V., K. Dewettinck, D. Verbeken, and I. Foubert (2006). Rheological behavior of crystallizing palm oil. European Journal of Lipid Science and Technology 108 (10), 864−870.

3.1 Problem statement and research strategy

In the past several techniques have been used to study primary crystallization of fats: differential scanning calorimetry (DSC), pulsed nuclear magnetic resonance (pNMR), and X-ray diffraction (XRD). These techniques however do have their limitations. DSC can only be used to investigate primary crystallization under static processing conditions, while pNMR does not allow on-line quantification. To evaluate primary crystallization by means of XRD, synchrotron radiation is needed, which makes this technique not suitable for everyday use. The primary crystallization process can also be followed by means of viscosity changes as a function of time. Before crystallization starts, the melt shows Newtonian behavior. With the formation and growth of crystals, the viscosity increases almost linearly with the amount of crystals in the suspension until it reaches a thermodynamic equilibrium (Breitschuh and Windhab 1998). This technique has also been used by Loisel et al. (1998), Toro-Vazquez et al. (2000) and Chen et al. (2002) to follow the isothermal crystallization of refined palm oil, chocolate and palm stearin, respectively. Toro-Vazquez et al. (2004, 2005) recently used a rheological approach to investigate the crystallization of cocoa butter under static as well as dynamic (shear applied) conditions. This technique has been widely applied in polymer science and this for several decades. In fat crystallization however, oscillatory rheology is not generally accepted as a tool to follow this process. Concerning the microstructural development, many authors limit their investigation to a qualitative follow-up by means of polarized light microscopy or confocal laser scanning microscopy (Herrera and Hartel 2000a; Tietz and Hartel 2000). Kawamura (1979) and Brunello et al. (2003) studied the microstructural development on a quantitative basis via microscopy and rheology, respectively. In the past, microstructure was almost exclusively investigated in terms of fractal dimensions and only the final microstructure was taken into consideration, while little attention was paid to the development of microstructure (Herrera and Hartel 2000a; Brunello et al. 2003; Litwinenko et al. 2002; Narine and Humphrey 2004).

In this chapter the different phases of the crystallization (primary crystallization, microstructural development, macroscopic properties) of palm oil under static isothermal conditions are evaluated with oscillatory rheology. These results are compared with crystallization data obtained with DSC and pNMR to highlight the possibilities of oscillatory rheology.

Table 3.1: Fatty acid composition (%)

C12:0	C14:0	C16:0	C16:1	C18:0	C18:1	C18:2	C18:3	C20:0
0.35	1.14	46.00	0.13	4.31	37.71	9.11	0.10	0.35
± 0.02	± 0.01	± 0.18	± 0.00	± 0.06	± 0.11	± 0.03	± 0.032	± 0.10

Table 3.2: Triacylglycerol composition (%)

OLL	PLL	LOO	PLO	PLP	OOO
0.05	0.85	0.72	9.79	8.96	2.64
± 0.01	± 0.01	± 0.05	± 0.09	± 0.17	± 0.06

POO	POP+PLS	PPP+SOO	POS	PPS	SOS
27.92	36.29	7.68	4.44	0.46	0.13
± 0.24	± 0.11	± 0.09	± 0.12	± 0.00	± 0.01

3.2 Methods and Materials

3.2.1 Substrate

Refined, bleached and deodorized palm oil of iodine value 52.3 was obtained from Loders Croklaan (Wormerveer, The Netherlands) and stored in the freezer at -24°C. Table 3.1 displays the average fatty acid composition and standard deviation as determined by gas chromatography according to the AOCS official method Ce 1-62. These averages are the result of duplicate analyses. The triacylglycerol composition was determined by reversed-phase HPLC with ELSD detector (Rombaut et al. 2008). The average and standard deviation of duplicate determinations are shown in Table 3.2

3.2.2 Oscillatory rheology measurements

Small deformation oscillatory experiments were performed on an AR2000 controlled stress rheometer (TA Instruments, Brussels, Belgium) using the starch pasting cell (SPC). This SPC consists of a jacket, mounted on the instrument, a removable cup and an impeller (Figure 3.1). A gap of 5500 μm is used, which is larger than that of plate-plate or concentric cylinders geometries and reduces the risk of clogging. Furthermore, in the SPC the impeller is immersed in a larger sample volume compared to the other geometries and

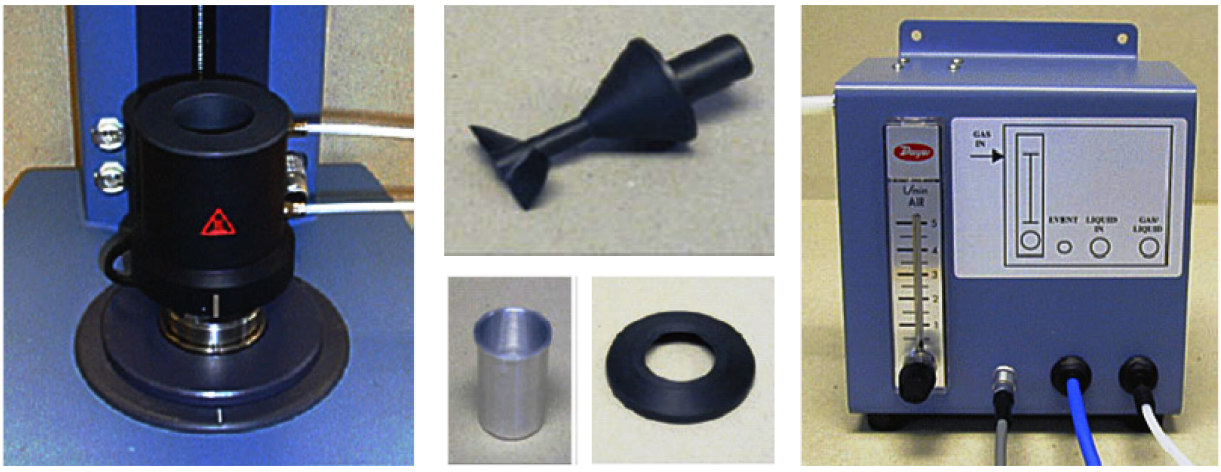

Figure 3.1: Starch pasting cell with removable impeller, cum and cap and the cooling control unit (TA Instruments)

crystallization is not limited to a narrow gap between rotor and stator. This geometry also allows performing crystallization experiments under shear. In addition, the SPC has a very efficient cooling system and fast cooling rates can be easily achieved, which are faster than for the more conventionally used geometries. Heating is accomplished through the electrical elements placed within the jacket, concentrically to the cup. The sample is cooled using water carried in a helical conduit in close proximity to the cup's outer walls. The cooling water flow is controlled through the cooling control unit (Figure 3.1), which is placed upstream of the cup. Purged air is used to displace the water from the conduit during heating. The temperature is read by a Pt 100 probe in close thermal contact with the bottom cup. The temperature is read by a Pt 100 probe in close thermal contact with the bottom cup. Since the impeller produces an ill-defined flow, analytical conversion factors are not available. Therefore a calibration was performed by the manufacturer to determine the conversion factors for shear rate (4.500) and shear stress (48600 m^{-3}).

The complex modulus G^* can be defined as the ratio of the shear stress to the applied deformation and consists of a real and an imaginary component, respectively, G' and G". G' is denoted as the elastic, storage or in-phase modulus and is a measurement for the solid nature of the sample. On the contrary, the viscous, loss or out-phase modulus G" is an indication for the fluid character of the viscoelastic system. The phase angle δ encompasses both G' and G'', evaluating in a quite sensitive way the viscoelastic changes of complex

systems. In a pure viscous system, such as a vegetable oil or completely melted palm oil, δ equals 90°. Once nucleation occurs and crystals start to grow, δ starts to decrease as the solid character of the crystallizing oil increases. This decrease can be quite drastically. At a δ above 45°, the sample displays a predominantly fluid character, while for values lower than 45°, the solid character prevails. Eventually, when the system becomes fully crystallized, δ approaches zero.

Oscillation measurements were conducted at a constant frequency of 1Hz and a strain of $4.500 * 10^{-3}$. This very low strain together with the low frequency of 1Hz was chosen to avoid disturbances to the crystallization process as much as possible while maintaining a sufficiently high data sampling rate. Rheograms were obtained by plotting the complex modulus ($|G^*|$) and phase angle (δ) of the crystallizing sample as a function of the crystallization time. The melted sample was transferred into the cup and the following time-temperature profile was applied:

- keeping isothermally for 10 minutes at 70 °C to erase all crystal memory;
- cooling at 10 °C per min to the desired crystallization temperature;
- oscillatory time sweep at the achieved crystallization temperature (isothermal period).

Each analysis was executed in triplicate.

3.2.3 DSC

The isothermal crystallization experiments were performed on a Q1000 DSC with a Refrigerated Cooling System (TA Instruments, Brussels, Belgium). The DSC was calibrated with indium (TA Instruments, Brussels, Belgium), azobenzene (Sigma Aldrich, Bornem, Belgium) and undecane (Acros Organics, Geel, Belgium) prior to analysis. Nitrogen was used to purge the system. Hermetic aluminum pans were used with air as reference. The sample was held isothermal at 70°C for 10 minutes to erase all crystal memory. Subsequently it was cooled at 10°C per min to the desired crystallization temperature and kept isothermal at the crystallization temperature until the end of the primary crystallization. Each analysis was executed in triplicate.

3.2.4 pNMR

pNMR experiments were performed with a Minispec pc 20 (Bruker, Karlsruhe, Germany). Liquefied fat was transferred into pNMR tubes and held at 65°C for 30 minutes to eliminate any thermal history. These tubes were subsequently placed in a thermostatic water bath at the crystallization temperature. Readings of the amount of solid fat were taken at appropriate time intervals and a separate tube was used for each measurement. The start of the isothermal period was taken one minute after transfer to the water bath. Each analysis was executed in triplicate.

3.3 Results and discussion

3.3.1 Rheological characterization of palm oil crystallizing at 18°C and 25°C

In Figure 3.2A the phase angle δ and complex modulus $|G^*|$ are plotted as a function of isothermal time for crystallization at 18°C. Although measurements are executed in triplicate, this graph represents one exemplary curve as there is very little variation between the repetitions. When looking at the evolution of the phase angle, it can be noticed that at the start of the isothermal time δ equals 90°, indicating the liquid behavior of the sample. After 1.3 min, however, δ starts to decrease to reach a plateau at 2.6 min isothermal time. At this stage the phase angle has decreased to 71°. This decrease indicates the formation of solid phase, thus reducing the liquid character of the sample. The following three minutes, δ does not vary. This can be interpreted as a period in which no additional crystallization takes place. After 5.6 min a second decrease occurs, leading to a minimum δ value of 23° at 8.7 min isothermal time.

Toro-Vazquez et al. (2004) attributed the evolution in phase angle, recorded during static cocoa butter crystallization, to crystallization in different polymorphic forms. Applied to the phase angle curve for palm oil crystallization, this would lead to the following hypothesis. During the first step, α crystals are formed as the phase angle decreases from 90° to 71°, which are converted via a solid phase transformation into β' crystals when the phase angle is stable at 71°. The subsequent decrease in phase angle from 71° to 23° and

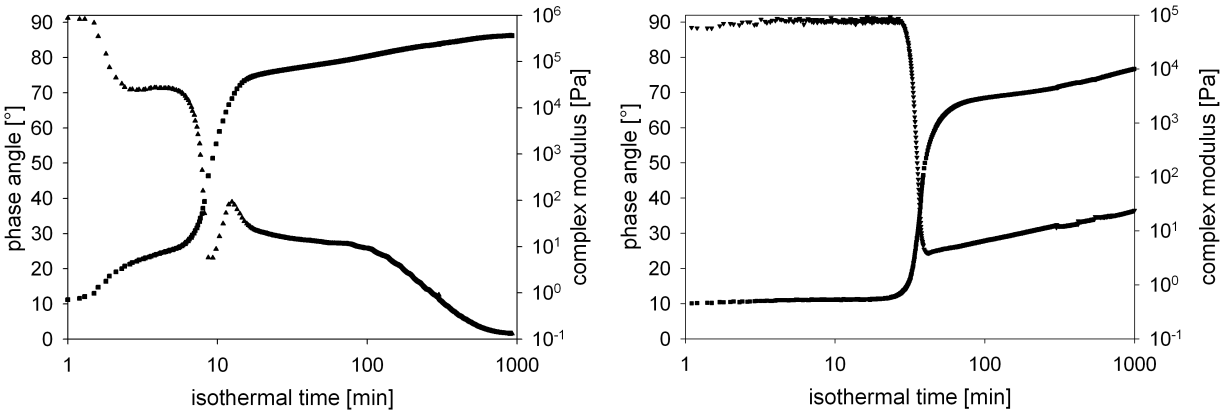

Figure 3.2: Evolution of the phase angle δ (▲) and complex modulus $|G^*|$ (■) during static isothermal crystallization of palm oil at (A) 18°C and (B) 25°C

the following peak might then be caused by β' crystal formation directly from the melt. This polymorphic transition hypothesis was worked out by Mazzanti et al. (2005) based on time resolved X-ray data for palm oil crystallization at 17 and 22°C and various shear rates and without shear. In literature (Chen et al. 2002; Litwinenko et al. 2002), there is no agreement on the critical temperature above which primary crystallization occurs in one step. Differences in critical temperature can be explained by the variations that can occur in palm oil composition caused by seasonal variations, origin and refining.

The second decrease in phase angle is immediately followed by a sharp increase so that at 15 min an intermediate maximum δ value of 39° is attained. It is hypothesized that during the decrease from 71° to 23° most of the liquid material crystallizes, thereby releasing a considerable amount of crystallization heat. This crystallization heat cannot be removed immediately, causing a temporary temperature rise. This temperature rise can locally cause crystals to melt, hereby loosening the network structure and thus leading to an increase in phase angle. Due to ongoing crystallization and aggregation, the phase angle decreases slowly to reach a final value of 1.5° after more than 15 hours.

The changes in the complex modulus correspond with the timescale of the variations in phase angle (Figure 3.2A). At 1.3 min $|G^*|$ has a value of 0.83 Pa. A first sigmoidal increase till 5.6 min leads to value of about 10 Pa, which corresponds with the first step of the primary crystallization process: formation of α crystals from the melt. This small

increase is followed by a more drastic one from 10 Pa to 50 000 Pa. This drastic increase is related to the polymorphic transition of α to β' crystals and to the formation of β' crystals from the melt. An increasing trend is maintained up to 15 hours isothermal time, when $|G^*|$ equals 360 000 Pa. This may be due to further strengthening of the network due to ongoing crystallization and recrystallization or aggregation.

The storage modulus G' follows the same pattern as the complex modulus. The loss modulus G'' initially displays the same pattern as G', but reaches a maximum at a certain stage, while G' further increases. The decrease in G'' is expected as G'' is related to the phase angle, which approaches zero (1.5° at 15 h isothermal time). According to Kloek (1998) the decrease of G'' will be due to relatively less energy dissipation during deformation. A possible explanation for a maximum in the G'' can be a gradual change in the type of interaction. During the initial stage of crystallization, the crystals are attracted to each other by van der Waals forces. These bonds may exhibit considerable relaxation and therefore cause energy dissipation. If these bonds become sintered due to ongoing crystallization or recrystallization, much less energy relaxation will occur, resulting in a decrease of the loss modulus (Kloek 1998).

For crystallization at 25°C the phase angle and complex modulus show a slightly different evolution as shown in Figure 3.2B. At about 28 min isothermal time the phase angle decreases from 90° to 24° in 15 min. Afterwards, the phase angle shows a slightly increasing trend, probably due to rearrangements in the network structure. At the same time scale the complex modulus increases from 0.5 Pa to 400 Pa, indicating crystal growth and formation of a primary network. The complex modulus further continues to increase so that at 1000 min the complex modulus almost equals 10 000 Pa. This straightforward behavior suggests that at 25°C the crystallization of palm oil is a single stage process. The storage and loss moduli curves are similar compared to the complex modulus curve. The larger induction time for crystallization can be explained by the decrease in driving force for nucleation compared to 18°C due to lower supercooling. Also, since at 25°C no α phase is developed and no α to β' transition occurs, β' nucleation takes longer because the only mechanism possible is direct crystallization from the melt.

3.3.2 Comparison of oscillatory rheology with DSC and pNMR

In the next paragraphs oscillatory rheology data are compared with DSC and pNMR results for the static isothermal crystallization of palm oil at 18°C. It must be kept in mind that, when using different equipment to follow crystallization, comparison between results must be done with caution. Differences in sample weight or volume, equipment design and its impact on the thermodynamics of the system and, heat and mass transfer conditions existing in each measurement device, may affect crystallization to a different extent.

Figure 3.3A presents an overlay of the heat flow recorded by DSC and the phase angle recorded by oscillatory rheology. The global time on the X-axis represents the total time of the analysis, including conditioning at 70°C to erase all crystal memory and the subsequent cooling stage (from 70°C to 18°C at 10°C/min). The isothermal period starts at 15 min global time. It can be derived from Figure 3.3A that the measured heat flow displays two exothermic peaks, of which the first one coincides with the equilibration step. The exothermic DSC peaks correspond with heat changes due to crystallization of the sample. The first peak indicates the formation of the α phase, while the second peak is related to the polymorphic transition of α to β' crystals and the formation of β' crystals from the melt. What is important in this graph, is that the two exothermic peaks in the heat flow curve more or less coincide with the two steps in the phase angle curve, which indicates that most probably the same events are recorded. However, some important differences can be noticed. DSC is only capable of measuring primary crystallization as can be seen in Figure 3.3A: the heat flow does not change anymore beyond 45 min. The phase angle however, still changes beyond 45 min, which could be an indication of structural rearrangements. The changes in phase angle beyond 45 min may be interpreted as changes in microstructural arrangement due to e.g. post hardening effects such as sintering and Ostwald ripening. Oscillatory rheology may thus also provide information on the second step of the crystallization process, namely the microstructural development.

Marangoni and his group demonstrated that equal solid fat contents do not necessarily lead to equal macroscopic properties such as hardness. In studies on factors affecting the hardness and spreadability of chemically and enzymatically interesterified milk fat (Marangoni and Rousseau 1996; Marangoni and Rousseau 1998b; Marangoni and

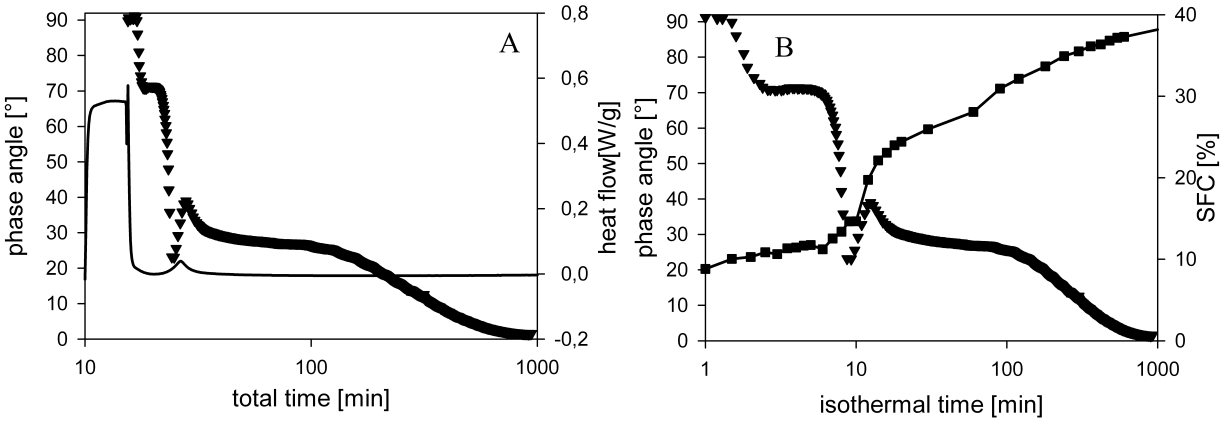

Figure 3.3: Overlay of the phase angle δ (▼) recorded by oscillatory rheology and (A) the heat flow (−) recorded with DSC and (B) the SFC (■) recorded with pNMR during palm oil crystallization at 18°C

Rousseau 1998a), palm oil, lard, cocoa butter, SalatrimTM and tallow (Marangoni and Rousseau 1998b; Marangoni and Rousseau 1998a; Narine and Marangoni 1999a; Narine and Marangoni 1999d) blended with canola oil, it was demonstrated that although the polymorphic nature and the solid fat content of the interesterified and non-interesterified fat system-canola oil blends were essentially the same, the rheological properties were very different. These results implicated that the mechanical strength of fat crystal networks is not only determined by the solid fat content but also by the microstructure. Singh et al. (2004) reached the same conclusion based on their experiments on enzymatically interesterified hydrogenated palm oil and partially hydrogenated palm oil. Their results suggested that the dynamics of structure formation are a key factor in influencing macroscopic properties of palm oil based fats. Furthermore, DSC is only capable of measuring primary crystallization under static crystallization conditions, while oscillatory rheology can also be used to follow the whole crystallization process under stirred process conditions and this with one single geometry.

The crystallization curve obtained by pNMR is compared with the phase angle curve in Figure 3.3B. The pNMR-curve represents the average of three measurements. The pNMR data lead to the same conclusion as the DSC results: primary crystallization of palm oil at 18°C occurs in two steps. As for the DSC results, the two steps in pNMR data also coincide more or less with the steps visible in the phase angle curve. In contrast to DSC,

the pNMR data show a slightly increasing trend throughout the whole measurement. This could be explained by a further crystallization of the network and may be related to the increase in complex modulus (Figure 3.2A).

Walstra (1987) already pointed out that ongoing crystallization and particularly recrystallization cause a growing together or sintering of the flocculated crystals, thereby greatly enhancing the strength of the bonds in the network, as can be seen by an increase of the elastic modulus. A specific study was done by Johansson and Bergensthl (1995), who made dispersions of crystals of pure triacylglycerols in oil. These aggregated to form a network, but did not show significant sintering. They also studied the effect of adding small amounts of crystallizable triacylglycerol mixtures. These mixtures were found to cause considerable sintering, as measured for instance by an increase in storage modulus. Sintering occurred if the newly added triacylglycerols crystallized in the same polymorph and if the melting point of the solution was below that of the original crystals. Sintering can already occur in a very early stage.

3.4 Conclusions

It was demonstrated that oscillatory rheology is a valuable complementary method to DSC and pNMR to measure primary crystallization under static processing conditions. Like DSC and pNMR, oscillatory rheology was found to be capable of differentiating whether crystallization occurs in a two-stage or single-stage process. Furthermore, oscillatory rheology offers the advantage that primary crystallization, microstructural development and macroscopic properties can be evaluated by one single analysis. The more classically used techniques like pNMR and DSC do not provide any information on aggregation or the crystal network formed.

Chapter 4

A microstructural approach on the isothermal crystallization of palm oil

Time is an illusion. Lunch time doubly so
The hitchhiker's guide to the galaxy - Douglas Adams (1952-2001)

4.1 Problem statement and research strategy

A lot of food products contain a substantial amount of fat, of which a significant part is present in the crystallized form. The final properties of the products are largely influenced by the physicochemical properties of the product components and the processing conditions. Many of the sensory attributes such as spreadability, mouth feel, snap of chocolate, texture etc. are dependent on the mechanical strength of the underlying fat crystal network (Narine and Marangoni 1999c; Narine and Marangoni 1999e; Foubert 2003). Thorough knowledge of the microstructure, obtained by microscopic techniques, in relation to the physicochemical characteristics and the macroscopic properties can offer new ways to improve existing products and to design new ones (Heertje 1993). Many microscopic techniques are available to study food microstructure, such as light microscopy (LM), electron microscopy (EM) and confocal scanning laser light microscopy (CSLM).

4.1.1 Research strategy

In this chapter, palm oil was isothermally crystallized at four different temperatures (18, 20, 22 and 25°C). DSC and pNMR were used to study the primary crystallization, including nucleation and crystal growth. In contrast, oscillatory rheology provided information on both primary crystallization and microstructural development. PLM and CSLM were used to probe the microstructure. The aim of this research was thus to gain more insight in the microstructural arrangement of crystallizing palm oil and the influence of crystallization temperature thereon.

4.2 Methods and Materials

4.2.1 Substrate

Refined, bleached and deodorized palm oil with an iodine value of 51 was obtained from De Smet Ballestra (Zaventem, Belgium) and stored in the freezer at -24°C until analysis. Table 4.1 displays the fatty acid composition as determined by gas chromatography according to the AOCS official method Ce 1-62. The triacylglycerol composition obtained by reversed-phase HPLC with ELSD detector (Rombaut et al. 2008) is shown in Table 4.2

Table 4.1: Fatty acid composition (%) (average and standard deviation of duplicate measurements)

C12:0	C14:0	C16:0	C16:1	C18:0	C18:1	C18:2	C18:3	C20:0
0.25	1.05	46.66	0.19	4.25	37.71	9.06	0.10	0.33
± 0.01	± 0.01	± 0.01	± 0.01	± 0.02	± 0.01	± 0.04	± 0.02	± 0.01

Table 4.2: Triacylglycerol composition (%) (average and standard deviation of duplicate measurements)

OLL	PLL	LOO	PLO	PLP	OOO
0.12	1.16	1.09	10.36	8.61	3.08
± 0.00	± 0.00	± 0.01	± 0.04	± 0.00	± 0.02

POO	POP+PLS	PPP+SOO	POS	PPS	SOS
25.25	33.95	8.47	5.377	0.76	0.33
± 0.01	± 0.13	± 0.05	± 0.02	± 0.00	± 0.01

4.2.2 pNMR

pNMR experiments were performed with a Minispec pc 20 (Bruker, Karlsruhe, Germany) according to the procedure described in section 3.2.4. Each analysis was executed in triplicate.

4.2.3 DSC (stop-and-return)

The isothermal crystallization curves were obtained with a TA Q1000 DSC (TA Instruments, New Castle, Delaware) with a Refrigerated Cooling System. The DSC was calibrated with indium (TA Instruments, New Castle, Delaware), azobenzene (Sigma-Aldrich, Bornem, Belgium) and undecane (Acros Organics, Geel, Belgium) before analyses. Nitrogen was used to purge the system. Melted fat (5-15 mg) was sealed in hermetic aluminum pans and an empty pan was used as a reference. The applied time-temperature program for the isothermal crystallization curves was as follows: holding at 70°C for 10 minutes to ensure a completely liquid state, cooling at 10°C /min to the appropriate crystallization temperature, holding for a given crystallization time and then heating at 20°C /min to 70°C. The crystallization time was varied in different experiments prior to remelting. The

area of the melting peak, which corresponds to the melting enthalpy, increased with increasing time at the particular crystallization temperature, proportional to the degree of crystallinity, developed after a given time lapse. Accordingly, the degree of crystallinity as a function of time at the crystallization temperature could be determined (Foubert et al. 2008).

4.2.4 Oscillatory rheology

Oscillatory rheology was applied to study the isothermal crystallization of palm oil 18, 20, 22 and 25°C. The geometry and settings as well as the applied temperature-time profile used in these experiments are described in section 3.2.2.

4.2.5 Polarized light microscopy (PLM)

Microscopic analyses were conducted with a Olympus BHS microscope (Olympus Belgium N.V., Aartselaar Belgium) equipped with a Linkam TMS 600 hot stage and a Linkam TMS 91 controller (Linkam, Surrey, United Kingdom). A droplet of liquid fat was applied to the carrier glass and covered with a cover slide. Subsequently, the sample was heated up to 80°C and kept at this temperature for 10 min to erase all crystal memory. In a next step, the sample was cooled down to the selected crystallization temperature at 10°C / min. Finally, the sample was kept isothermally at the selected crystallization temperature. The samples were imaged at magnification 100x at a 15s time interval with a JVC TK-C138 color video camera and the obtained data were stored with Leica Qwin software (Leika, Germany).

4.2.6 Confocal scanning laser microscopy (CSLM)

Palm oil was melted at 70°C and 0.02 wt % Nile blue and 0.0001 wt % Nile red were added. As reported by Herrera and Hartel (2000a) this dye system did not modify the nucleation kinetics when induction times were measured with turbidimetry. Nile blue was used to negatively stain the fat crystals. This lipophilic stain diffused into the oil phase and generates a deep yellow fluorescence, whereas the solid fat does not fluoresce, hence enhancing the contrast between crystal and background (Heertje et al. 1990). By using Nile red the crystal structures are more defined and the laser source can be used at lower

power, thus preventing the sample from melting or the dyes from burning. The sample with the dyes was kept at 70°C overnight to allow the dyes to dissolve. Afterwards, a droplet of the fat sample was placed on an objective slide and a cover slide was placed on top. The sample was then subjected to the same temperature-time profile as in the rheological and polarized light experiments. The samples were examined with a laser scanning confocal fluorescence microscope (Bio-Rad Radiance 2100, AGR-3Q AOTF, Hertfordshire, U.K.), attached to a Nikon Eclipse E800 upright microscope. The argon laser beam was set at 488nm excitation and 500nm long-pass emission filter. The images were acquired with a 60x (1.20 NA, WI Plan Apo, water immersion) objective, using the software LaserSharp2000 (Bio-Rad, Hermel Hempstead, U.K.).

4.3 Results and discussion

4.3.1 Isothermal crystallization behavior as measured by pNMR

Figure 4.1 presents the solid fat content (SFC) as a function of isothermal time for palm oil crystallizing at 18, 20, 22 and 25°C . The SFC increased faster and steeper when lower crystallization temperatures were applied. In addition, at all times higher SFC-values were recorded for lower crystallization temperatures. Based on Figure 4.1, it can also be inferred that, depending on the crystallization temperature, primary crystallization occurs via different mechanisms. The crystallization curves obtained at 18, 20 and 22°C clearly indicate that at these temperatures primary crystallization is a two-step process. In a first step, the SFC increased without a considerable induction time to reach a first plateau. After some time, the SFC again increased drastically in a second step and finally leveled off to a second plateau. In general, a two-step primary crystallization mechanism can be due to a polymorphic transformation, a fractionated crystallization or a combination thereof. In contrast, the solid fat content for crystallization at 25°C only displayed a single increase following an appreciable induction period.

4.3.2 Stop and return experiments by DSC

Figure 4.2 presents the melting curves of palm oil crystallized at 18, 20, 22 and 25°C. At 18, 20 and 22°C the endotherm clearly displays two minima (or negative peaks). At 18°C (Figure 4.2 A) the first peak, with a peak maximum at 29°C, was already present

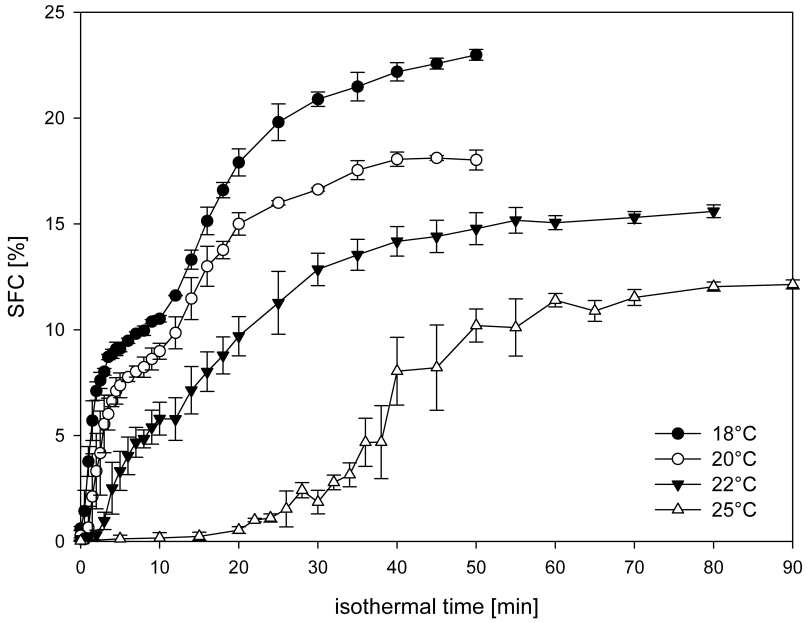

Figure 4.1: SFC as a function of isothermal time at various crystallization temperatures (average of three repetitions)

after 1 min of crystallization and gradually decreased at later times, with the second peak appearing as the first one decreased. From 10 min onwards, only the second peak prevailed. The peak maximum then shifts to 35°C, indicating a change to a higher melting polymorph. Additionally, a shoulder can be observed at higher temperatures, indicating the crystallization of the higher melting triaccylglycerols directly into the β' form. This shoulder is incorporated into the main peak as crystallization proceeds. Palm oil is known to exhibit a two-step crystallization below a certain cut-off temperature, depending on composition. Below this cut-off temperature palm oil is suggested to undergo an α mediated β' crystallization, while at higher temperatures β' crystals are directly formed from the melt (Chen et al. 2002; Mazzanti et al. 2005). The first peak in Figure 4.2 A might thus be attributed to the α polymorph and the second peak to the β' polymorph, possibly with extra β' formation directly from the melt.

The time frame of these events is visualized more clearly in Figure 4.2 E, where the peak depths (or intensity) of different peaks are plotted as a function of the isothermal time. Peak 1 corresponds with the formation of α crystals, peak 2 with the formation of β' crystals and peak 3 with the crystallization of the higher melting fraction directly into β'.

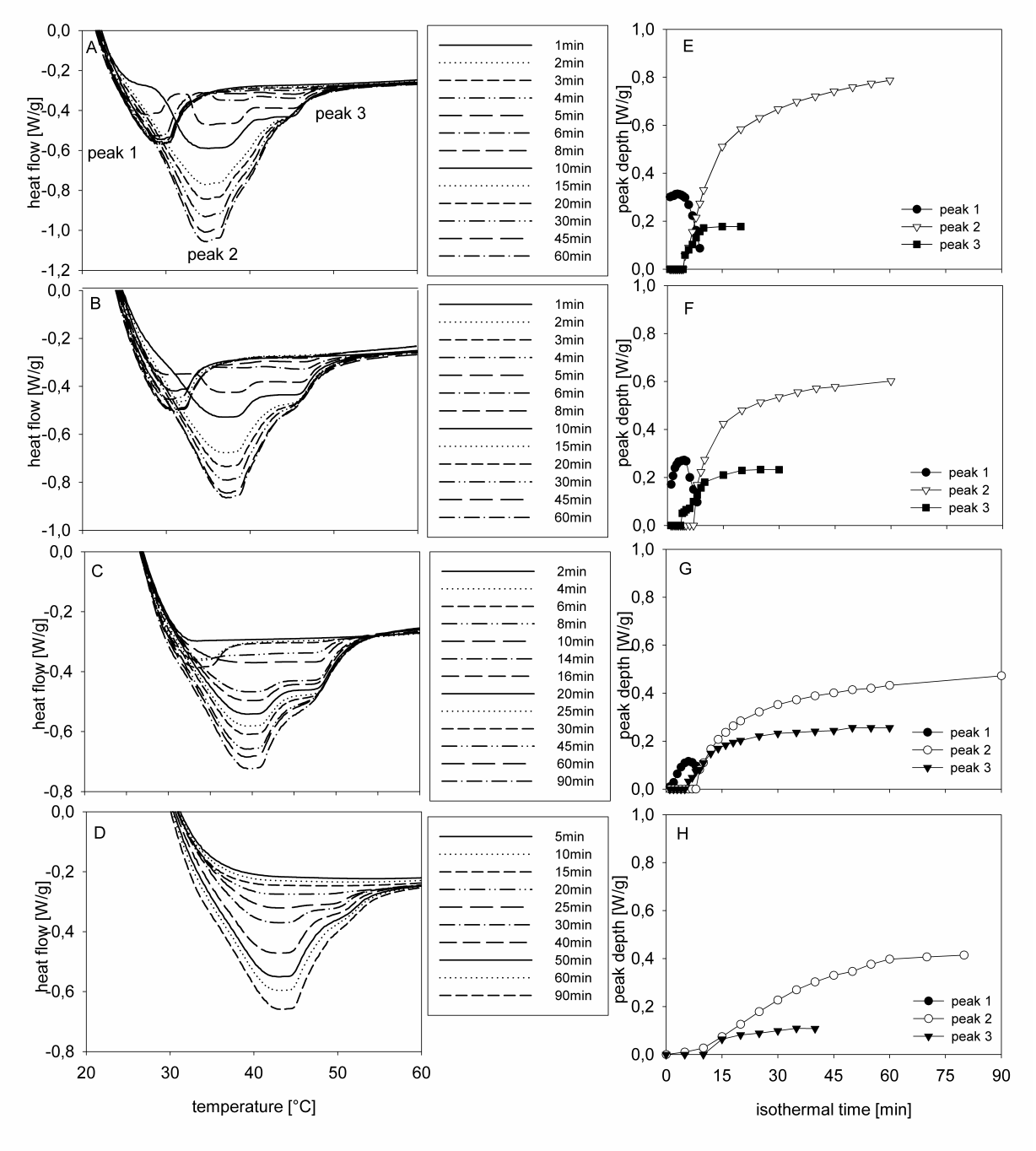

Figure 4.2: Melting curves of palm oil crystallized at (A) 18, (B) 20, (C) 22 and (D) 25°C (exo up) and peak depth as a function of isothermal time for (E) 18°C, (F) 20°C, (G) 22°C and (H) 25°C. Peak 1 corresponds with the formation of α crystals, peak 2 with the formation of β' crystals and peak 3 with the crystallization of the higher melting fraction directly into β'. (Note that single measurements have been done.)

As the intensity of peak 1, which is connected to the evolution of the α form, decreases, the intensity of peak 2 starts to increase, indicating the transformation from α to β' and additional β' formation from the melt. At the same time, peak 3 appears at the higher temperature side. As this shoulder is incorporated into peak 2, the intensity reaches a plateau value. The intensity of the second peak levels of as crystallization proceeds.

At 20 and 22°C (Figure 4.2 B and E, C and F), the same events were observed. After 1 min of isothermal crystallization at 20°C, a first peak at the lower temperature side was already present. Similar to 18°C, this first peak, with peak maximum at 31°C, gradually decreased while a second peak was formed. At the same time, a shoulder appeared at the higher temperature side, indicating the crystallization of higher melting triacylglycerols. After 9 min, the first peak had disappeared completely and only the second peak, with a peak maximum at 37°C remained. The shoulder at the higher temperature side (peak 3 in Figure 4.2 E) is gradually incorporated in largest peak (peak 2). At a crystallization temperature of 22°C (Figure 4.2 C and F), a less pronounced peak with peak maximum at 33.5°C existed between 2 and 8 min isothermal time. The second peak (peak maximum = 39.5°C) was formed at the expense of this lower melting peak. Beyond 8 min isothermal time only the higher melting peak was observed. At the higher temperature side, a shoulder (peak 3 in Figure 4.2 F) is formed that is gradually incorporated into the second peak.

However, the melting curve for palm oil crystallization at 25°C displayed only one peak with a small shoulder on the higer temperature side and a peak maximum at 43°C, indicating direct crystallization from the melt into the more stable polymorph β' (Figure 4.2 D and H). At this temperature only the peak 2 and peak 3 were detected as no α crystals are formed at this temperature. The larger induction time for crystallization at 25°C compared to 18°C can be explained by the decrease in driving force for nucleation due to lower supercooling. Also, since at 25°C no α phase is developed and no α to β' transition occurs, β' nucleation takes longer because the only mechanism possible is direct crystallization from the melt.

4.3.3 Isothermal crystallization behavior as measured by oscillatory rheology

The isothermal crystallization at the different crystallization temperatures was also investigated with oscillatory rheology. As pNMR and DSC provide information on primary crystallization only, oscillatory rheology provides information on all three steps of the crystallization process, namely primary crystallization, microstructural development of the fat crystal network and macroscopic properties (see Chapter 3). The fat crystal network is formed by the aggregation of fat crystals through van der Waals attraction (Kloek 1998; Walstra et al. 2001), which finally results in the formation of a continuous three-dimensional network. As a consequence of simultaneous crystallization and aggregation, a continuous network is already formed, while a substantial amount of fat still has to crystallize. This generally leads to sintering, i.e. the formation of solid bridges between aggregated crystals and aggregates (Kloek 1998). The number, size and shape of the particles and large clusters will define the microstructure, which will in turn determine the macroscopic properties of the fat (Marangoni 2002a).

The complex modulus as a function of isothermal time at the various crystallization temperatures is displayed in Figure 4.3. The point at which the complex modulus starts to increase can be considered as the onset of crystallization, which occurs at later isothermal times for higher crystallization temperatures. At 18 and 20°C, the complex modulus displays an initial plateau (during the induction time), followed by a first shallow increase (crystallization onset) and later a second increase with a steeper slope, after which the complex modulus further increases again at a shallower rate. The situation is less clear 22°C. At this temperature, the first increase is barely visible. At 25°C a much longer initial plateau can be observed, followed by a single step increase before the complex modulus levels off.

The increase in complex modulus is not only due to the primary crystallization, but also to microstructural development by aggregation. These two processes cannot be completely separated. Walstra (1987) already pointed out that ongoing crystallization and particularly recrystallization cause a growing together or sintering of the flocculated crystals, thereby greatly enhancing the strength of the bonds in the network, which can be

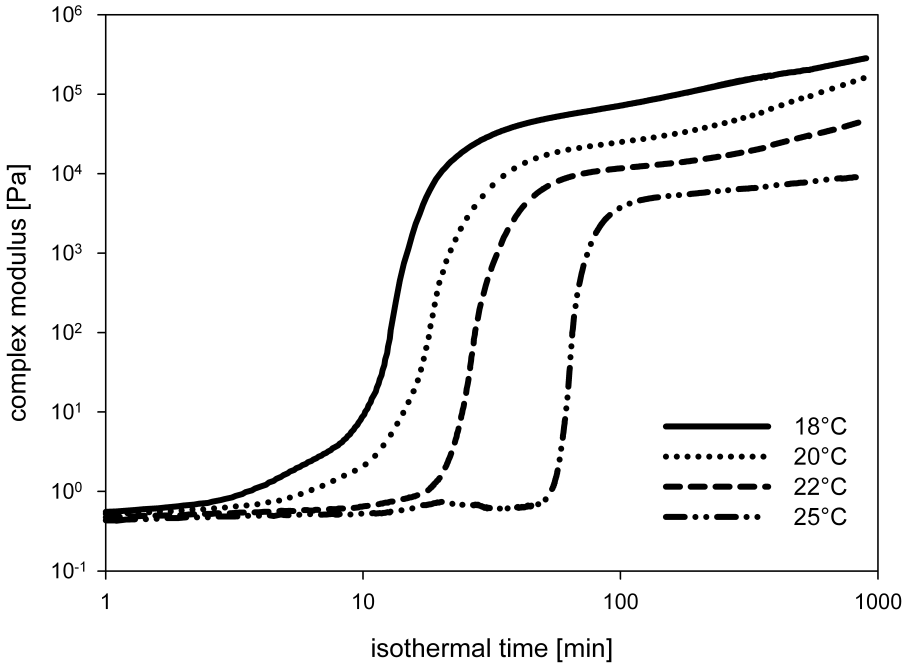

Figure 4.3: Complex modulus for isothermal crystallization of palm oil at 18, 20, 22 and 25°C

seen as an increase in complex modulus. Sintering can already occur at a very early stage (Johansson 1995). Figure 4.3 clearly shows higher complex modulus values for crystallization at lower temperatures, thus implicating that lower crystallization temperatures result in stiffer networks.

Compared to DSC and pNMR, oscillatory rheology shows a longer induction period. For instance, at 25°C the SFC started to increase after 20 min isothermal time, while oscillatory rheology only showed a significant increase after 50.9 ± 7.9 min. At the same time, DSC already provided clear melting curves after 25 min isothermal crystallization. This may indicate lower sensitivity for detecting the onset of crystallization by rheology compared to pNMR and DSC. However, it must be kept in mind that differences in sample weight or volume, equipment design, heat and mass transfer conditions may affect crystallization. In any case the three techniques commonly revealed the two-step character of the crystallization at 18, 20 and 22°C while at 25°C crystallization happens in a one-step process.

4.3.4 Visualization of the microstructure by polarized light microscopy

For crystallizing at 18 and 20°C, no induction period was detected by polarized light microscopy. The optical plane was already completely filled with small crystals suspended in the remaining liquid fat upon reaching the isothermal crystallization temperature, indicating that crystallization already started during the cooling step. During the following isothermal period no visible changes in microstructure took place. Figure 4.4A shows the microstructure of palm oil crystallized at 18°C for 40 min, which is representative for the complete isothermal period. Figure 4.4 B shows the microstructure for crystallizing 60 min at 20°C, which is also representative or the entire isothermal period. The major difference between these microstructures is the amount of liquid fat present between the crystals: more liquid fat remains when crystallizing at 20°C.

Upon reaching 22°C, some crystals were already visible in the liquid fat. With increasing isothermal time at 22°C, these crystals rapidly grew in size and new crystals appeared. After 5 min no further changes could be observed. Hence, the microstructure at 60 min isothermal time shown in Figure 4.4C is representative for the microstructure is representative for the microstructure irrespective of the time lapse following the initial 5 min. Compared to 18 and 20°C, the microstructure at 22°C showed considerably larger aggregates suspended a larger portion of remaining liquid fat.

At a crystallization temperature of 25°C , the first detectable crystals appeared around 3 min isothermal time. At this point, very few crystals were present in the liquid fat matrix and the amount of crystals did not change until after 12 min isothermal time when new crystals appeared. The crystals were of spherulitic nature with the crystals oriented along the spherulite radius, as was evidenced by the characteristic Maltese cross pattern. With time more material crystallized onto these spherulites but the associated birefringence was poor due to the overgrowth of randomly oriented crystals. After 120 min, large crystal clusters or aggregates were present in the remaining liquid fat as can be seen in Figure 4.4 D. Compared to the lower crystallization temperatures, the final crystal structures obtained at 25°C appeared to be less birefringent, except for the central part of the clusters.

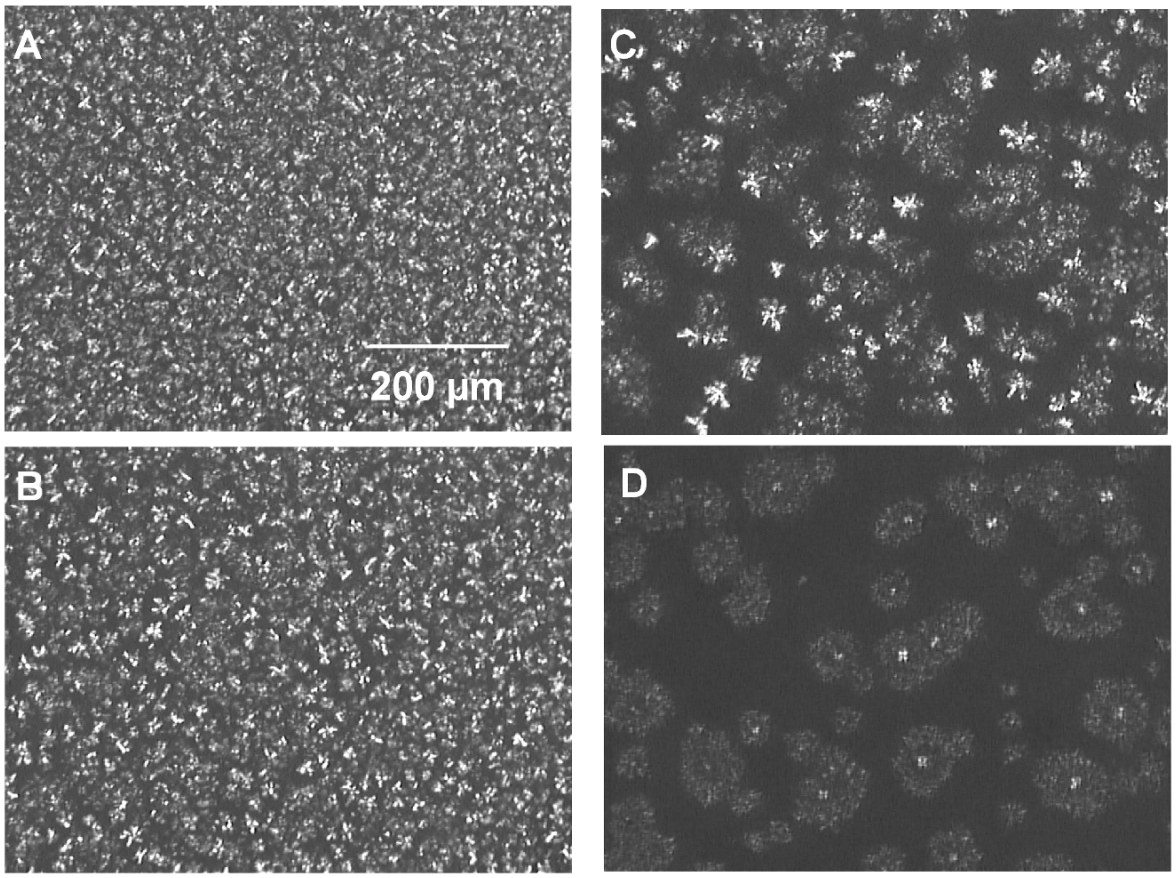

Figure 4.4: PLM of palm oil crystallizing for (A) 40 min at 18°C, (B) 60 min at 20°C, (C) 60 min at 22°C and (D) 120 min at 25°C

When comparing the PLM images, it becomes clear that the crystallization temperature has a large effect on the microstructure. For 18 and 20°C, similar microstructures are obtained: small crystals are quite uniformly distributed in the remaining liquid fat matrix. The major difference in microstructure at these temperatures lies in the presences of more liquid fat between the crystals at 20°C compared to 18°C. This observation corresponds to the lower SFC-values obtained at 20°C as was shown in Figure 4.1 and consequently to the lower complex modulus as indicated in Figure 4.3. Larger differences can be seen when considering the microstructures obtained at 22 and 25°C: fewer but larger crystal structures are formed and considerably more liquid fat can be observed in between these crystal structures. Crystallization at 25°C gave rise to a completely different microstructure. A possible explanation can be found in the DSC melting profiles shown in Figure 4.2. At 18, 20 and 22°C an α mediated β' crystallization was observed while at 25°C direct

crystallization in the β' form took place. As can be seen in Figure 4.2, the area under the melting curves that could be attributed to the α-polymorph and the associated time interval, decreased with increasing crystallization temperature and was very limited at 22°C, both in size and in duration. In this respect, the microstructure at 22°C might be considered as a 'transition structure' between the small aggregates at 18°C and 20°C, and the large aggregates at 25°C. In addition, the PLM data revealed that the polymorphic transformation from α to β' which is known to occur at 18, 20 and 22°C, did not result in a drastic change in crystal morphology. This observation is in agreement with the conclusions of Litwinenko et al. (Litwinenko et al. 2002) who used PLM to study the crystallization of palm oil based shortenings.

4.3.5 Visualization of the microstructure by confocal scanning laser microscopy

To gain more insight into the microstructure, the crystallization process was also monitored with confocal laser scanning microscopy (CSLM). The dyes are only soluble in the liquid fat; therefore the liquid fat will appear as white zones while the dark zones are the solid structures which do not fluoresce.

Figure 4.5 displays confocal microscopy images of palm oil crystallizing at 18°C for various isothermal times. Immediately upon reaching the crystallization temperatures, numerous small needle-like crystal structures appeared in the liquid fat matrix. These crystals grow in a feather like style (Figure 4.5 A). As crystallization continued, clearly distinct spherulitic structures can be appreciated from which tenuous filaments protrude. Via these filaments, the individual spherulitic structures interact and form aggregates (Figure 4.5 B-D). Figure 4.5 E shows that after 16h isothermal crystallization the microstructure is composed of a delicate crystal network in which larger crystalline structures are embedded. Tenuous filaments extend outwards from a core-structure and interact with the surrounding larger crystal structures. This can be observed in detail in Figure 4.5 F. Despite the limited amount of solid fat (Figure 4.1), a continuous network structure can be observed. The high complex modulus values (Figure 4.3) for palm oil crystallizing at 18°C can be explained by the numerous small crystals structures each interacting with their neighbors, leading to a strong network.

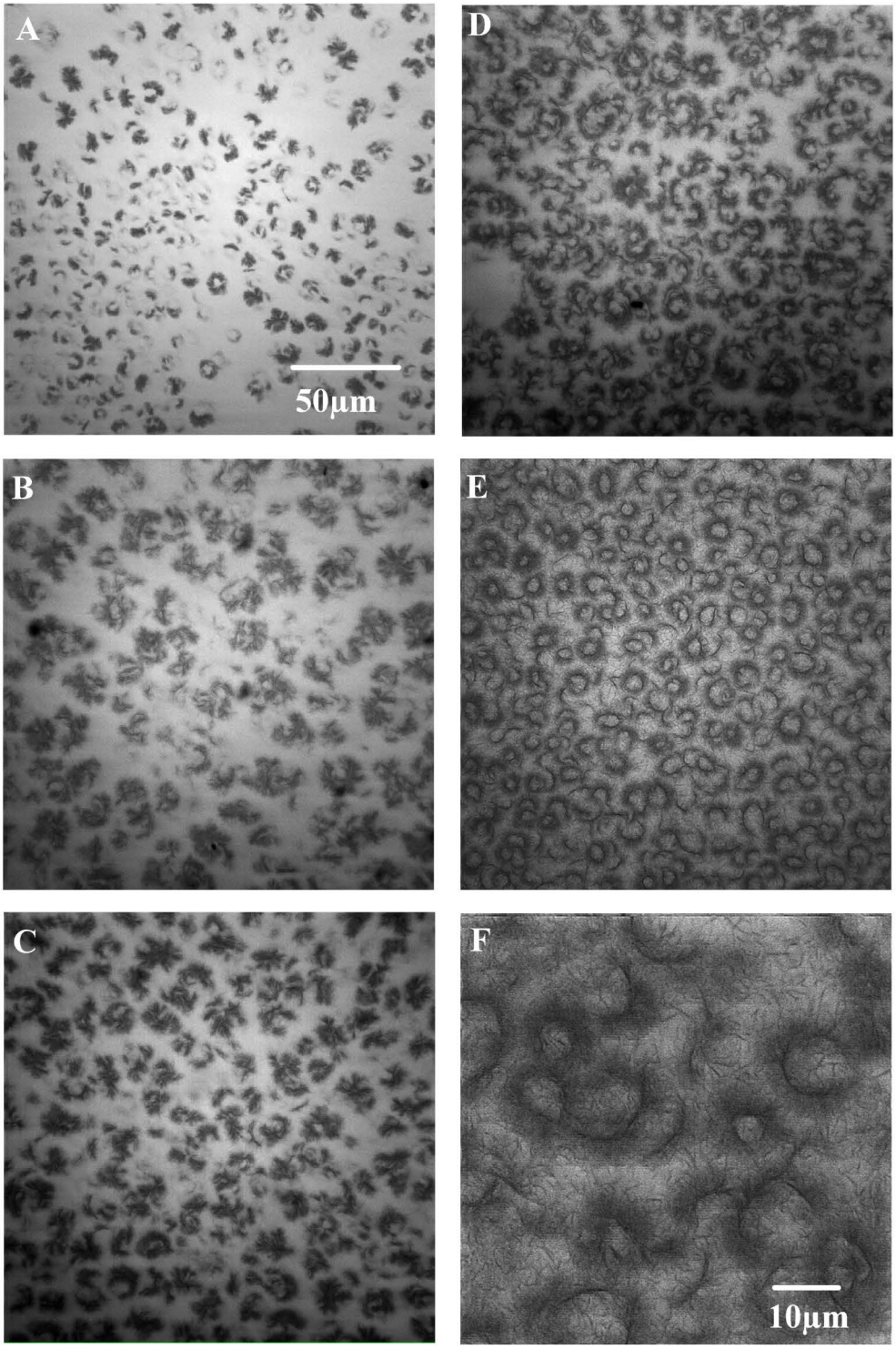

Figure 4.5: CSLM images of isothermal palm oil crystallization at 18°C during (A) 1 min, (B) 20 min, (C) 60 min, (D) 193 min and (E,F) 16 hours (A-E: 60x, F: 180x magnification)

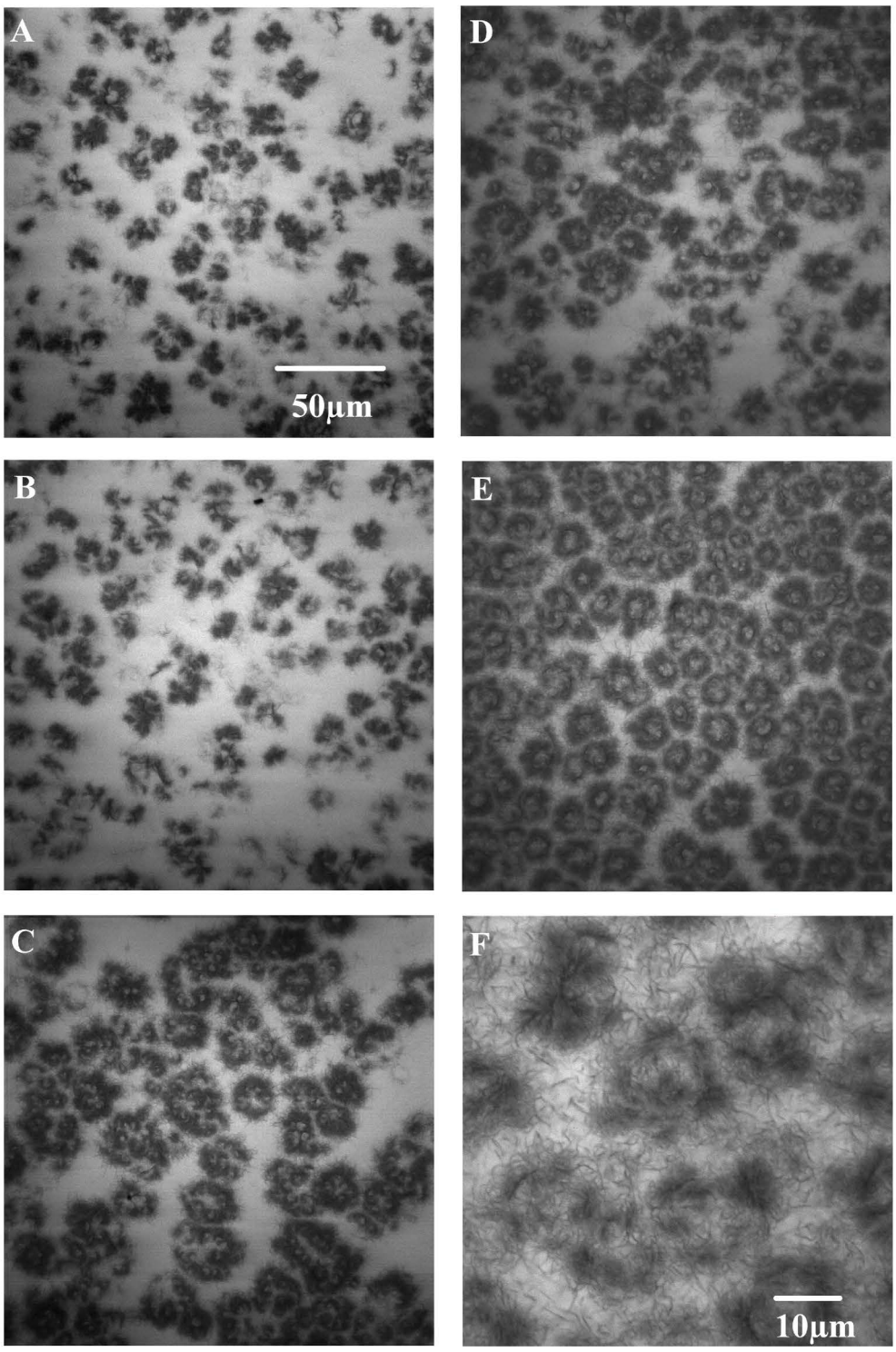

Figure 4.6: CSLM images of isothermal palm oil crystallization at 20°C during (A) 30 min, (B) 65 min, (C) 190 min, (D) 310 min and (E,F) 16 hours (A-E: 60x, F: 180x magnification)

At 20°C, the microstructural development is quite similar compared to the one at 18°C as is shown in Figure 4.6. Starting from feather-like structures, larger crystalline particles are formed from which thin filaments originate. As crystallization proceeds, aggregates and eventually a network is formed through interfilament interactions. Similar to 18°C, tenuous filaments originate from a denser core connecting the individual aggregates and thus forming a crystal network structure. However, some differences can be observed when comparing to the microstructure at 18°C. At 20°C, more liquid fat is present between and in the porous aggregates, corroborating the solid fat content data (Figure 4.1). In addition, the aggregates are larger and denser when crystallizing at 20°C. It can thus be concluded that at 20°C, less crystalline material is present, concentrated in fewer aggregates. Consequently, larger gaps exists between the aggregates, which have to be bridged by the thin crystal filaments as is clearly shown in Figure 4.6 E and F, and which results in less stiff network compared to at 18°C, as can be deduced from the complex modulus values (Figure 4.3.

An overview of the crystallization at 22°C is given in Figure 4.7. Crystallization proceeded more slowly at 22°C as fewer nuclei were formed in the liquid fat matrix. These nuclei developed to dense crystal cores form which, like at 18 and 20°C, filaments originate. The crystal structures aggregate to larger particles due to interactions via the filaments and compared to 18 and 20°C more liquid fat remains, as could be anticipated based on the solid fat content (Figure 4.1). It can also be seen that the amount of filaments increased strongly at longer isothermal times and that the final microstructure is made up of large aggregates which are loosely connected via the filaments. These large aggregates are suspended in the liquid fat matrix and are constructed of several crystal structures embedded in a large amount of tenuous filaments. This type of crystal network is weaker (less stiff) compared to the networks obtained at 18 and 20°C, as can be deduced from the complex modulus values in Figure 4.3.

At 25°C (Figure 4.8), fewer crystals were initially formed and these grew into larger crystal structures without the further generation of new crystals from the liquid. The most noticeable difference compared to the lower crystallization temperatures, apart from the degree of crystallinity, lies in the size and structure of these crystals. They are markedly

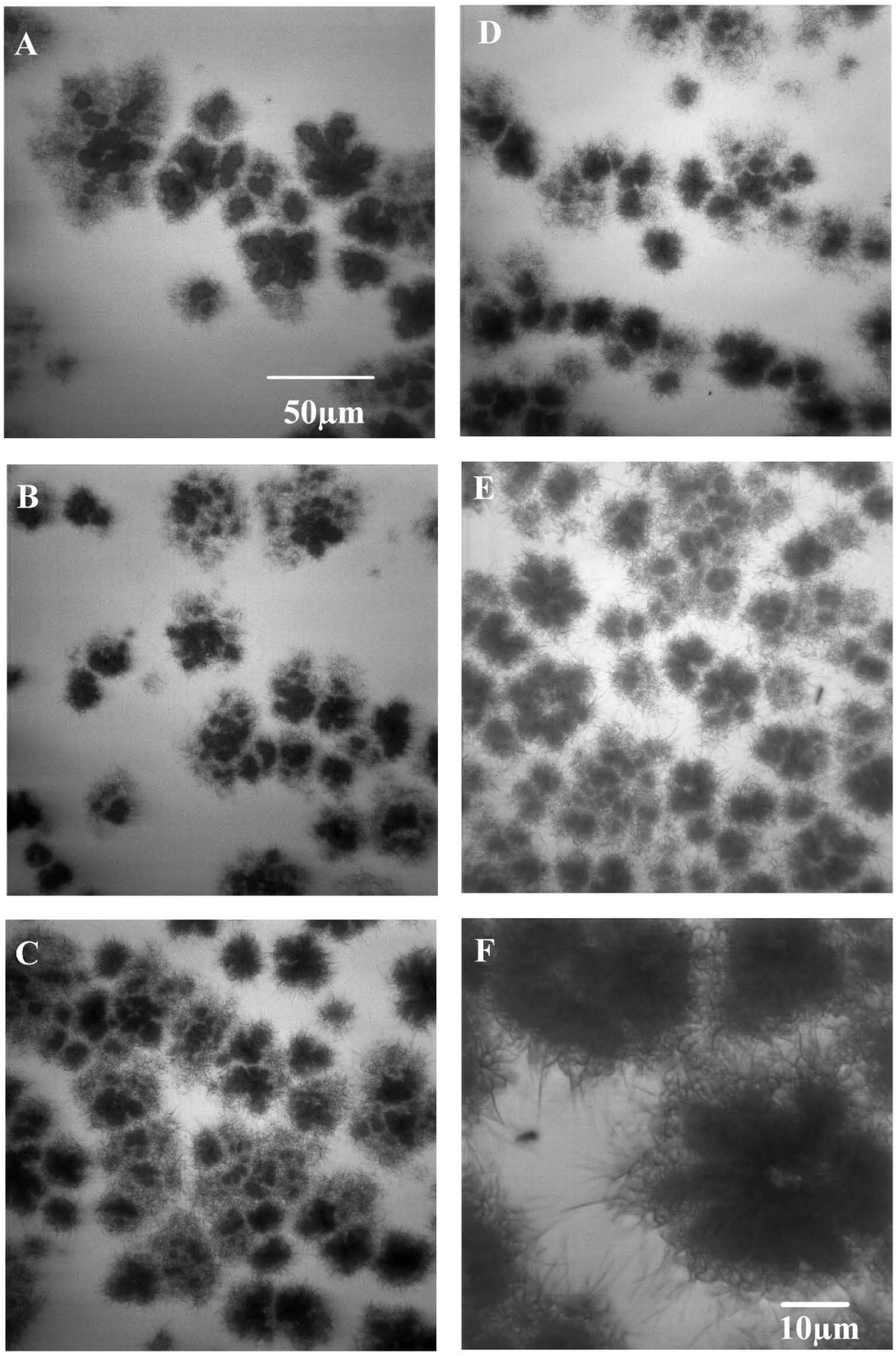

Figure 4.7: CSLM images of isothermal palm oil crystallization at 22°C during (A) 30 min, (B) 70 min, (C) 180 min, (D) 307 min and (E,F) 16 hours (A-E: 60x, F: 180x magnification)

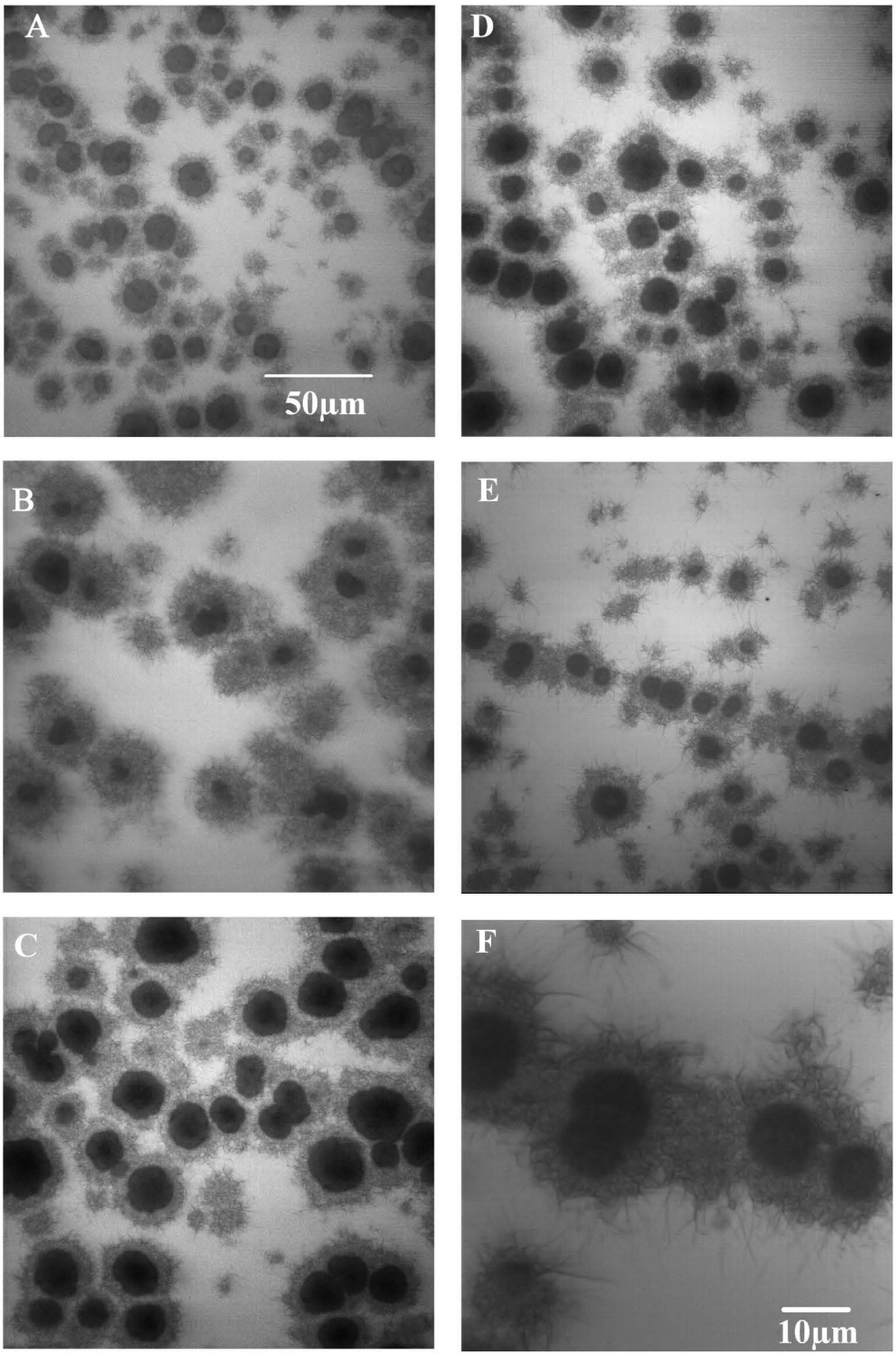

Figure 4.8: CSLM images of isothermal palm oil crystallization at 25°C during (A) 30 min, (B) 60 min, (C) 100 min, (D) 160 min and (E,F) 16 hours (A-E: 60x, F: 180x magnification)

larger with a much denser core structure. In addition, these crystals structure display a more regular shape as can be seen in Figure 4.8 A. These dense, round crystals structures are surrounded by a rather dense filamentous layer, which is quite similar to the observations at 22°C. Via these filaments crystals interact and aggregates are formed (Figure 4.8 B, C). In addition, these filaments also ensure the formation of a network structure (Figure 4.8 D, E), although a large portion of the fat is still present in the liquid state. The SFC-profile (Figure 4.1) already indicated that at 25°C about 12% solid fat was achieved after 90 min isothermal crystallization. Although the interactions between the aggregates at 22°C and 25°C appear similar, as visualized in Figure 4.7 F and Figure 4.8 F, lower complex modulus values were found at 25°C (Figure 4.1). Taking into account the CSLM-images, this can be explained by the lower amount of crystals and more importantly the fewer interacting bridges between these crystals.

4.4 Conclusions

Two different crystallization mechanisms were found for palm oil crystallizing at different temperatures: at 18, 20 and 22°C crystallization was an α mediated β' crystallization while at 25°C crystallization took place directly in the β' polymorph. These observations are in agreement with previous studies, reporting a cut-off temperature above which the crystallization process changes from a two-step to a one-step process. Oscillatory rheology showed that lower complex modulus values and thus lower network strength were obtained at higher crystallization temperatures. This is not only due to the smaller solid fat content at higher crystallization temperatures. Differences in microstructure have to be taken into account as well. At lower crystallization temperatures the fat crystallizes quickly, leading to the formation a large number of small crystals. When these crystals start to aggregate, a very compact network structure is formed, giving rise to a high modulus. At higher crystallization temperatures, fewer but larger crystals are generated that grow more slowly. As a result a looser network structure is formed, leading to a lower complex modulus. In addition, CSLM revealed that at lower crystallization temperatures, more bridging crystalline filaments exists that bridge the crystalline aggregates through the remaining oil fraction. Furthermore, using CSLM the fat crystal network is clearly visualized an detailed structures can be observed. While in this research the use of CSLM is was purely descriptive, the chanmmene for future research will be to use the CSLM approach to further

quantatively unravel the fat crystal network.

Chapter 5

Development of a rheological method to characterize palm oil crystallizing under shear[1]

There is nothing like looking, if you want to find something. You certainly usually find something, if you look, but it is not always quite the something you were after.
Lord of the rings - J.R.R. Tolkien (1982-1973)

[1]This chapter has been published in:
De Graef, V., B. Goderis, P. Van Puyvelde, I. Foubert and K. Dewettinck (2008). Development of a rheological method to characterize palm oil crystallizing under shear, European Journal of Lipid Science and Technology 110, 521-529.

5.1 Problem statement and research strategy

Shearing during the crystallization process of fats and fat rich products can have different effects. On the level of primary crystallization, shear can enhance nucleation and accelerate polymorphic transitions (Wesdorp 1990). Shear can also induce orientation in crystallizing fats (Mazzanti et al. 2003; Mazzanti et al. 2005). Furthermore, it can cause fracture of crystals, leading to smaller crystals. Aggregation is also affected by shear. Fat crystals attract each other due to van der Waals forces and, under static conditions, meet due to Brownian motion. Shear increases the collision frequency to an extent proportional to the shear rate. Above a critical shear rate, which depends on particle size and viscosity, collision of crystals due to shear dominates over that caused by Brownian motion (Kloek et al. 2005). Aggregating crystals tend to form voluminous aggregates with a volume much greater than the total volume of the primary crystals, causing viscosity to increase. However, increasing shear rate may cause aggregates to break up because of the shear forces acting upon them. Furthermore, shear may also induce internal rearrangement of the aggregates which, as a result, may become more compact (Kloek 1998; Walstra et al. 2001). If the aggregates have grown so far that a space-filling network has been formed, application of shear can break up the network and lead to internal rearrangement of the fragments. The solid bridges formed due to sintering can also be broken by the application of shear, and the resulting network fragments are attracted to each other by van der Waals forces. Such a change of prevailing interaction between structural elements can have a marked effect on the macroscopic properties of fats (Kloek et al. 2005).

Mazzanti et al. (2003, 2004a, 2005) used time resolved X-ray diffraction to assess the influence of various shear rates on the crystallization of palm oil, cocoa butter, milk fat and stripped milk fat. Sonwai and Mackley (2006) and MacMillan and Roberts (2002) used the same technique to elucidate the effect of various shear rates on the polymorphic transitions in cocoa butter. However, XRD only provides information on primary crystallization, and thus not on large-scale aggregation processes. Furthermore, the need for synchrotron radiation to perform these time resolved experiments makes this technique not suitable for everyday use. Herrera and Hartel (2000b) applied dynamic mechanical analysis (DMA) to evaluate the effect of shear, cooling rate, crystallization temperature, chemical composition and storage time on the complex, storage and loss moduli of a milk

fat model system. However, in this research the samples were crystallized in a separate vessel with mixer and subsequently transferred to the DMA-apparatus. Moduli were thus determined on the solid product, not as a function of time but as a function of frequency. Therefore, only the effect of shear on the final solid product and not on the complete crystallization process (primary crystallization, microstructural development, macroscopic properties) could be assessed.

Rheology is frequently used to evaluate an end product obtained under certain processing conditions (time, temperature, and shear rate) in terms of elastic and loss modulus. Few authors, however, have used oscillatory rheology to determine the moduli and phase angle as a function of time under shear conditions. In polymer science, parallel superposition rheology is used to measure these variables under shear. In this technique shear is superposed onto the oscillation and this superposition can cause interference from one motion on the response of another. If the amplitude of oscillation is sufficiently low, however, a linear region can be observed in which the parallel superposition moduli are independent of amplitude, and the oscillation can be regarded as a linear perturbation of the steady shear. In this region the oscillation probes the shear-induced steady-state structure (DeCostello 1997). Ojijo et al. (2004) applied this approach to olive oil/monoacylglycerol gel networks. However, if no region can be determined where the parallel superposition moduli are independent of amplitude, parallel superposition cannot be applied.

Bell et al. (2007) crystallized their fat samples in separate vessels and applied them to a rheometer after different periods of shearing. In doing so, rheological parameters could be determined as a function of time, although it is not an on line evaluation of the crystallization process. Garbolino et al. (2000) equipped a rheometer with ultrasonic sensors, allowing simultaneous measurements of torque, rate of temperature changes and ultrasonic properties as a function of time, temperature and shear rate. Although this technique allows on line evaluation of the entire crystallization process, only primary crystallization was considered. Their results do not mention anything on aggregation or macroscopic properties. Toro-Vazquez et al. (2004) evaluated the effect of shear on cocoa butter crystallization in terms of torque. Changes in torque were attributed to product changes.

In this chapter, a new rheological approach to evaluate crystallization under shear is presented. Apparent viscosity, complex modulus, loss modulus, storage modulus and phase angle were monitored as a function of isothermal time during the isothermal crystallization of palm oil at 18°C and various shear rates (1, 10 and 100s^{-1}). The thus obtained results were compared with crystallization data obtained via time resolved XRD and polarized light microscopy.

5.2 Methods and Materials

5.2.1 Substrate

Refined, bleached and deodorized palm oil with an iodine value of 51 was obtained from De Smet Ballestra (Zaventem, Belgium) and stored in the freezer at -24°C until analysis. The triacylglycerol and fatty acid composition is given in Section 4.2.1.

5.2.2 Rheology

Small deformation oscillatory experiments were performed on an AR2000 controlled stress rheometer (TA Instruments, Brussels, Belgium) using the starch pasting cell (SPC). This geometry is described in detail in section 3.2.2. The melted sample (30 mL) was transferred into the cup and subjected to a time-temperature-shear profile which is schematically represented in Figure 5.1. This profile can be split up into 5 different steps:

- Step a: keeping isothermal for 10 minutes at 70°C to erase all crystal memory;
- Step b: cooling at 10°C per min to the desired crystallization temperature (18°C) while applying the selected shear rate;
- Step c: keeping isothermal for a predefined period of time while shearing at the selected shear rate ;
- Step d: oscillating for 30s at the crystallization temperature without shear;
- Step e: heating to 70°C.

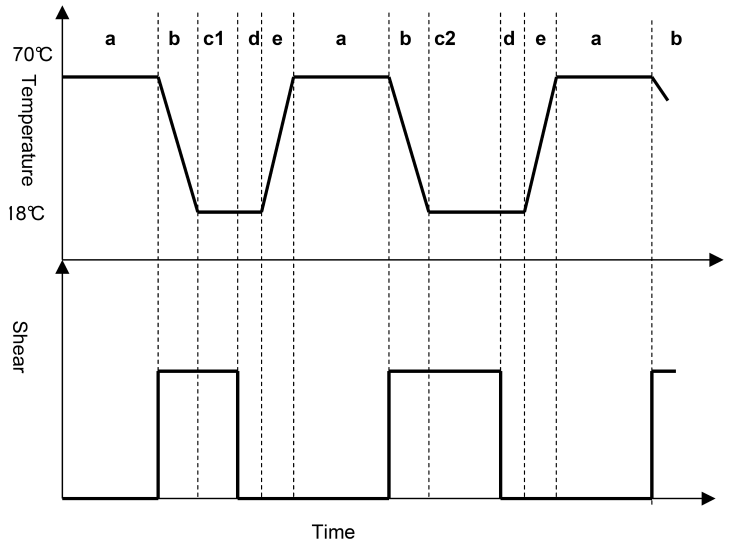

Figure 5.1: Schematic overview of the applied temperature-time-shear protocol

These 5 steps are continuously repeated for increasing lengths of step c (c1<c2<). During step b and c the crystallization process is monitored by apparent viscosity measurements, while in step d an oscillation measurement is performed at a frequency of 1Hz and a strain of $4.500 * 10^{-3}$, recording moduli and phase angle as obtained after step c. This very low strain was chosen to disturb the crystallization process as little as possible. As the crystallizing sample is continuously changing crystalline content and microstructure, it is however not possible to ascertain that oscillation measurements are executed within the linear viscoelastic region. However, by applying this very low strain, the risk of actually destroying the microstructure is limited. The low frequency of 1Hz was preferred also in order to influence the crystallization as little as possible while maintaining enough data points.

Viscosity and oscillatory measurements were executed in triplicate. It must be kept in mind that, although the liquid palm oil is Newtonian, its behavior becomes Non-Newtonian as soon as crystallization starts. As the calibration of the SPC is performed with Newtonian oil and Non-Newtonian oils, the values of apparent viscosity and shear are only nominal. It is difficult to know how much effect is produced by the particular flow patterns produced by the impeller and the range of shear rates that the material is subjected to. However, at the low shear rates used in this study, the occurrence of turbulence is unlikely.

Rheograms are constructed by plotting the value of the complex modulus ($|G^*|$) and phase angle (δ) at the end of step d, the oscillation step, as a function of isothermal time under shear in step c, the shear step. This is repeated for different lengths of step c (c1, c2,). These rheograms then represent the crystallization process under shear in terms of complex modulus and phase angle. The 30s period in which they are collected is considered to be short enough for the sample to retain the "sheared" characteristics.

5.2.3 Time resolved X-ray diffraction

Time-resolved X-ray diffraction (XRD) measurements using synchrotron radiation were performed on the Dutch-Flemish (DUBBLE) beam line BM26B at the European Synchrotron Radiation Facility (ESRF) in Grenoble (France). The experiments were executed at a fixed wavelength λ of 0.95 Å. The diameter of the point source at DUBBLE typically is 300 μm across. The spatial resolution at the 2D detector is 250 μm and has a total size of 13 by 13 cm. The sample to detector distance was 4 m. A 2D multiwire gas-filled detector was used for small angle X-ray scattering (SAXS). A Couette cell developed for XRD work under shear was constructed out of polycarbonate and basically consists of a central stator and an outer rotor. Taylor vortices are very unlikely in a configuration where only the outer cylinder is rotating (rotor) and the inner is stationary (stator). The dimensions of the polycarbonate cell (radius of the inner cylinder: 25 mm, gap: 0.5 mm) are identical to those reported earlier by others (Pople et al. 1998). The earlier reported design (Pople et al. 1998) was slightly adapted to allow for temperature control with air-flow powered heating units for both the rotor and the stator. Approximately 4 ml sample was used. The X-ray beam crossed the cell perpendicularly.

The following time-temperature program was applied: heating to 70°C, holding isothermally for 10 minutes, cooling at 10°C/min to 18°C and keeping isothermal at that temperature for 66 minutes. A shear rate of $10s^{-1}$ was applied from the cooling step onwards until the end of the isothermal period at 18°C. This protocol corresponds with the protocol applied during the rheological experiments. During the isothermal period 200 frames were recorded at 20s intervals. All scattering patterns were corrected for the detector response and normalized to the intensity of the primary beam which is measured by an ionization

chamber placed after the sample. No crystal orientation was observed and therefore the 2D patterns were azimuthally averaged into linear profiles. The intensities were converted into a color scale and plotted as a function of s [$Å^{-1}$], with s = $(2\sin\theta)/\lambda$ and θ half the scattering angle, and as a function of the isothermal time. The known reflections of silverbehenate were used to calibrate the scattering angles. Data are reported covering the s-range $0.016 < s < 0.028$ $Å^{-1}$, which corresponds to scattering at relatively low angles. In small angle X-ray scattering (SAXS), the long spacings can be determined. Apart from the packing mode (2L or 3L) and the length of the molecules, the long spacings also depend on the chain length of the fatty acids and the angle of tilt formed between the chain axis and the basal plane formed by the end methyl groups, which thus allows identifying polymorphic transitions (Timms 1984).

5.2.4 Polarized light microscopy (PLM)

Microscopic analyses were conducted with a Laborlux 12 Pol S microscope (Leica, Germany) equipped with a Linkam CSS450 shear cell with integrated cooling system (Linkam, Surrey, United Kingdom). Liquid samples were loaded at a gap setting of 80μm. Next, the liquid was heated to 70°C and kept there for 10 min after which it was cooled down to 18°C at 10°C/min for isothermal crystallization during 60 minutes. A continuous shear was applied from the start of the cooling step onwards until the end of the isothermal period. These conditions correspond to those used during the rheological and X-ray experiments. Samples were imaged with a Hamamatsu digital camera C4742-95 (Hamamatsu, Japan) every 6s, with an acquisition time of 20ms, at a magnification of 32x. Pictures were automatically recorded with the software program HiPic8 (Hamamatsu, Japan). Due to the high rotational speed of the bottom disc during shearing, no clear images could be recorded. To resolve this problem, shear was reduced to $0.1s^{-1}$ during the last 10s of every minute. The images obtained during this period provide clear views of the crystallizing material. After these 10s, the shear was immediately brought back to the selected shear rate. This approach was also used by Sonwai and Mackley (2006) in their study of the effect of shear on cocoa butter crystallization.

5.3 Results and discussion

5.3.1 Isothermal crystallization of palm oil at 18°C and a shear rate of $10s^{-1}$

5.3.1.1 Rheology

The crystallization of palm oil at 18°C and a shear rate of $10s^{-1}$ was monitored. Figure 5.2A shows the apparent viscosity, measured during the steady shear step, as a function of isothermal time under shear. Figure 5.2B and Figure 5.2C respectively show the phase angle and complex modulus as a function of isothermal time under shear. These three graphs can all be divided in six sections and the corresponding changes in rheological variables can be summarized as follows:

- Section 1: 0 - 4 min:
  - η*increases slightly from 0.05 to 0.10 Pa*s;
  - δ is close to 90°;
  - $|G^*|$ increases from 0.5 to 1 Pa;
- Section 2: 5 - 10 min:
  - η* increases faster from 0.10 to almost 0.30 Pa*s;
  - δ decreases from almost 90° to 80°;
  - $|G^*|$ increases faster to 3.5 Pa;
- Section 3: 11 - 15 min:
  - η* shows an even steeper increase from almost 0.30 to 1.00 Pa*s;
  - δ displays a second, steeper decrease from 80° to 13°;
  - $|G^*|$ sharply increases to 447 Pa;
- Section 4: 16 -25 min:
  - η* reaches a maximum of 1.40 Pa*s around 20 min;

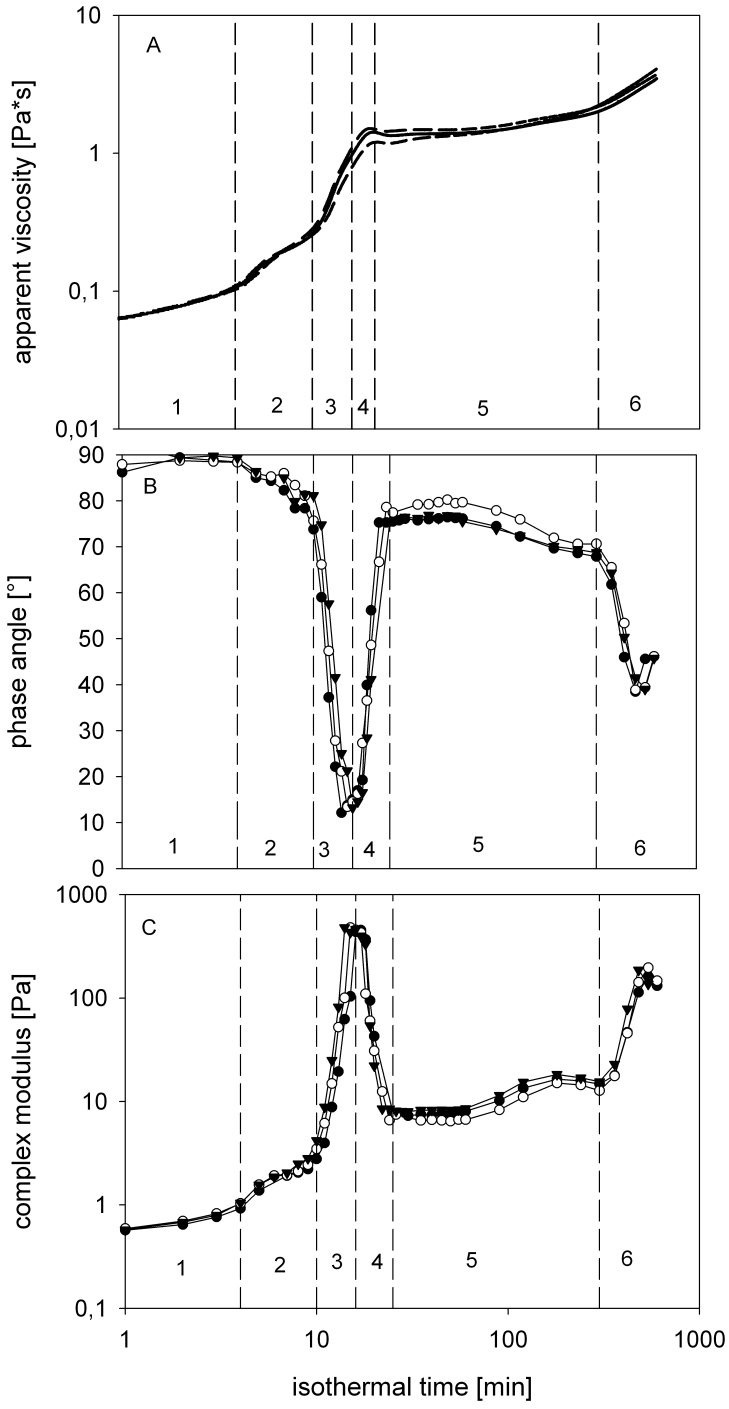

Figure 5.2: Apparent viscosity (A), phase angle (B) and complex modulus (C) as a function of isothermal time under shear for palm oil crystallization at 18°C and shear rate 10 s^{-1} (3 repetitions)

  - δ suddenly increases from 13° to 76°;
  - $|G^*|$ suddenly decreases to 7.6 Pa;

- Section 5: 26 - 300 min:
  - η^* remains more or less constant
  - δ gradually decreases from 76° to 69°
  - $|G^*|$ gradually increases to 14.3Pa

- Section 6: beyond 300 min:
  - η^* increases moderately leading to about 3.80 Pa*s at 600 min;
  - δ decreases from 69° at 300 min to 39° at 540 min and subsequently increases again;
  - $|G^*|$ increases to 181 Pa followed by another decrease.

5.3.1.2 XRD

To identify unequivocally the polymorphs formed during crystallization under shear at 18°C, palm oil was subjected to time resolved XRD. Figure 5.3 shows the SAXS-profile of palm oil crystallizing at 18°C while shearing at a shear rate of $10s^{-1}$ for a crystallization period of 60 min. The first peak at s = 0.021 $Å^{-1}$(d = 1/ s = 47.6 Å) was present from the start and increased until 6 min isothermal time after which it started to vanish. Concomitantly to the decrease of this peak a second peak appeared at s =0.024 $Å^{-1}$ (d = 1/ s = 41.7Å). At 10 to 11 min, only this second peak prevailed, which continued to increase until the end of the experiment at 60 min.

Mazzanti et al. (2005) studied the crystallization of palm oil at 17 and 22°C under static conditions and at shear rates ranging from 45 to 2880 s^{-1}. They concluded that at both temperatures α crystals nucleate from the melt and act as nucleation sites for the formation of β' crystals which grow at the expense of the α crystals as well as from the melt. Based on the results of Mazzanti et al. (2005) the first peak in Figure 5.3 can be attributed to the α-polymorph and the second one to the β' polymorph. The shift to higher s-values is caused by the tilted fatty acid chains with respect to the methyl end group plane

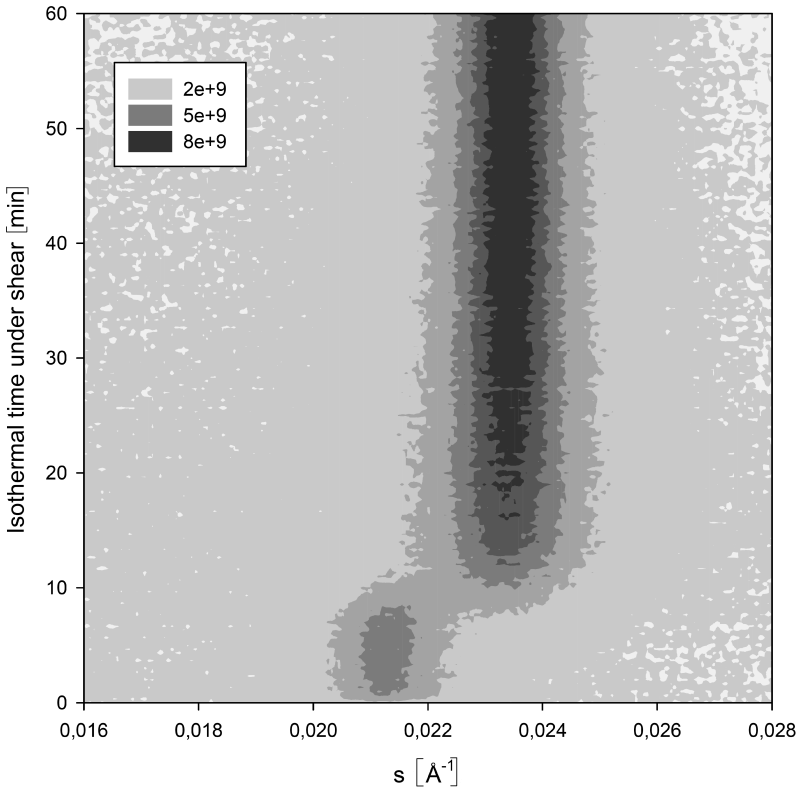

Figure 5.3: SAXS diffraction patterns of the isothermal crystallization of palm oil at 18°C and a shear rate of $10s^{-1}$

in the β'-polymorph (Timms 1984). This second peak increases at the expense of the α crystals and due to the formation of extra β'-crystals from the melt (Mazzanti et al. 2005).

5.3.1.3 PLM

PLM experiments were performed to assess the changes on the microstructure, which cannot be evaluated by means of XRD. PLM demonstrated that the first crystals were formed just before the crystallization temperature of 18°C was reached. At 1 min isothermal time (Figure 5.4A) a large number of crystals were present in a matrix of liquid fat. Visible aggregation occurred from approximately 9 to 10 min isothermal time onwards. Simultaneous primary crystallization and aggregation continued further on in the following sections. As aggregation went on, a primary network was formed. This was not a firm network as its 'building blocks', the aggregates, were continuously attaching and detaching under

the influence of the applied shear rate. Between 10 and 16 min isothermal time under shear (Figure 5.4B), the PLM images showed larger aggregates, apparently consisting of interconnected smaller aggregates, continuously moving in the shear field. Beyond 16 min, these aggregates were remarkably smaller, moving around in the shear field more individually. Between 16 and 60 min (Figure 5.4C) the microstructure was quite similar to the one at 60 min. The PLM experiments showed a very open structure at 60 min, consisting of separate aggregates suspended in some remaining liquid fat. Although this shear rate of $10s^{-1}$ might increase the collision rate, it is possible that no real aggregation and network formation can occur as the shear forces generated are high enough to dominate the van der Waals attraction and act as network destructing forces (Sonwai and Mackley 2006). As the impact of collision is higher for heavier objects, it is possible that an initially weak network breaks down when colliding with a mature aggregate.

5.3.1.4 Discussion

In Section 1 (Figure 5.2B), δ equaled 90° indicating the completely liquid nature of the sample. During this first period, η^*(Figure 5.2A) and $|G^*|$(Figure 5.2C) increased slightly, but their values were still very low. However, according to XRD and PLM there is already some crystallinity from the start. This can be due to the difference in sensitivity for detecting the onset of crystallization between XRD and PLM on the one hand and rheology on the other hand. Furthermore, it must be kept in mind that, when using different equipment to follow crystallization, comparison between results must be done with caution. Differences in sample weight or volume, equipment design and its impact on the thermodynamics of the system and, heat and mass transfer conditions existing in each measurement device, may affect crystallization to a different extent. Based on the XRD data the decrease in δ and increase in $|G^*|$ and η^* in Section 2 can be related to the formation of α-crystals from the melt. Consequently, the changes in δ, η^* and $|G^*|$ in Section 3 can then be attributed to a polymorphic transformation of α to β' crystals, possibly with extra β' formation from the melt.

However, the changes in Section 2 and 3 can not only be attributed to primary crystallization. Walstra (1987) already pointed out that ongoing crystallization and in particular recrystallization causes a growing together or sintering of the flocculated crystals, thereby greatly enhancing the strength of the bonds in the network, which can be seen as an in-

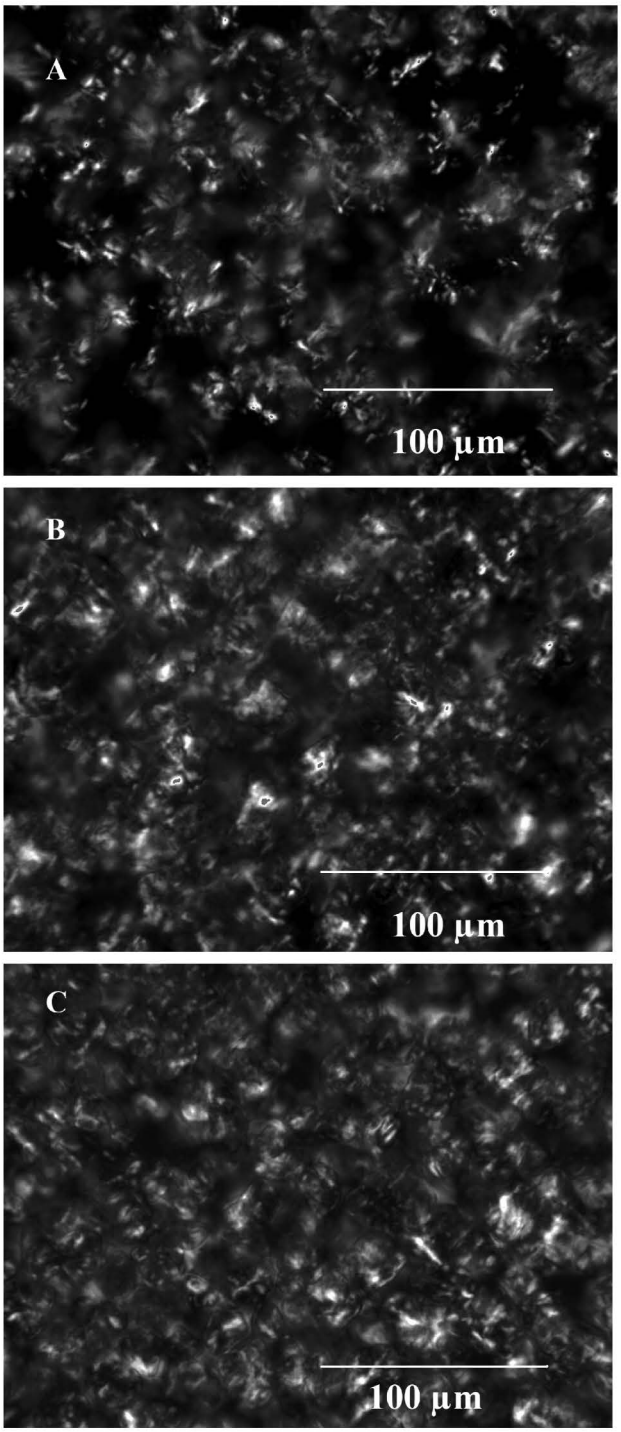

Figure 5.4: PLM images of palm oil crystallizing at 18°C and $10s^{-1}$ for (A) 1 min, (B) 16 min and (C) 60 min

crease in $|G^*|$. Therefore, primary crystallization cannot be completely separated from aggregation as it can already occur at very low volume fractions of crystalline material (Walstra 1987). Furthermore, viscosity is not only a result of increasing amounts of solids present in the liquid, but is also influenced by the crystal size distribution as well as the interactions between the different crystals. Aggregating crystals tend to form voluminous aggregates with a volume much greater than the total volume of the primary crystals, causing viscosity to increase (Kloek 1998; Walstra et al. 2001). Therefore, the increase in η^* and $|G^*|$ as well as the decrease in δin Section 2 and 3 are likely to be not only due to primary crystallization, but also to aggregation and crystal network formation.

In Section 4 (Figure 5.2A, B and C) a sudden decrease in $|G^*|$ and η^* and increase in δ around 16 min was observed, while no major changes were detected in Section 5 (Figure 5.2A, B and C). The rheological events in these Sections cannot be fully explained by XRD. This technique only revealed β' formation in Section 4 and 5. Clearly, XRD allows unambiguous determination of the polymorphs and of the amount of crystals (peak intensity) but not of the way larger aggregates are arranged in space. Consequently, the changes in δ, η^* and $|G^*|$ in Section 4 and 5 are probably situated at the micron level, indicating the break down of the primary network under the influence of the applied shear rate. This leads to a loss of structure, resulting in decreasing η^* and $|G^*|$ in Section 4. The loss of structure also results in a decreasing δ, although crystals and/or aggregates will still be present. These aggregates then possibly behave "liquid like" within the shear field. The increasing XRD peak intensity between 30 and 50 min isothermal time might be related to the increase in $|G^*|$ and η^* and decrease in δ in Section 5, although this section continues up to 300 min.

The remainder of Section 5 and Section 6 cannot be related to XRD as profiles were only recorded up to 60 min. For sure, changes in δ, η^* and $|G^*|$ beyond 60 min will not be related to polymorphism as palm oil is known to be β' stable (Yap et al. 1989). The PLM results suggest some change in the way the aggregates behaved in the shear field. Beyond 16 min the aggregates were smaller and moved around in the shear field more individually, thus changing the microstructure of the crystallizing sample compared to shorter shearing times. Furthermore, it can be assumed that, as the rheological variables did not return to their initial values of Section 1 after the changes in Section 4, some degree of structure must still be present. This structure can possibly originate from aggregates remaining

after structure breakdown. The PLM experiments confirmed the existence of aggregates throughout the experiment up to 60 min. In Section 6 η^* and $|G^*|$ increased more strongly while δ decreased. This might indicate the (re)formation of a network structure. However, beyond 540 min structure breakdown is likely to occur again as can be concluded from the increase in δ and the corresponding decrease in $|G^*|$.

5.3.2 Isothermal crystallization of palm oil at 18°C and at shear rates of 1, 10 and 100s^{-1}

Figure 5.5 presents the apparent viscosity (Figure 5.5A) and the complex modulus (Figure 5.5B) as a function of isothermal time under shear for palm oil crystallizing at 18°C at various shear rates (1, 10, 100s^{-1}). For all shear rates, the apparent viscosity and complex modulus increased strongly to a maximum and subsequently decreased. For shearing at 10s^{-1}, the apparent viscosity and complex modulus have been discussed extensively in the previous sections.

Both apparent viscosity and complex modulus show a clear effect of shear rate. As shear was already applied during the cooling step, the effect of shear rate was already noticeable when reaching the isothermal temperature. At 1 min of isothermal shear, the apparent viscosity and complex modulus had clearly reached higher values when a shear rate of 100s^{-1} was applied. No clear difference can be noticed between 1 and 10s^{-1}. However, at increasing isothermal time under shear, the apparent viscosity (Figure 5.5A) increased significantly when shearing at 1 and 10s^{-1}, while for 100s^{-1} only a minor increase could be noted. From 15 min isothermal time onwards, an explicit effect of shear rate on apparent viscosity can be seen, with a higher shear rate leading to a lower apparent viscosity. As discussed earlier, the increase of viscosity during crystallization can be related to the increase in amount of fat crystals present and thus to the degree of crystallinity (Sonwai and Mackley 2006). This increase includes the formation of primary crystals as well as the aggregation into an interconnected crystal network.

The onset of the major increase in complex modulus (Figure 5.5B) occurred earlier in time with increasing shear rate, indicating that the sample crystallized faster or formed a

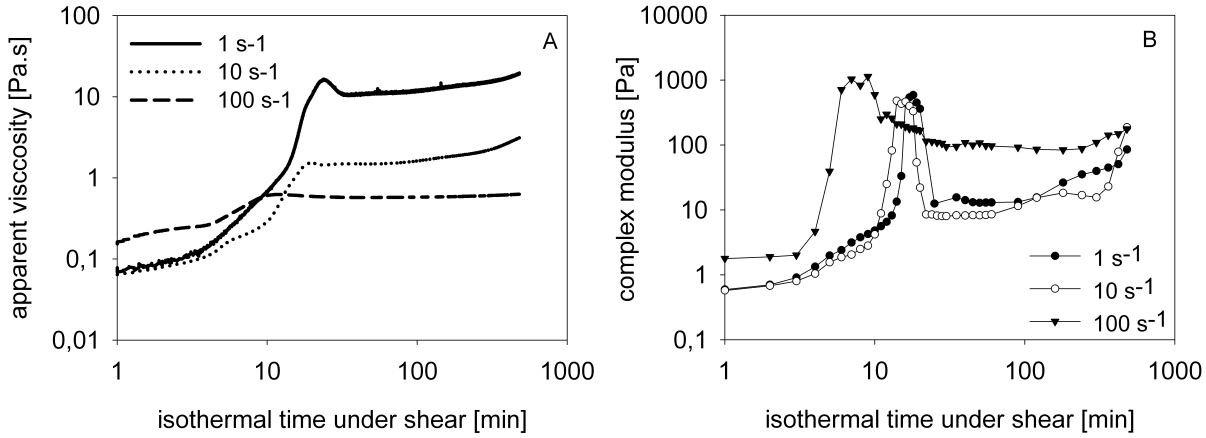

Figure 5.5: Apparent viscosity (A) and complex modulus (B) of palm oil crystallization under shear (1, 10, 100s^{-1}) at 18°C

network earlier at higher shear rates. Toro-Vazquez et al. (2005) and Dhonsi and Stapley (2006) reported an increase in a rheological parameter (torque for the former, viscosity for the latter) as an onset of crystallization took place, and an increase in the applied shear rate resulted in shorter crystallization induction times.

Furthermore, as can be seen in Figure 5.5B, the complex modulus as a function of time has the same shape for all shear rates investigated: a first gradual increase followed by a larger increase, and consequently a decrease. It was demonstrated in the previous section that the minor increase is related to the formation of α-crystals and the second one to the transformation of these α-crystals to β'-crystals and the formation of extra β'-crystals directly from the melt. However, as discussed earlier, primary crystallization and aggregation cannot be completely separated, thus the increase in complex modulus is also related to aggregation and network formation.

Mazzanti et al. (2005) demonstrated that shear did not influence the onset of formation of α-crystals, while the onset of β' formation was enhanced with increasing shear rate. Figure 5.5B clearly shows that the major increase in complex modulus, which is said to be related to the formation of β'-crystals, occurs sooner when higher shear rates are applied, although the difference between 1 and 10s^{-1} is rather limited.

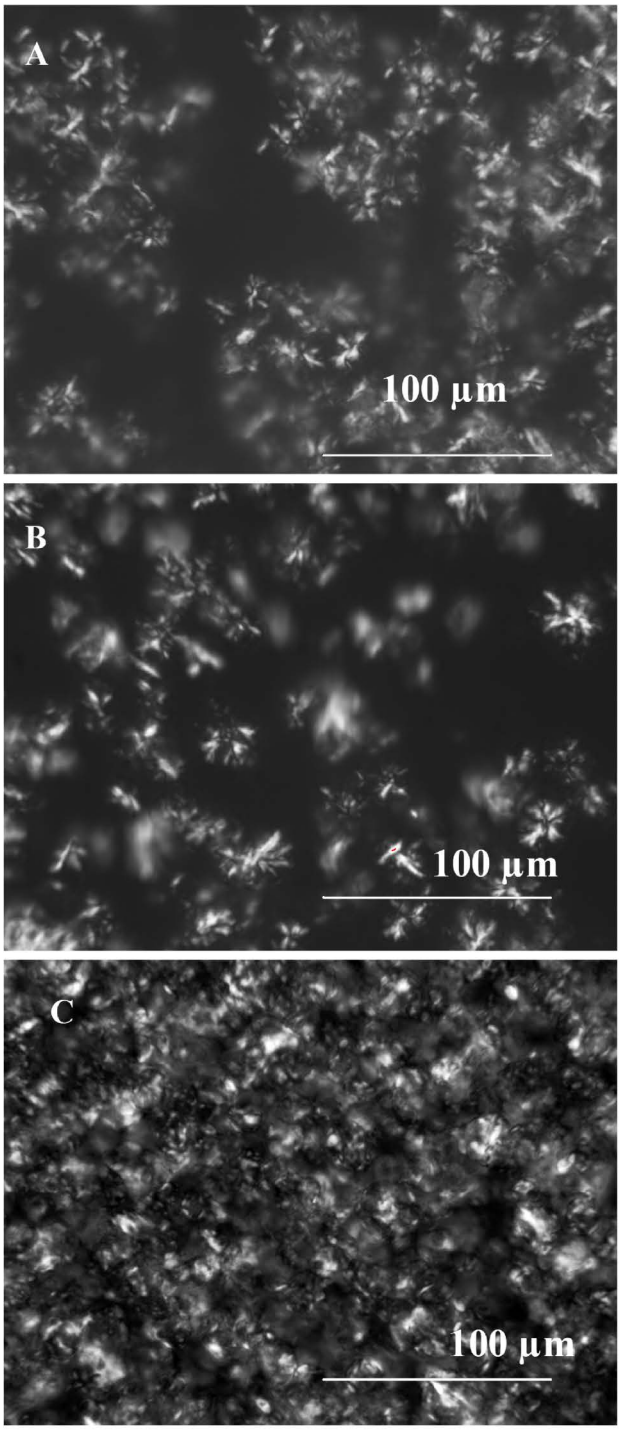

Figure 5.6: PLM images of palm oil at 18°C and 10 min isothermal time at different shear rates: (A) 1, (B) 10 and (C) 100s^{-1}

Figure 5.6 presents polarized light images of palm oil crystallizing at 18°C for 10 min isothermal time at different shear rates. When shearing at $1s^{-1}$ (Figure 5.6A) crystals already started to aggregate and to form a preliminary network structure. However, shearing at $10s^{-1}$ for 10 min (Figure 5.6B) resulted in single growing crystals, which were not yet aggregating. A completely different structure was obtained for shearing at $100s^{-1}$. At 10 min isothermal crystallization at $100s^{-1}$ (Figure 5.6C) individual crystals cannot be identified. The crystals have already aggregated and, compared to shearing at $1s^{-1}$, more of these aggregates are present. Although some liquid fat still remains, the aggregates appear to be volume filling.

These PLM observations can be related to the rheological data. At 10 min isothermal time under shear, the highest complex modulus (Figure 5.5B) was obtained when shearing at $100s^{-1}$, thus indicating the highest degree of structure. For shearing at $1s^{-1}$ and $10s^{-1}$, the complex modulus did not largely differ at 10 min isothermal time under shear. However, Figure 5.5A shows that up to 10 min isothermal time a higher apparent viscosity was found for shearing at 1 s^{-1} compared to shearing at $10s^{-1}$. At later times, aggregates are present at all shear rates. For $100s^{-1}$ the observed structure did not change visibly in time: throughout the experiment loosely connecting aggregates were observed. These findings are in accordance with the apparent viscosity and the complex modulus, which were more or less constant beyond 10 min and only slightly increased towards the end of the experiment. Beyond 15 min isothermal time under shear, no clear differences were observed between the microstructure obtained when shearing at $1s^{-1}$ compared to the one obtained when shearing at $10s^{-1}$.

5.4 Conclusions

It was demonstrated that oscillatory rheology can be applied to evaluate crystallization of palm oil while shear is applied. The proposed method is capable of measuring moduli and phase angle for crystallization under shear. Using rheological parameters, the comparison between static and dynamic crystallization modes can be facilitated in terms of rheological variables. Furthermore, this method offers the advantage that primary crystallization and microstructural development can be evaluated in one single analysis, while XRD only provides information on the amount and type of crystals. The main disadvantage of the developed method is that it is rather time consuming.

Chapter 6

Influence of shear flow on polymorphic behavior and microstructural development during palm oil crystallization[1]

There is a theory which states that if every anybody discovers exactly what the universe is for ans why it is here, it will instantly disappear and be replaced by something even more bizarre and inexplicable. There is another theory that this has already happened.
The hitchhicker's guide to the galaxy - Douglas Adams (1952-2001)

[1]This chapter has been submitted for publication in:
De Graef, V., P. Van Puyvelde, B. Goderis and K. Dewettinck. Influence of shear flow on polymorphic behavior and microstructural development during palm oil crystallization, European Journal of Lipid Science and Technology accepted

6.1 Problem statement and research strategy

A number of studies have reported on the effect of shear on fat crystallization. Mazzanti et al. (2003, 2004a, 2005) used time resolved X-ray scattering to assess the influence of various shear rates on the crystallization of palm oil (with shear ranging from 45 to 2880 s^{-1}), cocoa butter, milk fat and stripped milk fat. Sonwai and Mackley (2006) and MacMillan and Roberts (2002) used the same technique to elucidate the effect of various shear rates on the polymorphic transitions in cocoa butter. Dhonsi and Stapley (2006) and Toro-Vazquez et al. (2004) used a rheological approach to study cocoa butter crystallization under continuous shear, while Garbolino et al. (2000) equipped a rheometer with ultrasonic sensors to asses the effect of shear on crystallization of a confectionery fat. These experiments were all carried out with continuous shear throughout the whole experiment, except for the study of Sonwai and Mackley (2006). They applied a steady shear step (50-1500 s^{-1}) for a short period (250s) after which the sample was further monitored by means of a dynamic time sweep. They concluded that a steady shear step applied to the sample for only a short time during the crystallization substantially accelerated an apparent secondary crystallization process of cocoa butter.

In this chapter, the effect of low to medium high shear rates (0-100s^{-1}) was investigated at four crystallization temperatures (18, 20, 22, 25°C). In a first part, the effect of continuous shear on palm oil crystallization was studied by time-resolved X-ray analysis. In a second part, the influence of a shear step, starting during the cooling phase and comprising the first part of the isothermal period (1, 15, 30 min), was studied by rheological measurements and polarized light microscopy.

6.2 Methods and Materials

6.2.1 Substrate

Refined, bleached and deodorized (RBD) palm oil with an iodine value of 52 (Loders Croklaan Wormerveer, The Netherlands) was used for the time-resolved X-ray scattering experiments (results reported in part 4.1), while the rheological and polarized optical microscopy measurements were executed on RBD palm oil (De Smet Ballestra, Zaventem,

Belgium) with an iodine value of 51 (results reported in section 6.3.2). Samples were stored in a freezer at -24°C until analysis. The triacylglycerol and fatty acid compositions are given in Sections 3.2.1 and 4.2.1 respectively.

6.2.2 Time-resolved X-ray diffraction to study the effect of continuous shear on the crystallization of palm oil

Time-resolved small angle X-ray scattering (SAXS) measurements using synchrotron radiation were performed on the Dutch-Flemish (DUBBLE) beam line BM26B at the European Synchrotron Radiation Facility (ESRF) in Grenoble (France). The experiments were executed at a fixed wavelength λ of 1.0335 Å. A 2D multi wire gas-filled detector at 1.5 m from the sample was used to collect the SAXS data. The same Couette cell as described in section 5.2.3 was used.

The following time-temperature program was applied: heating to 70°C, holding isothermally for 10 minutes to erase all crystal memory, cooling at 10°C/min to the desired crystallization temperature (18, 20, 22 or 25°C)and keeping isothermal at the specified crystallization temperature. Shear was applied from the start of the cooling step until the end of the isothermal period, which was 60 min for 18, 20 and 22°C and 90 min for 25°C. Three different shear rates were investigated: 0, 1 and $5s^{-1}$. All scattering patterns were processed according to the procedure described in section 5.2.3.

6.2.3 Rheology to study the effect of a shear step on the crystallization of palm oil

Small deformation oscillatory experiments were performed on an AR2000 controlled stress rheometer (TA Instruments, Brussels, Belgium) using the starch pasting cell (SPC). This geometry is described in detail in section 3.2.2. In this study three variables were investigated, namely temperature (18, 20, 22, 25°C), shear rate (1, 10, 100 s^{-1}) and shear time (1, 15, 30 min), resulting in 36 experimental combinations. Each combination was rheologically analyzed in triplicate.

The melted sample was applied to the cup of the cell and subjected to the following time-temperature-shear protocol:

- step a: keeping isothermal at 70°C for 10 min to erase all crystal memory;
- step b: cooling down at 10°C/min to the crystallization temperature (18, 20, 22, 25°C) while shearing at the selected shear rate (1, 10, 100 s^{-1});
- step c: the selected shear rate is maintained for a predefined period (1, 15, 30 min) at the selected crystallization temperature;
- step d: isothermal crystallization without shear.

In step b and c the crystallization process was monitored by the apparent viscosity (η^*), which is measured during the steady shear step, while in step d oscillatory rheology was used. The oscillatory measurements probe the dynamic moduli ($G', G", G^*$) and the phase angle (δ) at a strain of $4.500 * 10^{-3}$ and a fixed frequency of 1 Hz. This very low strain together with the low frequency of 1Hz was chosen to avoid disturbances to the crystallization process as much as possible while maintaining a sufficiently high data sampling rate. Viscosity and oscillatory measurements were executed in triplicate.

6.2.4 Polarized light microscopy

The effect of a shear step on palm oil crystallization was studied with polarized light microscopy (PLM) at crystallization temperatures of 18 and 25°C. Microscopic analyses were conducted with a Laborlux 12 Pol S microscope (Leica, Germany) equipped with a Linkam CSS450 shear cell with integrated cooling system (Linkam, Surrey, United Kingdom). Liquid samples were loaded at a gap setting of 80μm. Next, the liquid was heated to 70°C and kept there for 10 min after which it was cooled down to 18°C or 25°C at 10°C/min. The sample was then kept at the selected temperature for isothermal crystallization. A continuous shear was applied from the start of the cooling step until some predefined time lapse in the isothermal period (step b and c). These conditions correspond to those used during the rheological experiments. After this initial shear step (step c), samples were imaged under static conditions (step d) with a Hamamatsu digital camera C4742-95 (Hamamatsu, Japan) every 6s at a magnification of 32x. Pictures were automatically recorded with the software program HiPic8 (Hamamatsu, Japan).

6.3 Results and discussion

6.3.1 The effect of continuous shear on crystallization kinetics

The crystallization of palm oil was followed at four temperatures (18, 20, 22 and 25°C) under three different shear rates (0, 1 and 5 s^{-1}). Figure 6.1 shows SAXS patterns of palm oil crystallized at 18°C without and with shear and crystallized at 25°C without shear.

The first peak at s = 0.021 $Å^{-1}$(d = 1/ s = 47.62 Å) in Figure 6.1A (crystallization without shear) was present 1 min after reaching 18°C and reached its maximum intensity at 8 min isothermal time after which it started to vanish. Concomitant to the decrease of this first peak a second peak appeared at s =0.024 $Å^{-1}$ (d = 1/ s = 41.67 Å). From 12.5 min onwards, only this second peak prevailed, which continued to increase until the end of the experiment at 60 min. Based on the results of Mazzanti et al. (2005) the first peak in Figure 6.1A can be attributed to the α-polymorph and the second one to the β' polymorph. The shift to higher s-values is caused by the tilted fatty acid chains with respect to the methyl end group plane in the β'-polymorph (Timms 1984). This second peak increases at the expense of the α crystals and due to the formation of extra β'-crystals from the melt (Mazzanti et al. 2005).

Figure 6.1B shows the same two peaks at s=0.021 $Å^{-1}$ and s =0.024 $Å^{-1}$. When applying a shear rate of $1s^{-1}$, the first peak, which is connected to the α-polymorph, also appeared after about 1 min isothermal time but it reached its maximum at 3 min isothermal time, which is 5 min earlier compared to crystallization without shear (Figure 6.1A). During its decrease from 3 min onwards, the second peak, which is associated with the β'-crystals, increased as the α-crystals underwent a polymorphic transformation to β'-crystals. From 11 min isothermal time onwards, only the β'-peak prevailed. Increasing the shear rate to 5 s^{-1} shifted the α-peak maximum intensity to 2.5 min again without any noticeable changes to the onset time, as is shown in Figure 6.1C. After 2.5 min, the α-peak decreased, while the β'-peak increased. From 9.5 min onwards, only the β'-peak could be detected.

Based on these results, it can be concluded that applying shear during crystallization influences the polymorphic behavior of palm oil. In the shear rate range used in this study,

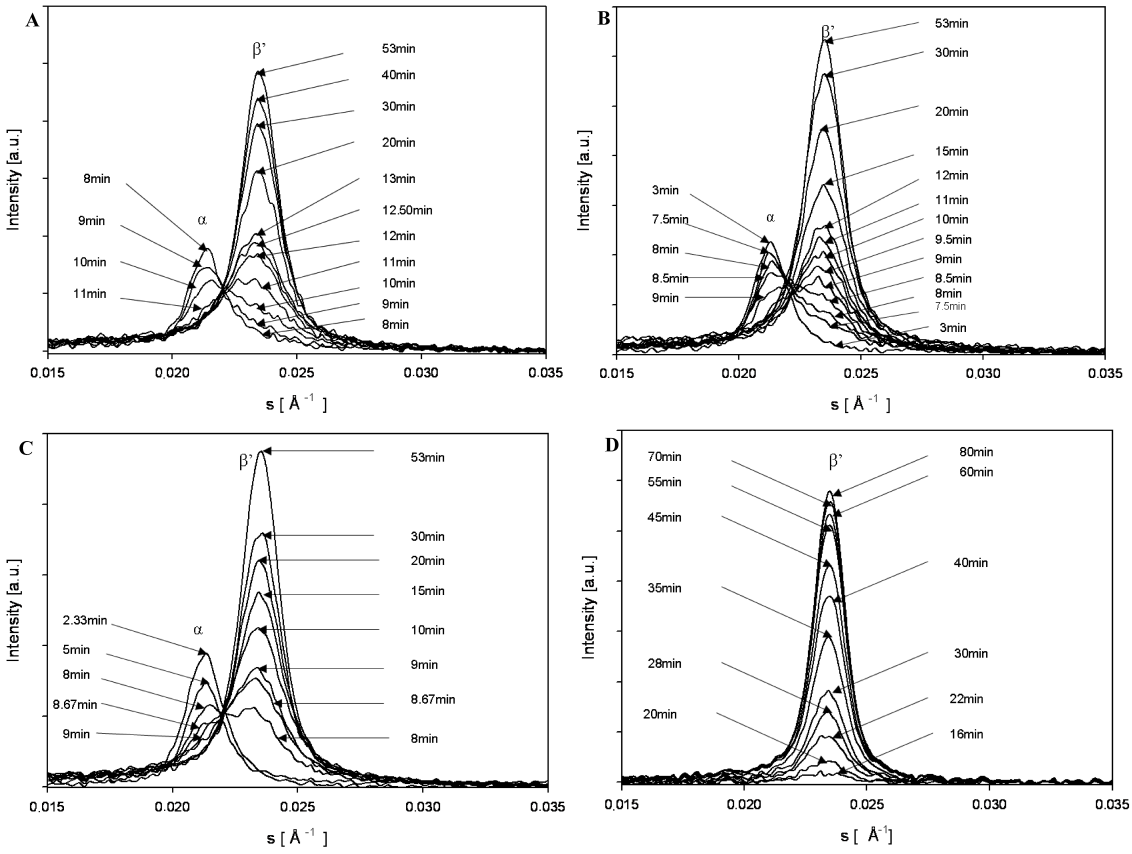

Figure 6.1: SAXS-profiles of palm oil crystallization at 18°C and a shear rate of (A) $0s^{-1}$, (B) $1s^{-1}$, (C) $5s^{-1}$ and (D) 25°C at $0s^{-1}$

no obvious effect of shear rate on the onset time of β'-crystal formation was found. However, the transformation of α- crystals to β'-crystals seems to be enhanced by applying shear. As the applied shear rate increased, the time needed to transform all α-crystals into β'-crystals was reduced. Similar effects were recorded at crystallization temperatures of 20°C and 22°C. At 20°C increasing the shear rate from 0 to $5s^{-1}$ caused a shift in the occurrence of the maximum of the α-peak from 8.5 min at $0s^{-1}$ to 7 min at $5s^{-1}$. Without shear the β'-peak was the only peak to be detected from 13 min onwards while at $5s^{-1}$ this was already the case at 11 min isothermal time. At 22°C the maximum at the α-peak position occurred 5 min sooner when shearing at $5s^{-1}$ compared to when no shear is applied. The β' peak prevailed at 18 min isothermal time when no shear was applied. Shearing at $5s^{-1}$ at 22°C resulted in a single β' peak from 11 min isothermal time onward in contrast to 18min at $0s^{-1}$. These findings are in agreement with the results of Mazzanti et al. (2005)

who studied the crystallization of palm oil at 17 and 22°C under static conditions and at shear rates ranging from 45 to 2880 s^{-1}, which are significantly higher shear rates than the ones used in the present study.

In contrast to 18, 20 and 22°C, only one peak was found in the SAXS patterns for palm oil crystallizing at 25°C. At this temperature, palm oil crystallized directly into the β' polymorphic form, as can be seen in Figure 6.2D. Here, the influence of shear on the crystallization kinetics was also studied but revealed no clear effect on the time at which the β'-peak appeared.

6.3.2 The effect of a shear step on the crystallization of palm oil

In this part of the study, palm oil (IV 51) was crystallized at four different crystallization temperatures (18, 20, 22 and 25°C) by applying three shear rates (1, 10, 100 s^{-1}) for three different isothermal shear periods (1, 15, 30 min: step c), followed by further crystallization without shear. During the shear step (step c) the crystallization process was monitored by apparent viscosity measurement. The subsequent static crystallization (step d) was evaluated plotting the complex modulus as a function of isothermal time. In addition, polarized microscopy experiments were performed to gain more insight in the effect of a shear step on the microstructural development during the subsequent crystallization when no shear was applied (step d). Although measurements are executed in triplicate, the plotted rheological parameters represent one exemplary curve as there was very little variation between the repetitions.

6.3.2.1 Crystallization during the shear step

Figure 6.2A shows the apparent viscosity (η^*) of palm oil during a shear step of 30 min at various isothermal crystallization temperatures and a shear rate of $100s^{-1}$. This graph clearly illustrates the effect of temperature on the crystallization process. The apparent viscosity increased faster and reached higher values when lower crystallization temperatures were adopted. At a crystallization temperature of 25°C, no significant crystallization occurred while shearing at $100s^{-1}$. This can be easily understood in terms of supercooling: the larger the supercooling (thus the lower the temperature), the higher the driving force, and thus the earlier the crystallization will start. The increase in viscosity of the sample

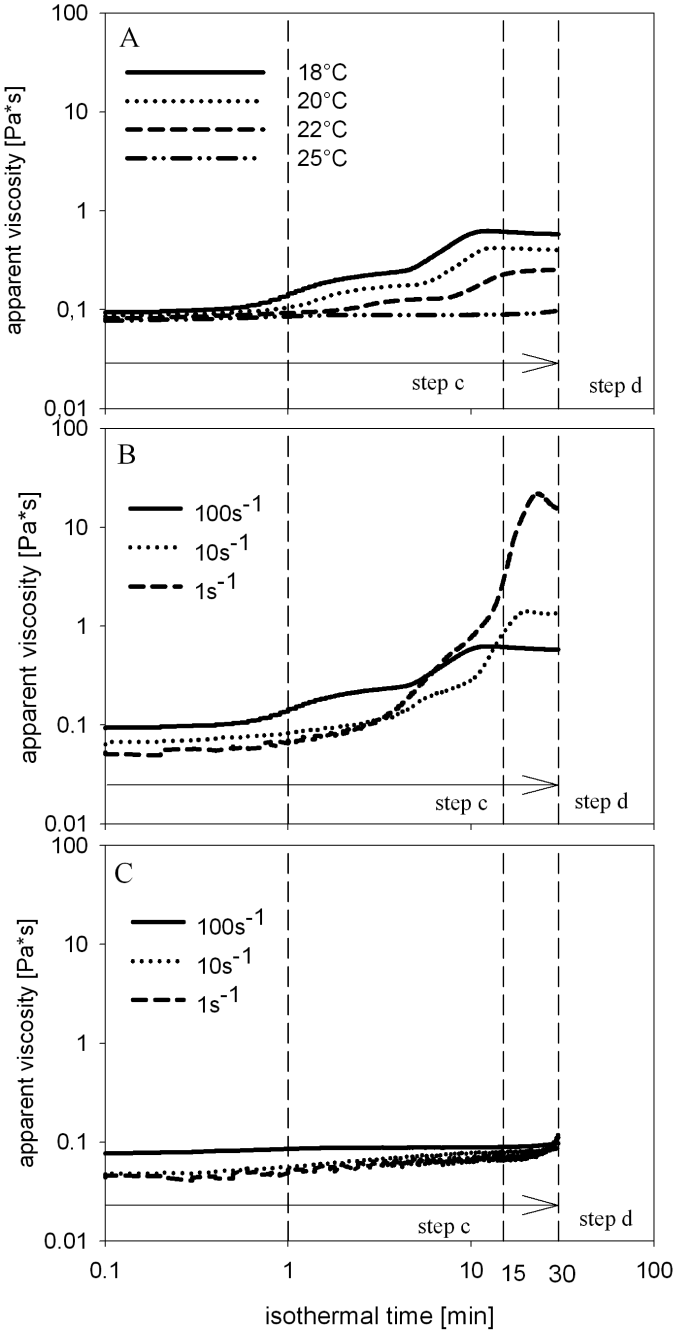

Figure 6.2: Apparent viscosity of palm oil (A) at different crystallization temperatures during 30 min shearing at $100s^{-1}$, (B) during 30 min crystallization at various shear rates and a crystallization temperature of 18°C and (C) during 30 min crystallization at various shear rates and a crystallization temperature of 25°C

during crystallization can be related to an increase in the amount of fat crystals present and thus to the degree of crystallinity (Sonwai and Mackley 2006). However, viscosity is not only a result of increasing amounts of solids present in the liquid, but is also influenced by the crystal size distribution as well as the interactions between the different crystals. Aggregating crystals tend to form voluminous aggregates with a volume much greater than the total volume of the primary crystals, causing viscosity to increase (Kloek 1998; Walstra et al. 2001). Therefore, the major increase in η^* is likely to be not only due to primary crystallization, but also to aggregation and crystal network formation.

Furthermore, two steps can be seen in the apparent viscosity for 18, 20 and 22°C. As was demonstrated with SAXS (although on another sample), palm oil exhibits a two-step crystallization at 18, 20 and 22°C, with the first step being the formation of α-crystals from the melt and the second step the polymorphic transformation of these α-crystals to β'-crystals and additional β' formation from the melt. At 25°C, palm oil crystallized directly in the β'- polymorphic form. Therefore, the two steps seen in the apparent viscosity for 18, 20 and 22°C can be related to the formation of α-crystals and their subsequent polymorphic transformation to β'-crystals. At 25°C, however, only a minor increase in ?* can be noticed due delayed crystallization immediately in the β'-form. The very low η^* values at 25°C indicate that no substantial crystallization has occurred while shearing at $100s^{-1}$.

Figure 6.2B and C show the effect of various shear rates, applied during the shear step (step c), on the apparent viscosity at crystallization temperatures of 18°C and 25°C respectively. At a crystallization temperature of 18°C (Figure 6.2B), the initial apparent viscosity (η^*) depends on the applied shear rate. For $100s^{-1}$, the initial η^* was significantly higher than for 1 and $10s^{-1}$, displaying equal initial η^* values. This difference is most likely due to the fact that shear was already applied during the cooling step (step b) where it induced some ordering or crystallization prior to reaching the isothermal segment. In fat systems, it has been proposed that an ordering process of molecules into lamellae act as a precursor to the formation of a solid crystalline phase (Sato 1999). The shape and size of these lamellar structures changes with the diffusion rate of the molecules (Larsson 1994). As shear influences the diffusion and convection mechanism, it will also affect the viscosity. However, based on these data, the possibility that some crystallization had already

occurred during the cooling step cannot be excluded.

The applied shear rate also influences the evolution of η^* with isothermal time as is illustrated in Figure 6.2B. As isothermal time increased, η^* increased substantially at all shear rates. This increase includes the formation of primary crystals as well as the aggregation into an interconnected crystal network and was more pronounced when lower shear rates were applied. All curves show two steps and the first increase in η^* occurred sooner as higher shear rates were applied. As discussed in Figure 6.2A, the two steps in the η^* curve can be related to the formation of crystals in the α polymorph and the subsequent transformation to β' with the additional formation of β' crystals directly from the melt. In addition, η^* clearly reached a maximum when shearing at $1s^{-1}$. The subsequent decrease indicates the break down of the primary network under the influence of the applied shear rate, which is in correspondence with previous results on palm oil crystallizing under continuous shear 5. During the 30min initial shear step at $10s^{-1}$ and $100s^{-1}$ this breakdown was less pronounced as no major decrease in η^* was observed. Beyond 15 min isothermal time under shear, higher shear rates clearly result in lower η^* values. This can be understood by considering that η^* is not only proportional to the amount of solids present but that it is also influenced by the crystal size distribution and the mutual crystal interactions (Kellens et al. 2007). The present results therefore suggest that shear, besides enhancing the primary crystallization, also influences the microstructural development.

At a crystallization temperature of 25°C (Figure 6.2 C), however, no significant increase in η^* could be noticed during the 30 min isothermal initial shear step at any shear rate. As at 18°C, the initial η^* was higher for $100s^{-1}$ compared to 1 and $10s^{-1}$. This difference is most likely due to some ordering effect of shear applied during the cooling step before reaching the isothermal segment. During the shear step, only a limited increase in η^* was recorded. This small increase occurred mostly toward the end of the shear step, suggesting the onset of crystallization.

Subsequent to the initial shear period (step c), the sample was allowed to crystallize further under static conditions (step d). As such, the total crystallization time, i.e. the isothermal shear period + static crystallization time, amounts up to 15.5 h. This static crystallization process was monitored by oscillatory rheology, recording the complex mod-

ulus ($|G^*|$) as a function of isothermal time. In the following sections, the effect of shear time and shear rate on subsequent static crystallization will be discussed for the crystallization temperatures 18 and 25°C. The crystallization temperature of 18°C is chosen as typical for a two-step primary crystallization of palm oil, while crystallization at 25°C is exemplary of single step crystallization. Results obtained for 20 and 22°C were similar to those for 18°C and will thus only briefly be discussed.

6.3.2.2 Crystallization at 18°C after shearing

As can be seen in Figure 6.3A, shearing for 1 min at $1s^{-1}$ and $10s^{-1}$ at a crystallization temperature of 18°C yields identical evolutions of $|G^*|$: the two curves completely coincide. The shape of the complex modulus curves are similar for all shear rates applied during the shear step. However, at a shear rate of $100s^{-1}$, 1 min of initial shear caused an upward shift of $|G^*|$, which resulted in a significantly higher final $|G^*|$, indicating a stiffer network structure. These observations corresponds to the η^* measured during the shear step as can be seen in Figure 2A at 1 min isothermal time: higher η^* values were obtained when shearing at $100s^{-1}$, while shearing at $1s^{-1}$ and $10s^{-1}$ did not result in a major difference in η^*. These results indicate that the crystallization process is enhanced even when shearing for only 1 min at the crystallization temperature, provided that the applied shear rate is sufficiently high.

After 15 min shear at 1 and $10s^{-1}$, no obvious differences in $|G^*|$ were found either at that particular time. However, a shearing at $100s^{-1}$ clearly altered the further evolution of $|G^*|$ in time. These observations can also be related to the evolution of the η^* during the shear step. During the 15 min shear at 1 and $10s^{-1}$, η^* did not reach its maximum before the end of the shear step. As this maximum and subsequent decrease in η^* is related to the formation and breakdown of a preliminary network structure 5, it can thus be concluded that after 15 min shear at these shear rates the microstructure developed under shear was still intact. However, when a shear rate of $100s^{-1}$ was applied, the maximum in η^* occurred before the end of the shear step. Although the decrease in η^* is very minor in this case, it can still be concluded that due to the high shear rate some breakdown of the network structure occurred. During the subsequent isothermal crystallization without shear, those effects are translated into a change in shape of the complex modulus curve, and thus in

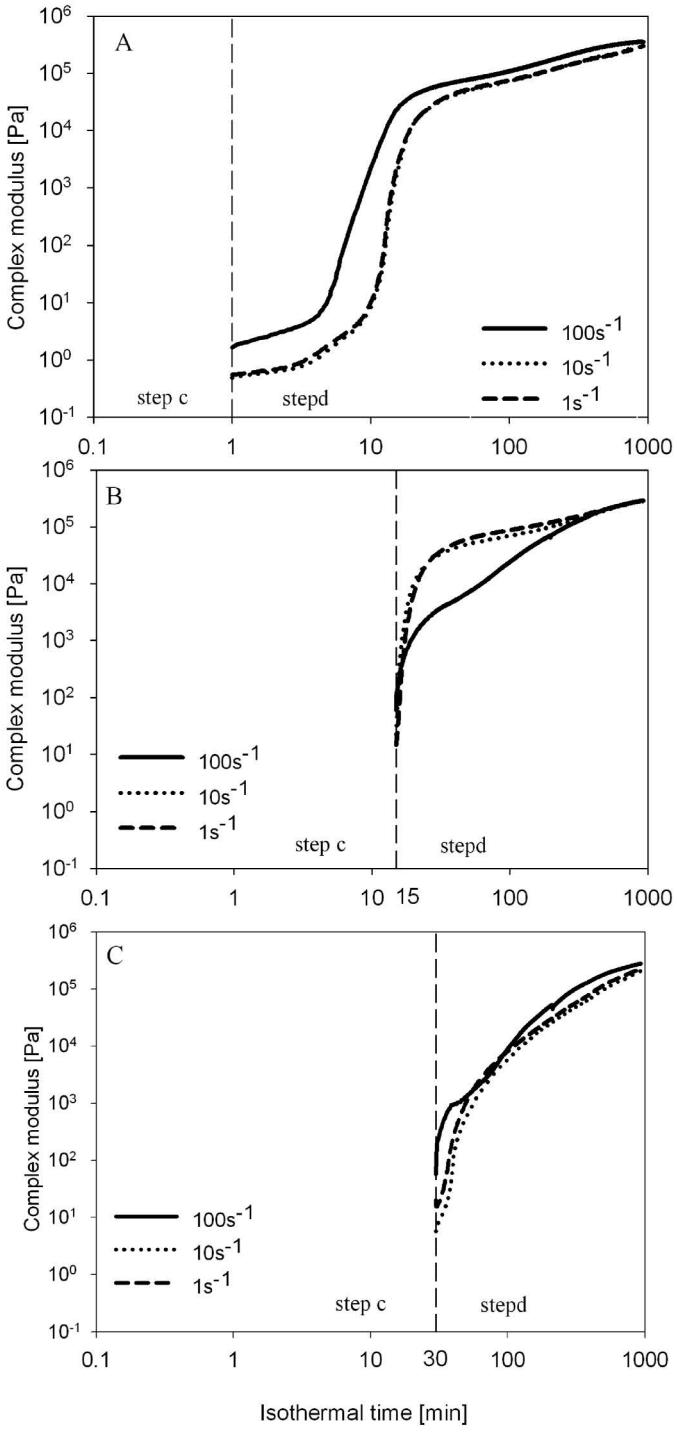

Figure 6.3: Complex modulus of palm oil at 18°C after a shear step of (A) 1, (B) 15 and (C) 30 min at shear rates of 1, 10 and 100 s^{-1}

the microstructural development, when a shear rate of $100s^{-1}$ was applied during the shear step. After a shear step of 15 min at 1 and $10s^{-1}$, the microstructural development during the static crystallization the microstructural development as expressed by the evolution of the complex modulus, resembles the one after a shear step of 1 min. In Figure 6.3A as well as in Figure 6.3B, similar $|G^*|$ curves can be seen for shearing at 1 and $10s^{-1}$: neither an effect of shear rate nor of the duration of the shear step could be appreciated. Despite the effect of shearing at $100s^{-1}$ on the evolution of $|G^*|$, no significant differences in final $|G^*|$ were found compared to shearing at 1 and $10s^{-1}$.

In contrast, a shear step of 30 min, (Figure 6.3C) resulted in significant differences between all shear rates. The initial $|G^*|$ after 30 min shear was significantly higher for 100 s^{-1} compared to $1s^{-1}$ and $10s^{-1}$, while shearing at $10s^{-1}$ led to a significantly lower value than shearing at $1s^{-1}$. It is likely that a shear step of 30 min at $100s^{-1}$ enhanced the crystallization process to such an extent that after 30 min more crystalline material was present, leading to a higher complex modulus. The difference between $1s^{-1}$ and $10s^{-1}$ can be sought in the interactions between the crystals: at lower shear rates more interactions will be able to form, thus leading to larger aggregates while at $10s^{-1}$ the aggregation might be hindered due to the higher shear rate. Furthermore, all shear rates caused a change in curve shape compared with the graphs obtained after a shear step of 1 min (Figure 6.3A), indicating a combined effect of shear time and shear rate.

The complex modulus curve recorded after shearing at 1 and $10s^{-1}$ is again similar for a shear step of 30 min. However, taking into account the complex modulus curves obtained after 1 min and 15 min shear, a major difference in shape can be seen. This shape difference can be explained by looking at the apparent viscosity measured during the shear step. During 30 min shearing, η^* reached a maximum and then decreased, whereas this maximum was not yet attained during the 15 min shear. As indicated earlier, the decrease in η^* is said to be related to the breakdown of a preliminary crystal network under the influence of the applied shear rate. This network breakdown during the shear step causes the complex modulus curve to change shape during the subsequent crystallization period without shear. Shearing at $100s^{-1}$ also changed the evolution of the complex modulus, again indicating the effect of not only shear rate but also of the length of the shear step. The significant effect of shear rate is maintained in the final $|G^*|$ ($100s^{-1}$>$1s^{-1}$>$10s^{-1}$).

For all shear rates studied, the lowest final complex modulus for crystallization at 18°C was found for a shear time of 30 min.

Polarized light microscopy was used to gain more insight in the microstructural development after a shear step. Immediately after 1 min shear at $100s^{-1}$ (Figure 6.4A), more and smaller crystals were obtained compared to $10s^{-1}$ and $1s^{-1}$. The microstructures obtained after 1 min shear at 10 (Figure 6.4B) and $1s^{-1}$ (Figure 6.4C) were rather similar and showed more liquid fat compared to $100s^{-1}$. The presence of more crystalline material immediately after the shear step is again an indication that the crystallization process is enhanced by shear, even at a shear step of only 1 min, provided that the applied shear rate is sufficiently high. During the static crystallization period following the shear step, additional material crystallized on and in between the crystals, resulting in larger aggregates. At 45 min total isothermal crystallization time including 1 min shear, no clear differences could be seen between the samples that were subjected to different shear rates during the 1 min shear step as can be seen in Figure 6.5A, B and C.

The effect of shear rate on the microstructure could be clearly seen immediately after a shear step of 15 min at 18°C. A shear rate of $100s^{-1}$ (Figure 6.4D) resulted in a large amount of compact crystals, whereas at $10s^{-1}$ (Figure 6.4E) and $1s^{-1}$ (Figure 6.4F) fewer crystal structures were formed with a larger remaining amount of liquid. Figure 6.4E and Figure 6.4F also illustrate that, although the crystal concentration is rather low, aggregation and network formation took place during the shear step. After an additional 30 min of crystallization without shear (total isothermal time = 15 min shear + 30 min without shear = 45 min) no obvious changes in microstructure were found in the sample that was sheared at $100s^{-1}$: the microstructure at 45 min isothermal time (Figure 6.5D) was quite similar to the one immediately after the shear step of 15 min, likely to be because the crystals were almost volume filling immediately after the shear step (Figure 6.4D).

The microstructures obtained after shearing at lower shear rates showed some additional crystallization and aggregation. Both the sample sheared at $10s^{-1}$ (Figure 6.5E) and the one sheared at $1s^{-1}$ (Figure 6.5F) displayed a network structure after 45 min isothermal time, which is more pronounced in the sample that was subjected to a shear rate of $1s^{-1}$ during the shear step. At 18°C, the shear rate applied during a shear step of 15 min

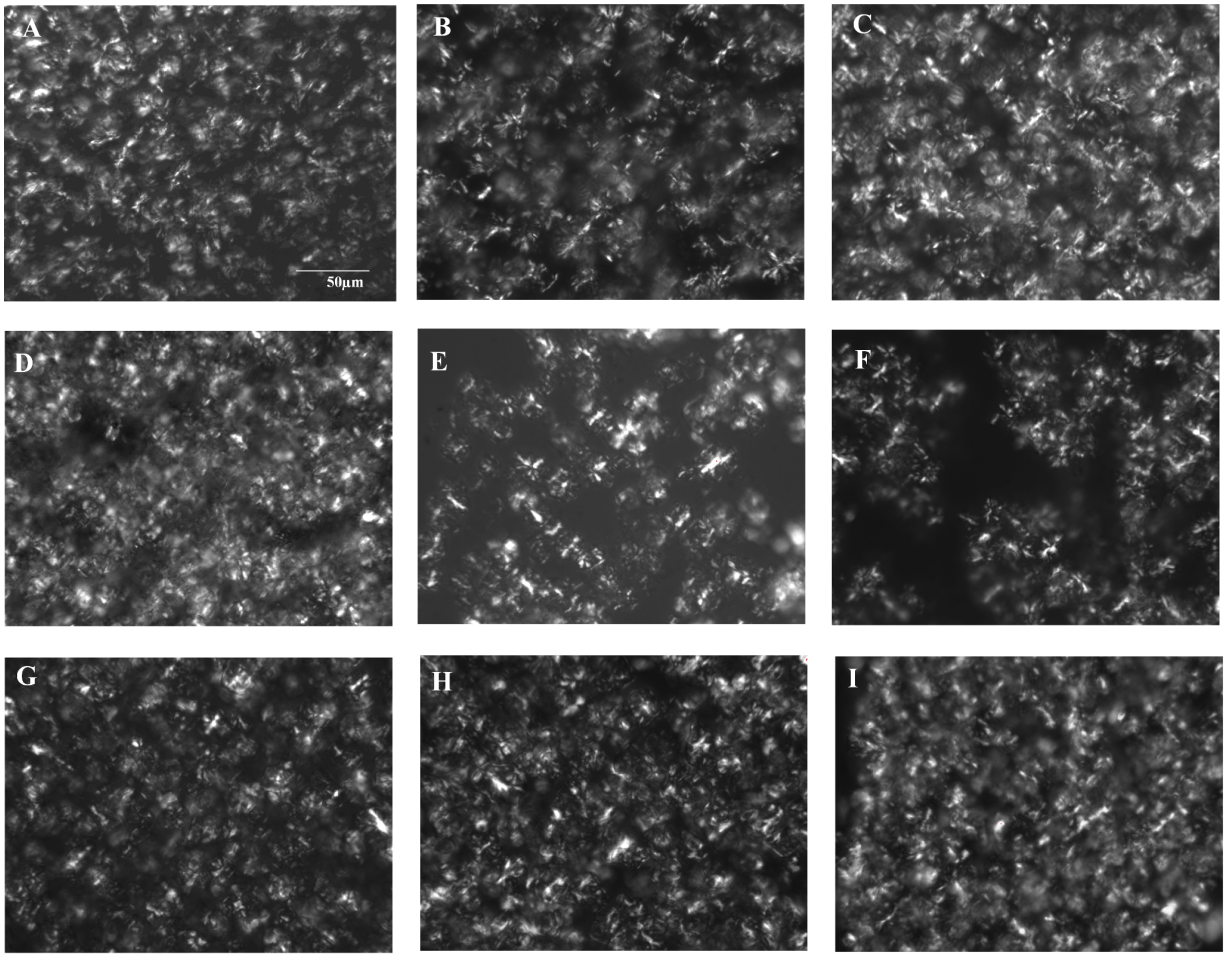

Figure 6.4: PLM images of palm oil at 18°C immediately after a shear step (horizontally: 1, 15 and 30 min) at various shear rates (vertically: 100, 10 and 1s^{-1})

influenced the microstructural development, but the final network stiffness as measured by the complex modulus was not affected. The differences in microstructure visualized with PLM correspond to the rheological analyses where a shear rate of 100s^{-1} caused the complex modulus to change shape, while this was not the case for shearing at 10s^{-1} or 1s^{-1}.

Shearing for 30 min at 100s^{-1} and 10s^{-1} at 18°C resulted in quite similar microstructures: aggregates were suspended in some remaining liquid fat. Shearing for 30 min at 1s^{-1} resulted in less aggregates compared to the higher shear rates (Figure 6.4G, H, I). During 15 min additional isothermal crystallization without shear (total isothermal crystallization time = 30 min shear + 15 crystallization without shear), clear differences could be detected

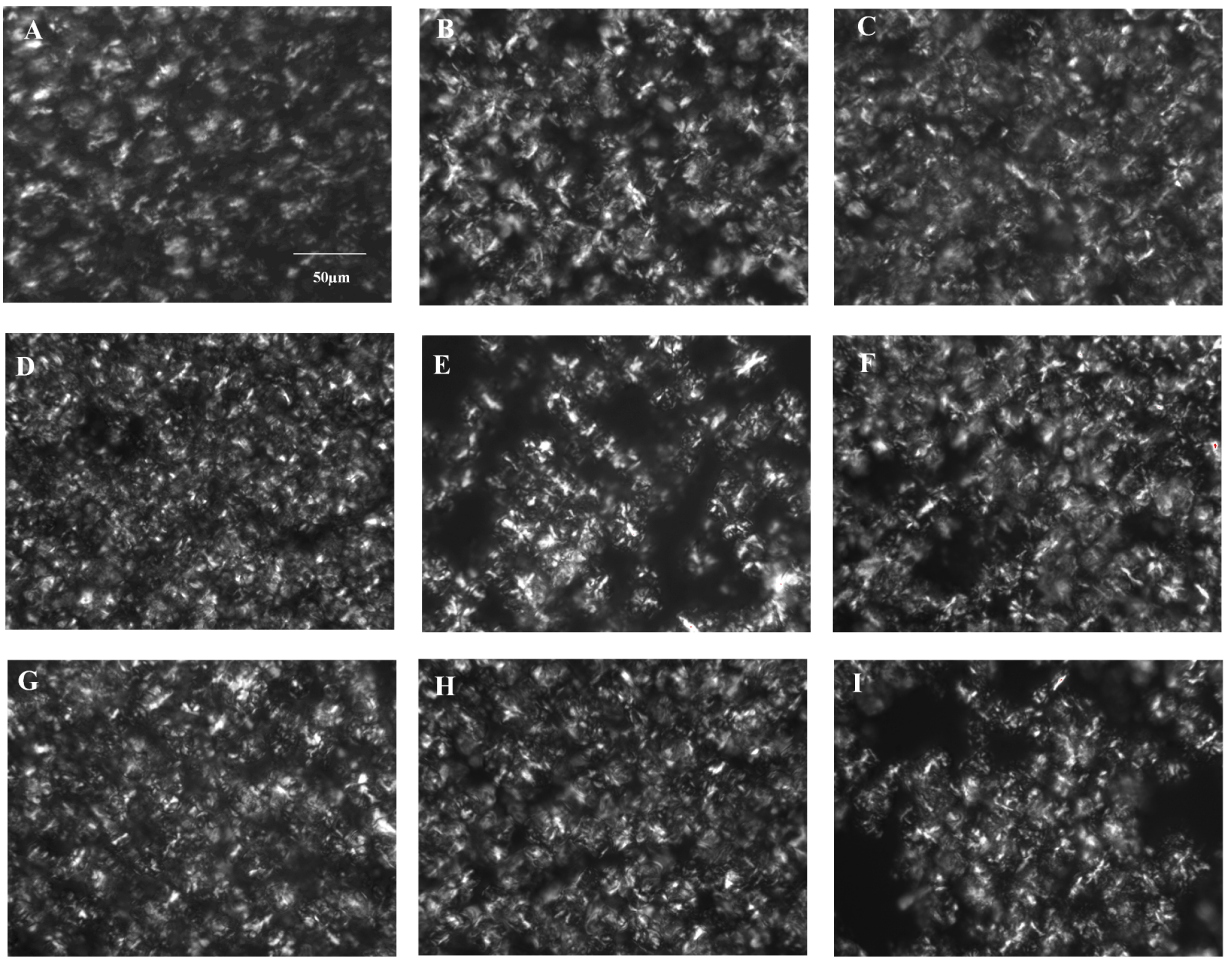

Figure 6.5: PLM images of palm oil at 18°C after 45 min isothermal crystallization including the shear step (horizontally: 1, 15 and 30 min) at various shear rates (vertically: 100, 10 and 1s^{-1})

compared to immediately after the shear step. Figure 6.5G and Figure 6.5H show similar structures, while Figure 6.5I seems to be characterized by a larger portion of liquid fat. Figure 6.3C, showed no significant difference in complex modulus after shearing at 10s^{-1} and 1s^{-1}. Based on Figure 6.2B it was said that that during the shear step a preliminary network structure was formed, which was subsequently broken down again by the ongoing shear. As soon as shear was stopped, the aggregates could form a firmer network structure by for instance sintering which is the formation of solid bridges between existing crystal structures.

6.3.2.3 Crystallization at 25°C after shearing

Figure 6.6 presents $|G^*|$ for static crystallization at 25°C after shearing for 1, 15 and 30 min at 1, 10 and 100s^{-1}. After 1 min shearing (Figure 6.6A), no major crystallization had taken place, as can be concluded from the low $|G^*|$. At 100s^{-1}, shearing for 1 min led to a significantly shorter induction time for $|G^*|$ compared to 1 and 10s^{-1}. However, no significant differences were detected in the final $|G^*|$ values.

The effect of the applied shear rate becomes more evident when considering the $|G^*|$-plot for static crystallization after 15 min shearing (Figure 6.6B). Again the induction time is considerably shorter for shearing at 100s^{-1} compared to 1 and 10s^{-1}, although shearing at different shear rates did not result in a significant effect on the initial $|G^*|$. The final $|G^*|$ was significantly higher after shearing at 1s^{-1}. No significant difference was found between 10 and 100s^{-1}. The reduction in induction time is most likely not only caused by a faster nucleation and crystal growth but also by an increased aggregation rate as these two phenomena cannot be completely separated and aggregation already occurs at very low volume fractions of crystalline material (Walstra et al. 2001).

Shearing for 30 min (Figure 6.6C) at 100s^{-1} enhanced crystallization to the extent that no induction time could be seen in $|G^*|$. In contrast, a short induction time was still present for shearing at 1 and 10s^{-1}. Furthermore, the slope of $|G^*|$ after shearing 30 min at 100s^{-1} has also changed compared to 1 and 10 s^{-1}, while this was less obvious after shearing for 1 and 15 min. Shear did not affect the initial $|G^*|$, while the final $|G^*|$ was significantly higher after shearing for 30 min at 1s^{-1} compared to 10 and 100s^{-1}: a stiffer network was obtained after shearing at lower shear rates.

Generally, it can be concluded that the effect of a shear step, as visualized by the complex modulus recorded during the subsequent isothermal crystallization without shear, was more pronounced when crystallizing at 18°C than at 25°C. In contrast to 18°C, the effect of shear time was less pronounced at 25°C. This can be explained by the fact that at 18°C crystallization largely took place during the shear step, while at 25°C crystallization and aggregation took place at later times due to the difference in supercooling. At both temperatures, the major increase in complex modulus occurred earlier in time when a

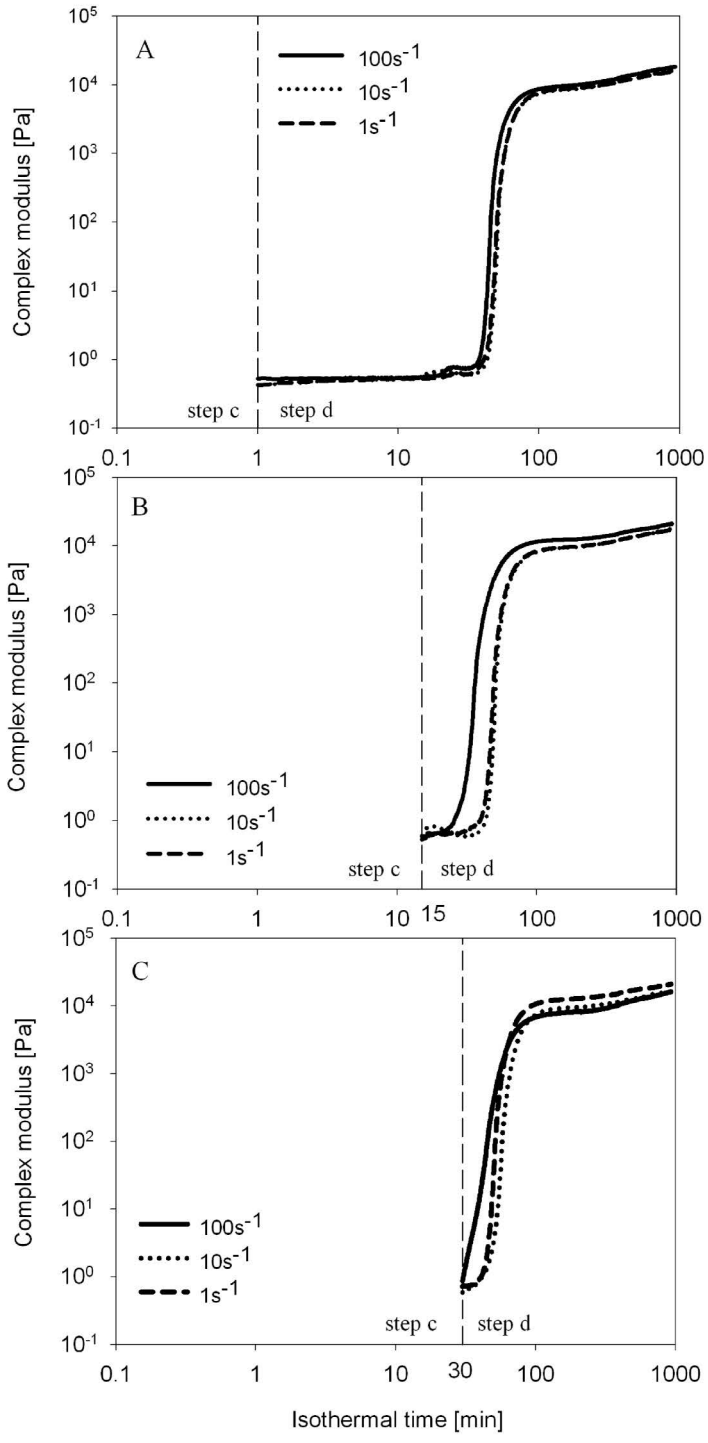

Figure 6.6: 6 Complex modulus of palm oil at 25°C after a shear step of (A) 1, (B) 15 and (C) 30 min at shear rates of 1, 10 and 100 s^{-1}

higher shear rate was applied during the shear step, indicating that the sample crystallized faster and with a higher level of crystallinity. The effect of a shear step on the crystallization kinetics, evaluated by rheological measurement, corresponds to the findings of Sonwai and Mackley (2006), Dhonsi and Stapley (2006) and Toro-Vazquez et al. (2004), who all studied the effect of continuous shear on the crystallization kinetics of cocoa butter. They reported an increase in rheological parameter (viscosity or torque) at the crystallization onset and a shorter crystallization induction time when higher shear rates were applied. Furthermore, Sonwai and Mackley (2006) also studied the effect of a steady shear step of 250s at shear rates ranging from 0 to 1500s^{-1} on cocoa butter crystallization and came to the same conclusions as when continuous shear was applied: a significant effect of the applied shear rate on the onset of the rheological change.

The microstructural development at 25°C was also studied with PLM (6.7). During the static crystallization following a shear step of 1 min, at all shear rates a limited amount of crystals was formed, which slowly increased in size. During this process, the birefringence of material that crystallized around the center was much less. The bright center might be related to the crystallization of the high melting triacylglycerols into compact assemblies, while the less bright outer parts can be the result of the crystallization of lower melting triacylglycerols into more branched and less dense crystal aggregates. An additional static isothermal crystallization period following the shear step resulted in similar microstructures for all shear rates as is illustrated in Figure 6.7A, B and C for a total isothermal crystallization period of 60 min including 1 min shear at 1s^{-1}, 10s^{-1} and 100s^{-1} respectively. After a shear step of 15 min at different shear rates, smaller and fewer crystals were found for a shear rate of 1s^{-1} compared to higher shear rates. For 10s^{-1} and 100s^{-1}, the crystals had already started to aggregate. In addition, toward the end of the 15 min shear at 100s^{-1}, the crystals already seemed to form a preliminary network structure (Figure 6.7F).

The difference in microstructure, due to the different shear rates applied in the shear step is maintained in the subsequent static crystallization as can be seen in Figure 6.7D, E and F for a shear rate of 1s^{-1}, 10s^{-1} and 100s^{-1} respectively. During this static crystallization, the crystal aggregates grew larger and new material crystallized in between the aggregates, thus creating a network structure. Larger crystal structures were found after

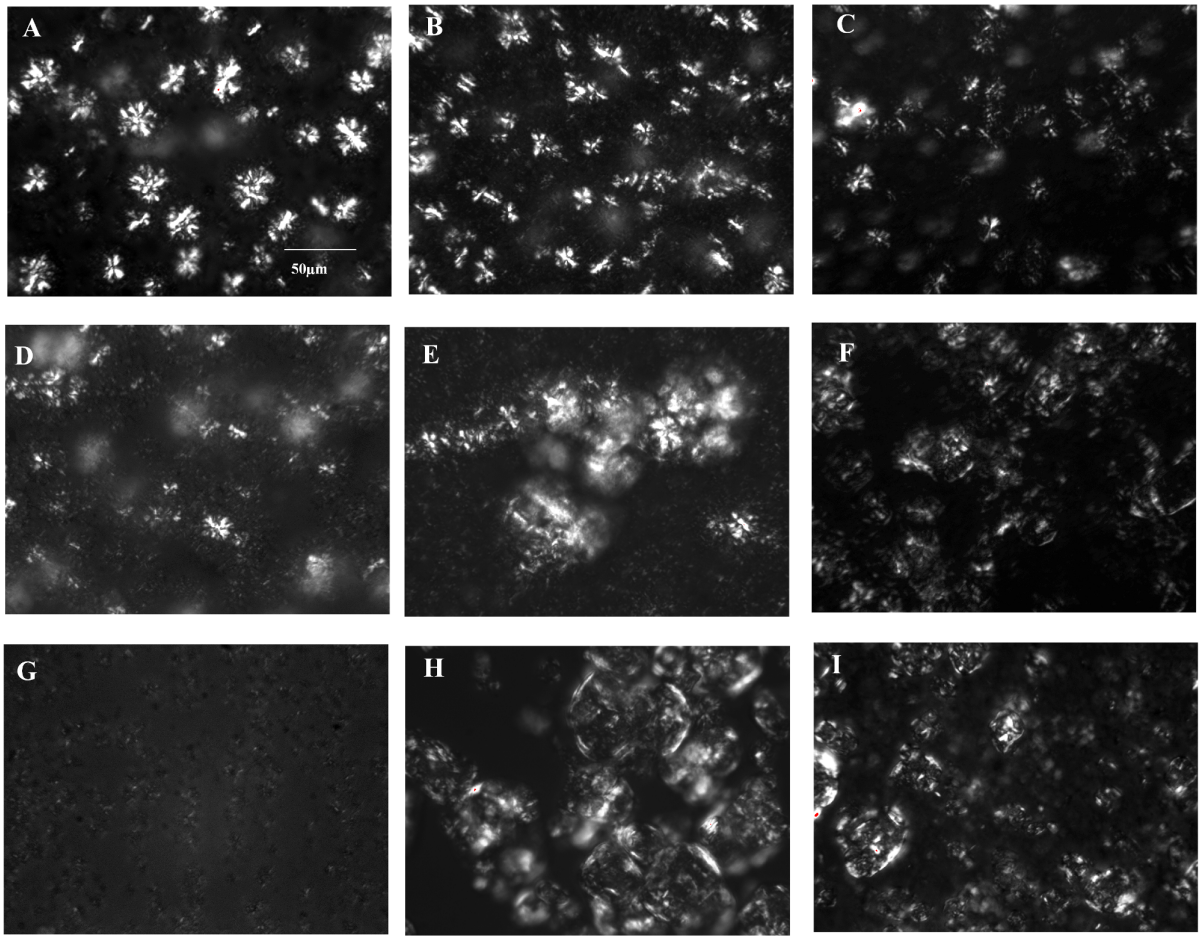

Figure 6.7: PLM images of palm oil crystallizing at 25°C during 60 min including a shear step (horizontally: 1, 15 and 30 min) at various shear rates (vertically: 1, 10 and 100s^{-1})

a shear step of 30 min at 10s^{-1} and 100s^{-1}, in contrast to shearing at 1s^{-1} which resulted in many smaller crystals. This microstructural difference was maintained during an additional static crystallization period. Figure 6.7H shows the microstructure of palm oil after 60 min crystallization at 25°C, of which 30 min shear at 10s^{-1}. A similar microstructure was obtained for 100s^{-1}(Figure 7I), although more extra crystalline material could be seen in between the aggregates at 60 min total isothermal time. No large aggregates were notices after shearing at 1s^{-1}. However, this image does not provide conclusive evidence due to bad picture quality.

Based on the rheological results (Figure 6.6), a large effect of shear (duration as well as shear rate) was not anticipated as the shape of the complex modulus curve did not alter significantly in contrast to crystallization at 18°C. Nevertheless the PLM images revealed an effect of the applied shear rate and shear time an the microstructure: larger crystal structures were obtained during the subsequent crystallization for longer shear times at higher shear rates, which is likely due to a higher coalescence rate of the crystals during the shear step.

6.3.2.4 Crystallization at 20 and 22°C after shearing

As stated earlier, the crystallization at 20 and 22°C will only be discussed briefly as the observed trends are similar to those discussed above. Figure 6.8 shows the complex modulus curves for crystallization at 20 and 22°C after a shear step of 1, 15 and 30 min at various shear rates. In Figure 6.8A the complex modulus evolution following a 1 min shear step at various shear rates at 20°C, is very similar to one in Figure 6.3A for 18°C: only the complex modulus curve 1 min shear at $100s^{-1}$ deviates as it occurs at higher values compared to after shearing at 1 and $10s^{-1}$ did not result in a significant difference. Some larger variations compared to 18°C can be noticed after 15 (Figure 6.8B) and 30 min shear (Figure 6.8C), although the trends are similar. Figure 6.8B demonstrates that after 15 min shear at $100s^{-1}$ the complex modulus curve changed shape, as was also observed at 18°C. Furthermore, shearing for 30 min at 18°C resulted in a change in curve shape for the complex modulus at all shear rates. At 20°C this effect was only observed when shearing 30 min $100s^{-1}$ and $10s^{-1}$.

Shearing for 1 min at 22°C seemed to be less shear rate sensitive. A shear step of 1 min at $100s^{-1}$ caused an earlier onset of crystallization, but no further effect of shear rate was observed as the complex modulus curves completely coincide. At 22°C, 15 min shear at $100s^{-1}$ (Figure 6.8E) did not result in an equally large change in curve shape as was the case at 18 and 20°C. However, the 30 min shear at $100s^{-1}$ clearly affected the complex modulus as is depicted in Figure 6.8F.

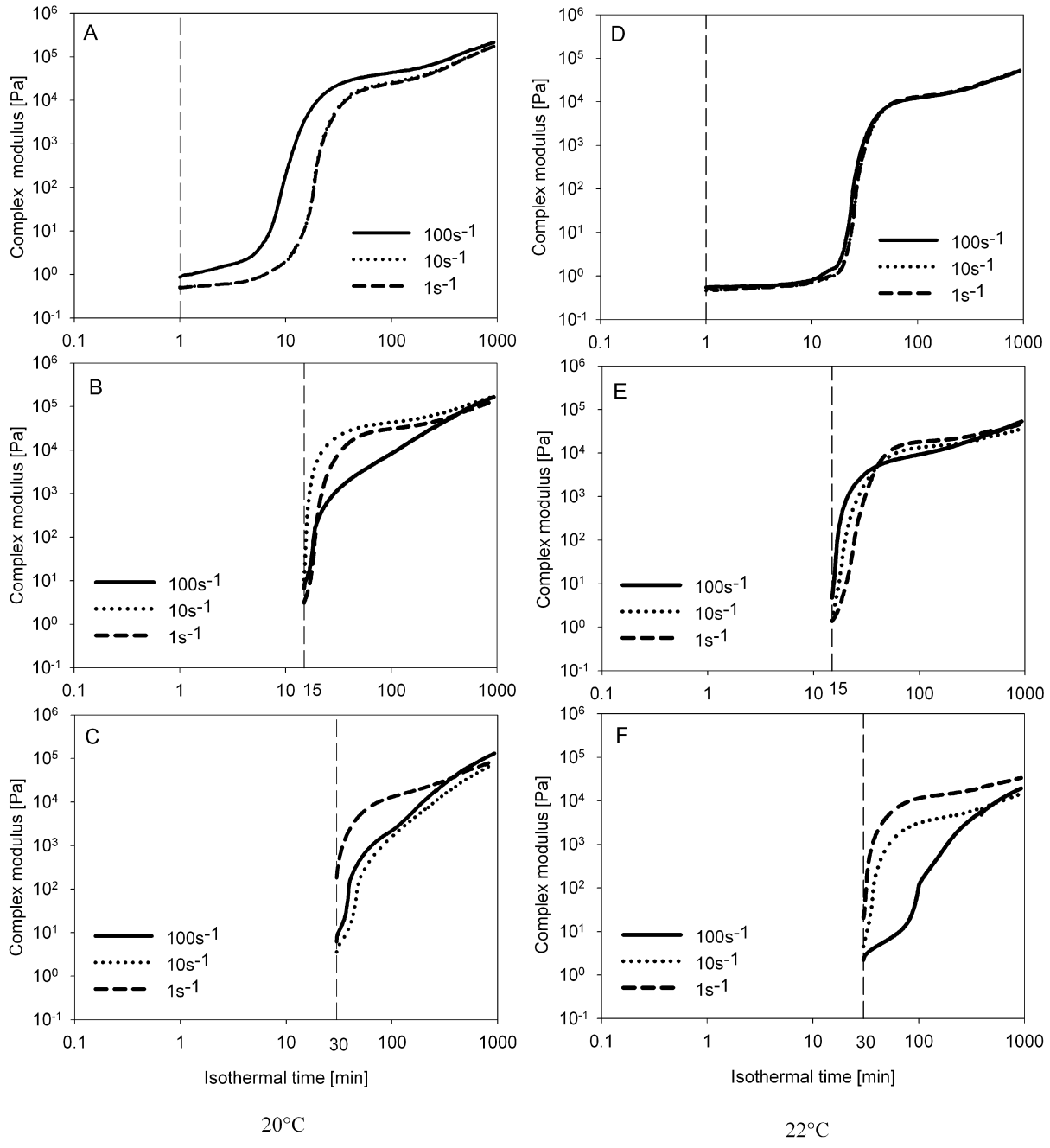

Figure 6.8: Complex modulus of palm oil at 20°C and 22°C after a shear step of (A and D) 1, (B and E) 15 and (C and F) 30 min at shear rates of 1, 10 and 100 s^{-1}

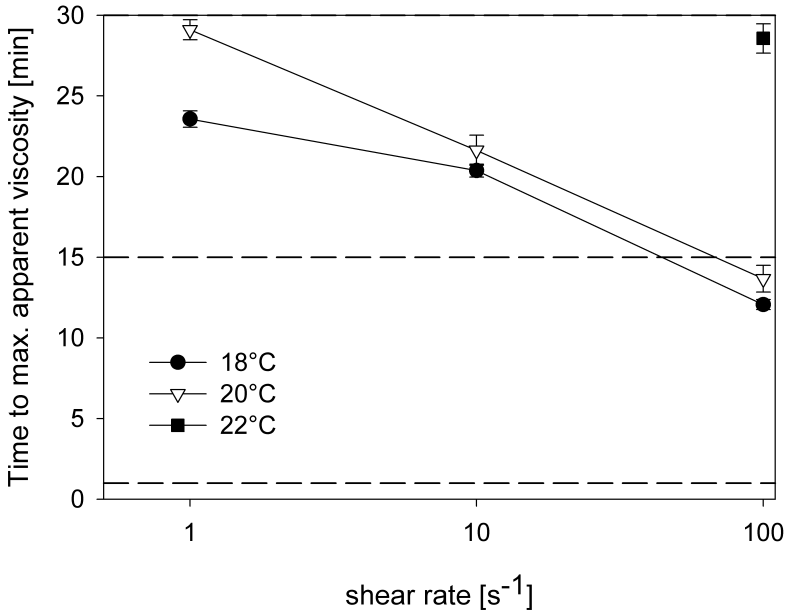

Figure 6.9: Time to reach maximum apparent viscosity during the shear step as a function of shear rate and temperature

It has been discussed in the previous sections that the duration of and the shear rate applied during the shear step influences the shape of the complex modulus curve during further crystallization without shear. Figure 6.9 displays the isothermal time to reach the maximum apparent viscosity within the duration of the shear step as a function of shear rate and temperature. The dotted-lines in Figure 6.9 indicate the different shear times used in this study. For 18 and 20°C, the maximum apparent viscosity is clearly reached sooner at increasing shear rates. At 25°C, no maximum is reached within the duration of the shear step and consequently this temperature is not included in Figure 6.9. During the shear step at 25°C only a minor increase in apparent viscosity was recorded. Correspondingly, no maximum was reached within the duration of the shear step when shearing at 1 and 10s^{-1} at 22°C, and these data are thus also not included in Figure 6.9. For 30 min shear at 100s^{-1} the maximum apparent viscosity at 22°C is reached at 28.57 $\pm$ 0.9 min, just before the end of the shear step. Taking into account Figures 6.3, 6.6 and 6.8 it becomes clear that the shape-change in complex modulus only occurs when the shear step is longer than the time needed to reach the maximum apparent viscosity (Figure 6.9).

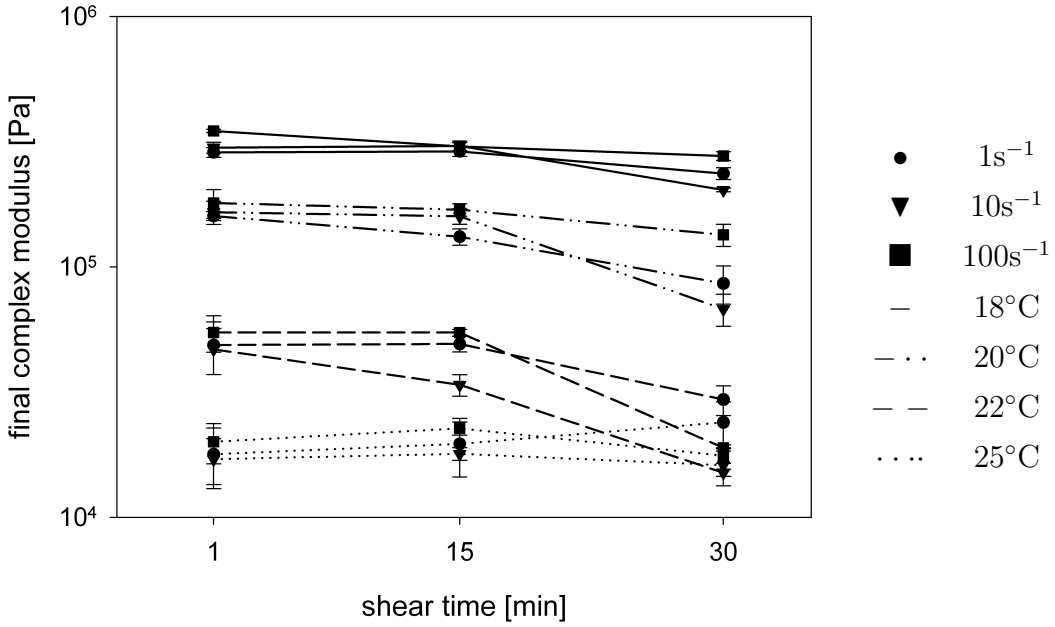

Figure 6.10: Final complex modulus after 930 min isothermal crystallization as a function of the duration of the shear step for all applied shear rates and temperatures

To summarize, for none of the temperature-shear rate combinations the maximum apparent viscosity was reached during a shear step of 1 min and correspondingly, no effect on the shape of the complex modulus curve was observed. A shear step of 15 min at 100^{-1} did affect the complex modulus at 18 and 20°C, which corresponds with the fact that the maximum apparent viscosity was reached before the end of this shear step. In addition, 30 min shear at 18°C and 20°C caused the shape-change of the complex modulus regardless of the applied shear rate. At 22°C, this shift was only recorded when shearing 30 min at $100s^{-1}$.

6.3.2.5 Effect of shear time, shear rate and temperature on the final complex modulus

The effect of shear time, shear rate and temperature on the final complex modulus is summarized in Figure 6.10. It can be clearly seen that the highest complex modulus values are found when crystallizing at 18°C, irrespective of the applied shear rate and shear time. The second highest values are recorded when crystallizing at 20°C which is also not affected by the applied shear rate or shear time. At these temperatures the largest

effect of shear rate and shear time are found after a shear step of 30 min. Shearing for 30 min at $100s^{-1}$ resulted in the highest final complex modulus while the lowest was found after 30 min shearing at $10s^{-1}$. At 22°C the final complex modulus following 1 min shear at all shear rates is significantly higher than at 25°C and significantly lower than at 20 and 18°C. The same observation can be made for a shear step of 15 min. After 30 min shear however, the results are less straightforward. No significant differences can be observed due to the higher standard deviations on the rheological measurement at these temperatures.

6.4 Conclusions

It has been demonstrated that shearing influences the further static crystallization process and alters the microstructural arrangement. The extent of the effect of the shear step is determined by both the duration and the applied shear rate but also by the crystallization temperature. Rheological analyses showed an earlier increase of the complex modulus provided that the applied shear rate was high enough and applied during a sufficiently long period. At 18°C, the crystallization process was already enhanced by applying a shear step of 1 min at $100s^{-1}$, while at 25°C this effect was only obtained when shearing at least 15 min at $100s^{-1}$. At 18°C a shear step of 30 min significantly altered the microstructural development as the majority of the crystallization took place during the shear step i.e. when shear was applied: more liquid fat between the aggregates was seen for increasing shear rates, which resulted in a less homogeneous microstructure and reduced network stiffness. This change in microstructural properties will also affect the macroscopic properties (for instance hardness) of the final product. Furthermore, the crystallization temperature also plays an important role as lower final complex moduli and different microstructures were found at 25°C compared to 18°C. The effect of crystallization temperature on the microstructural development should thus also be kept in mind.

Chapter 7

Crystallization behavior and texture of trans containing and trans free palm oil based confectionery fats[1]

The wise speak only of what they know.
Lord of the rings - J.R.R. Tolkien (1982-1973)

[1]This chapter has been published in:
De Graef, V., I. Foubert, K.W. Smith, F.W. Cain and K. Dewettinck (2007). Crystallization behavior and texture of trans containing and trans free palm oil based confectionery fats, Journal of Agricultural and Food Chemistry 55, 10258-10265.

7.1 Problem statement and research strategy

Recently, the pressure to ban trans fatty acids from food has dramatically increased because of their negative health implications. The major source of trans fatty acids are partially hydrogenated vegetable oils, which are frequently used in shortenings and confectionery products. To replace these partially hydrogenated fats, manufacturers have to turn to alternatives like palm oil and palm oil fractions. However, these alternatives should provide the same product functionality as the original product containing the unwanted trans containing fats.

The solid fat content (SFC) is a major factor determining the texture of fat, but the latter is also influenced by the polymorphism and the microstructure of the fat crystal network, which are in turn determined by the fat composition and crystallization conditions (Marangoni and Hartel 1998; Marangoni and Narine 2002). Therefore, all these structure levels (primary crystallization, microstructural development, macroscopic properties) have to be studied to gain more insight in the effect of trans fatty acids on the final product texture. However, until now few studies have addressed this issue in its full complexity. Foubert et al. (2006) studied the relationship between crystallization, microstructure and macroscopic properties in a trans containing palm based and trans free lauric based coating fat with DSC, microscopy and hardness measurements. Bell et al. (2007) used a rheological approach to compare the crystallization of fats differing in composition (low trans and high trans) but with similar melting profiles.

The aim of this chapter, which has a more applied nature, was thus to gain more insight into the role of trans fatty acids on crystallization and texture of palm oil based confectionery fats. Therefore, a series of trans containing and trans free palm oil based confectionery fats were analyzed with several techniques to asses their crystallization behavior and texture at 10°C. Differential scanning calorimetry (DSC) and pulsed nuclear magnetic resonance (pNMR) were applied to evaluate the primary crystallization, while oscillatory rheology provided information on primary crystallization, microstructural development and macroscopic properties. Texture was evaluated in terms of hardness determined by penetrometry.

7.2 Methods and Materials

7.2.1 Substrates

Loders Croklaan (Wormerveer, The Netherlands) supplied two series of palm based confectionery fats, one trans containing and one trans free. Samples were stored in the freezer.

7.2.2 Fatty acid composition

Fatty Acid Methyl Esters (FAME) were produced and subsequently analyzed on a Varian GC (Varian, Sint-Katelijne Waver, Belgium) with WCOT CP-sil88 column, split injector and FID according to the AOCS official method Ce 1-62 (1997). Each analysis was executed in triplicate.

7.2.3 Triacylglycerol composition

High resolution separation for triacylglycerols was achieved using an Agilent 6890+ GC system fitted with an automated on column injection onto a Quadrex 15m 0.25 mm 0.1 μm film 65% phenyl-methyl silicone GC column. The samples were dissolved in iso-octane at approximately 0.1 mg/mL. The injection volume was 0.1 μL. The helium carrier gas was set at constant flow of 1ml/minute. The oven program with injector in oven track mode was 80°C for 0.5 minutes, ramping up to 330°C at 50°C/minute, with triacylglycerols separation being achieved from 330°C to 350°C ramping at 1°C/minute. Detection was via FID.

The carbon number distribution was obtained using a Perkin Elmer AUTOXL GC system fitted with a 10m x 0.53mm 0.1μL. Quadrex Scientific methyl-5% phenyl DB-5 capillary column. The samples were dissolved into iso-octane at a concentration of approximately 2mg/ml and 0.5μL was used as injection volume. The injector program was 70°C for 0.1 minutes, ramping up to 350°C at 200°C/minute and holding at 350°C for 3 minutes. The oven program was 200°C at 0.0 minutes, ramping up to 325°C at 10°C/minute, with triacylglycerols separation being achieved from 325°C to 355°C ramping at 5°C/minute. Helium was used as carrier gas and detection was via FID.

7.2.4 pNMR

pNMR experiments were performed with a Minispec pc 20 (Bruker, Karlsruhe, Germany). Liquefied fat was transferred into pNMR tubes and held at 65°C for 30 minutes to eliminate any thermal history. Subsequently, the tubes were placed in a thermostatic water bath at 10°C. Readings of the amount of solid fat were taken at appropriate time intervals and a separate tube was used for each measurement. Each analysis was executed in triplicate.

7.2.5 DSC (stop and return)

The primary crystallization mechanism was further investigated with stop-and-return DSC experiments. The principle of the stop-and-return technique is to interrupt the primary isothermal crystallization at different moments in time and, subsequently, heat the sample to obtain the melting profile of the crystals formed during the immediately preceding isothermal period. Based on this melting profile, information on the primary crystallization process can be obtained (See also section 4.2.3). The applied time-temperature program for the isothermal crystallization curves was as follows: holding at 70°C for 10 minutes to ensure a completely liquid state, cooling at 5°C per min to the 10°C (0.05°C), holding for the required crystallization time and then heating at 20°C per min to 70°C.

7.2.6 Polarized light microscopy

Microscopic analyses were conducted by the use of a Leitz Diaplan microscope (Leitz Diaplan, Leica, Germany) equipped with a Linkam PE94 temperature control system (Linkam, Surrey, U.K.). Samples were imaged with a Nikon Coolpix 4500 (Nikon, Melville, New York). To allow unhindered crystal growth, a cavity was formed on a glass slide by means of gluing some cover slips to the edges of the carrier glass. The melted sample was applied to this cavity and allowed to crystallize without a cover slip, thus allowing unhindered crystal growth in a three dimensional space.

7.2.7 Oscillatory rheology

The crystallization process was monitored by oscillatory rheology using the geometry and settings specified in section 3.2.2. The melted sample was transferred into the cup and the following temperature profile was applied:

- keeping isothermally for 10 minutes at 70°C to erase all crystal memory;
- cooling at 5°C per min to 10°C;
- oscillatory time sweep at 10°C (isothermal period).

Rheograms were obtained by plotting the complex modulus ($|G^*|$) and the phase angle (δ) of the crystallizing sample as a function of isothermal time at 10°C. Each analysis was executed in triplicate.

7.2.8 Hardness

Penetration tests were used to determine the hardness of the samples. The hardness of a fat is an important property that strongly influences the perceived texture of the fat containing food product (Brunello et al. 2003). Samples were cooled on a copper plate in which cooling water of 10°C circulated and was placed inside a thermostatic cabinet at 10°C to eliminate temperature fluctuations from the environment. Samples were crystallized at 10°C for 30, 60 and 90 minutes after which the hardness was measured with a penetration test. This penetration test was performed on a Texture Analyzer TA 500 (Lloyd Instruments, Hampshire, United Kingdom) with a load cell of 500N and a cylindrical probe with a diameter of 4.51 mm (CNS Farnell, Hertfordshire, United Kingdom), penetrated the product at a constant speed of 10 mm/min to a distance of 10 mm. To ensure that measurement of the hardness at the specified temperature the texture analyzer was placed in a temperature controlled cabinet at 10°C (0.5°C) (Lovibond, Dortmund, Germany). Hardness was defined as the maximum penetration force (N) and each measurement was executed seven times.

7.3 Results and Discussion

7.3.1 Characterization of the samples: fatty acid composition

Table 7.1 presents the fatty acid composition of the trans containing (HTF: high trans fat) and the trans free (NTF: no trans fat) fat series. The HTF-series contained 31 to 42% elaidic acid (C18:1trans), while for the NTF no trans fatty acid was detected. Both fat series were high in palmitic acid (C16:0) and oleic acid (C18:1c) due to their palm

Table 7.1: Fatty acid composition of high trans fat (HTF) and non-trans fat (NTF) samples (wt%) as determined by gas chromatography

	C12:0	C14:0	C16:0	C18:0	C18:1t	C18:1c	C18:2 n-6	Other	Sat. /Unsat.	(Sat.+C18:1t) /Unsat.
HTF-1	0.31	1.27	39.98	7.49	31.44	19.32	-	0.19	0.97	4.17
	± 0.02	± 0.04	± 0.2	± 0.05	± 0.17	± 0.10	-	± 0.02		
HTF-2	0.87	1.47	35.71	7.53	34.54	19.58	-	0.30	0.84	4.09
	± 0.02	± 0.04	± 0.09	± 0.01	± 0.23	± 0.32	-	± 0.03		
HTF-3	0.28	0.72	23.86	11.66	41.71	21.13	-	0.64	0.58	3.70
	± 0.02	± 0.01	± 0.18	± 0.01	± 0.05	± 0.13	-	± 0.03		
NTF-1	0.24	1.26	50.28	5.04	-	35.18	7.67	0.33	1.33	1.33
	± 0.01	± 0.02	± 0.07	± 0.04	-	± 0.06	± 0.04	± 0.01		
NTF-2	0.16	1.13	54.06	4.82	-	33.36	6.14	0.33	1.52	1.52
	± 0.01	± 0.03	± 0.16	± 0.02	-	± 0.14	± 0.02	± 0.02		
NTF-3	0.09	0.94	59.53	6.04	-	30.29	2.77	0.34	2.01	2.01
	± 0.01	± 0.02	± 0.16	± 0.02	-	± 0.15	± 0.03	± 0.01		

Table 7.2: Carbon number distribution of high trans fat (HTF) and non-trans fat (NTF) (wt%) as determined by gas chromatography (* Note that single measurements have been made)

	C42	C44	C46	C48	C50	C52	C54	C56	C58	C60
HTF-1	0.06	1.27	0.22	2.51	29.68	52.14	14.58	0.73	0.00	0.01
HTF-2	0.16	1.47	0.27	2.30	22.74	54.40	18.66	0.99	0.19	0.12
HTF-3	0.11	0.72	0.70	1.84	14.98	25.11	51.96	3.72	0.90	0.58
NTF-1	0.06	0.07	0.47	3.99	53.24	33.20	8.23	0.49	0.13	0.06
NTF-2	0.04	0.17	0.45	3.91	61.40	27.54	6.04	0.41	0.14	0.00
NTF-3	0.02	0.10	0.54	4.28	71.94	19.36	3.27	0.32	0.15	0.04

oil based nature. Within the HTF-series, the fats differed mostly in C16:0 and C18:1t content, and to a minor extent in amount of C18:0 and C18:1c. For the NTF-series, the major differences occurred in C16:0 content and amount of unsaturated fatty acids. These compositional differences can also be represented by the ratio of saturated to unsaturated fatty acids. This ratio was the highest for NTF-3 and the lowest for HTF-3. If C18:1t is assumed to behave more like a saturated fatty acid than an unsaturated one, the ratio of saturated + C18:1t to unsaturated can also be calculated. This ratio yields the highest value for HTF-1 and the lowest for NTF-1.

The carbon number composition of the HTF- and NTF-series is displayed in Table 7.2. When comparing the two series, the HTF-series proves to be higher in C52 and C54 compared to the NTF-series, but lower in C50. Within the HTF-series, the amount of C48 and C50 decreased from HTF-1 to HTF-3, while C54 increased. The highest percentage of C54 was found in HTF-3. HTF-3 stood out from HTF-1 and HTF-2 as it was lower in C52 (25.11% compared to 52.14% and 54.40% respectively), but high in C56 (3.72% compared to 0.73% and 0.99% respectively). Within the NTF-series, C52 and C54 decreased from NTF-1 to NTF-3, while C50 increased. NTF-3 also showed a slightly higher C48 compared to NTF-1 and NTF-2 (4.28% compared to 3.99% and 3.91% respectively).

High resolution GC-analysis was unable to separate the wide range of cis-trans isomers present in the HTF-samples and therefore only Carbon Number GC-data can be reported

Table 7.3: Triacylglycerol composition of non-trans fat (NTF) (wt%) obtained with high resolution GC (wt%) (positional isomers have not been separated)(* Note that single measurements have been made)

		NTF-1	NTF-2	NTF-3
C46	MMP	0.33	0.38	0.47
	MOM	0.14	0.07	0.07
C48	PPP	1.41	1.63	2.48
	MOP	2.04	1.96	1.62
	MLP	0.54	0.33	0.15
C50	PPS	0.82	0.21	0.80
	POP	42.93	52.56	65.80
	PLP	9.30	8.38	5.18
	MLO	0.15	0.05	0.00
	MLL	0.24	0.31	0.35
C52	PSS	0.36	0.02	0.64
	POS	7.85	10.15	13.09
	POO	16.04	11.21	3.47
	PLS	1.79	1.28	0.95
	PLO	5.99	4.03	1.00
	PLL	1.23	0.86	0.20
C54	SSS	0.16	0.01	0.13
	SOS	1.10	1.43	2.04
	SOO+SLS	2.08	1.48	0.40
	OOO	2.66	1.92	0.33
	SLO	0.76	0.54	0.04
	OLO	1.27	0.62	0.13
	OLL	0.20	0.03	0.19
others		0.60	0.56	0.44

for these samples. The triacylglycerols composition of the NTF-series, obtained with high resolution GC, is presented in Table 7.3. Within this series the amount of PPP, POP, POS and SOS increased from NTF-1 via NTF-2 to NTF-3, while the percentage of PLP, POO, PLO, SOO+PLS and OOO decreased.

7.3.2 Isothermal crystallization behavior at 10°C

Figure 7.1 presents the SFC as a function of time at 10°C for the HTF- (Figure 7.1A) and NTF-series (Figure 7.1B). As can be seen in Figure 7.1A, the three HTF-fats showed a very similar primary crystallization. They all started to crystallize very rapidly and quickly reached an equilibrium value which was quite high. This equilibrium value was significantly (p=0.05) different within the HTF-series: HTF-3 reached a slightly higher equilibrium value ($95.50 \pm 0.07\%$) compared to HTF-2 ($93.51 \pm 0.01\%$) and HTF-1 ($87.89 \pm 0.06\%$). These differences can be attributed to the different amount of trans fatty acid in the three HTF-fats (Table 7.1), being lowest for HTF-1 and highest for HTF-3. Although HTF-3 had the lowest ratio of (saturated fatty acids + C18:1t) to unsaturated fatty acids, it reached the highest SFC equilibrium value, which is probably related to the higher amount of C18:1t as trans fatty acids tend to crystallize faster than their cis-equivalents, as has been demonstrated in a recent study by Vereecken et al. (2007). However, with the ratio of (saturated fatty acids + C18:1t) to unsaturated fatty acids being rather similar for the three HTF-fats, no major differences were expected, despite the differences in chemical composition. In carbon number composition (Table 7.2) the C54-content (higher melting) increases from HTF-1 to HTF-3, while the C48 and C50 content decreases. These compositional differences can be an explanation for the differences in primary crystallization.

The NTF-series showed major differences in primary crystallization as is illustrated in Figure 7.1B. NTF-3 crystallized very rapidly and, like the HTF, quickly reached a high equilibrium value ($96.14 \pm 0.01\%$). NTF-2 and NTF-1 crystallized much slower and their equilibrium value was significantly (p=0.05) lower, $79.14 \pm 0.30\%$ and $64.72 \pm 0.46\%$ respectively. Based on Table 7.3 it can be seen that NTF-3 is higher in PPP, POP, POS and SOS compared to NTF-2 and NTF-1 respectively, which is in agreement with the order of crystallization. Taking into account the ratio of saturated to unsaturated fatty acids (Table 7.1), NTF-3 is indeed expected to crystallize faster than NTF-2 and NTF-1.

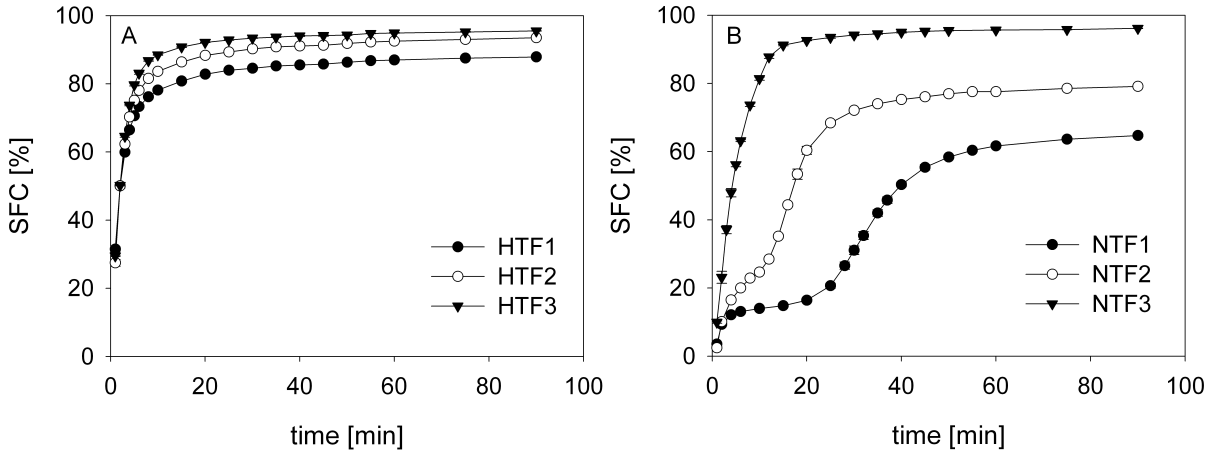

Figure 7.1: SFC of (A) HTF and (B) NTF as a function of time at 10°C obtained with pNMR (NTF=no trans fat; HTF=high trans fat)

However, this ratio does not explain why the HTF-fats, having a lower ratio of saturated to unsaturated fatty acids, crystallized so much faster.A possible explanation lies in the presence of C18:1t in the HTF-series. Based on the structure of trans fatty acids, which is more similar to that of saturated fatty acids rather than to cis-unsaturated fatty acids, it might be assumed that they behave more as saturated fatty acids. The ratio of saturated fatty acids + C18:1t to unsaturated fatty acids (Table 7.1) is much higher for the HTF-series compared to the NTF-series, which is in agreement with the order of crystallization.

Based on Figure 7.1, it can also be assumed that the NTF- and HTF-series possess a different primary crystallization mechanism. In Figure 7.1A, the HTF-series display a single step primary crystallization, while in Figure 7.1B, NTF-1 and NTF-2 clearly exhibit a two-step primary crystallization. Based on Figure 7.1B, a single step primary crystallization process could be assumed for NTF-3. In general, a two-step primary crystallization mechanism can be due to a polymorphic transformation, a fractionated crystallization or a combination thereof.

Figure 7.2B represents the melting curves of NTF-3 at different isothermal times at 10°C. Although Figure 7.1B did not reveal a two-step primary crystallization mechanism, Figure 7.2B proves otherwise. The melting curves clearly display two peaks, one with a minimum at 18°C and one with a minimum at 25°C. The first peak was already present

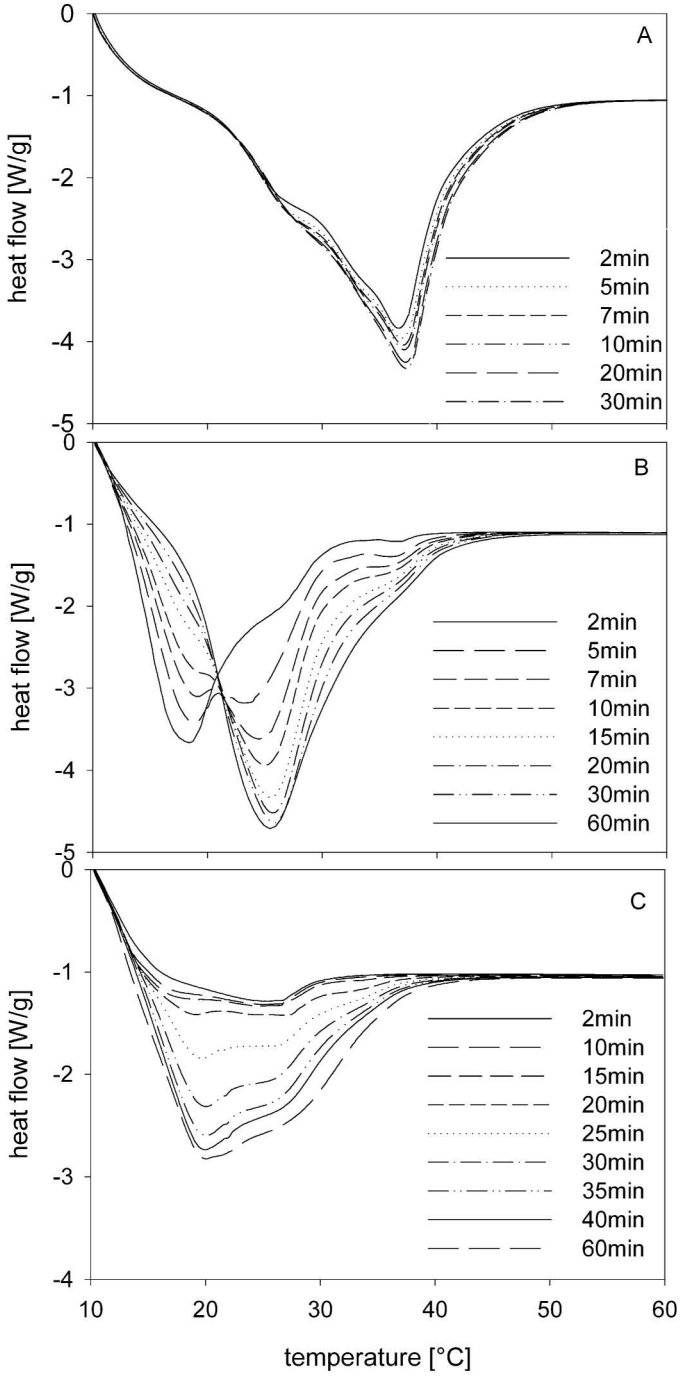

Figure 7.2: Melting curves of (A) HTF-2, (B) NTF-3 and (C) NTF-1 and at 10° obtained with DSC (NTF=no trans fat; HTF=high trans fat)

after 2 minutes of crystallization and gradually decreased at later times, with the second peak appearing as the first one decreased. Palm oil is known to exhibit a two-step crystallization below a certain cut-off temperature, which depends on composition. Below this cut-off temperature palm oil is said to undergo an α mediated β' crystallization, while at higher temperatures β' crystals are directly formed from the melt (Chen et al. 2002; Mazzanti et al. 2005). The first peak in Figure 7.2B might thus be attributed to the α polymorph and the second peak to the β' polymorph, possibly with extra β' formation directly from the melt.

Figure 7.1B already suggested a two-step primary crystallization for NTF-1 and NTF-2. Stop-and-return results confirmed that for NTF-2 this two-step primary crystallization was due to a polymorphic transition. For NTF-1 (Figure 7.2C), however, this two stepped mechanism appeared to be caused by a fractionated crystallization into a high melting and a low melting fraction, possibly both directly in the β' polymorph. This is apparent since the high-melting peak appears first and grows a little before the low-melting peak appears and increases in size. This suggests a high-melting fraction begins to crystallize at the start, later joined by the lower-melting fraction. The difference in mechanism is most likely due to compositional differences as expressed in the carbon number profile (Table 7.2) and the triacylglycerol composition (Table 7.3). Compared to NTF-2 and NTF-3, NTF-1 has a lower percentage of PPP, POP, POS and SOS, while being higher in PLP, POO, PLO, PLL, SOO+PLS, OOO, SLO and OLO. It can thus be supposed that at 10°C, NTF-2 and NTF-3 undergo an α mediated β' crystallization, while NTF-1 crystallizes directly in the β' polymorph, with the two step character due to a lower-melting and a high-melting fraction.

For the HTF-fats, a single step primary crystallization process was hypothesized, which is illustrated in Figure 7.2a. Figure 7.2A show the melting curves of HTF-2 at different isothermal times at 10°C. In contrast to Figure 7.2B, only a single peak is present with a minimum at 37°C, probably indicating a direct crystallization in a more stable polymorph. Based on these data, it cannot be concluded whether the HTF-fats crystallize in the β' or β polymorph. Taking into account that the HTF-series is palm oil based, it is likely that the HTF-samples crystallize directly in the β'-polymorph (Chen et al. 2002; Yap et al. 1989). The different primary crystallization mechanism of the NTF- and HTF-series could be explained by the difference in fatty acid composition. A higher ratio of (saturated fatty

acids + C18:1t) to unsaturated fatty acids appeared to cause a direct crystallization in the β' polymorph.

7.3.3 Oscillatory rheology at 10°C

The isothermal crystallization at 10°C was also investigated with oscillatory rheology. This technique allows recording all three steps of the crystallization process, namely primary crystallization, microstructural development of the fat crystal network and macroscopic properties as is demonstrated in Chapter 3. Crystallization curves were obtained by plotting the complex modulus and the phase angle as a function of isothermal time at 10°C, which is illustrated in Figure 7.3 and Figure 7.4. As some of the samples began to crystallize during the cooling step, the cooling time is included as a negative isothermal time.

Figure 7.3A presents the phase angle and complex modulus of NTF-3. Although measurements are executed in triplicate, this graph represents a typical curve as there is very little variation amongst the repetitions. The evolution of the phase angle in time can be divided in five different sections as indicated by the dotted lines. As shown by Toro-Vazquez et al. (2002, 2004) and De Graef et al. (2006)(Chapter 3, these different sections can be attributed to crystallization into different polymorphic forms. The discussion of these sections is based on Figure 7.3A of NTF-3, but also applies to NTF-2.

- Section 1: δ is close to 90°, indicating a fully melted sample
- Section 2: δ decreases sharply from 90° to 24°. This decrease can be attributed to crystallization in the α polymorph.
- Section 3: δ remains more or less unchanged. The α crystals formed in section 1 are converted into β' crystals via a solid state transformation, as seen in the DSC results. The variation in phase angle during this step is probably caused by the crystallization heat released during section 1. This crystallization heat can induce a temperature rise, locally causing crystals to melt. This then leads to a loosening of the network structure and an increase in phase angle.
- Section 4: δ decreases again to 1°. This decrease is caused by the formation of β' crystals directly from the melt, aggregation and network formation.

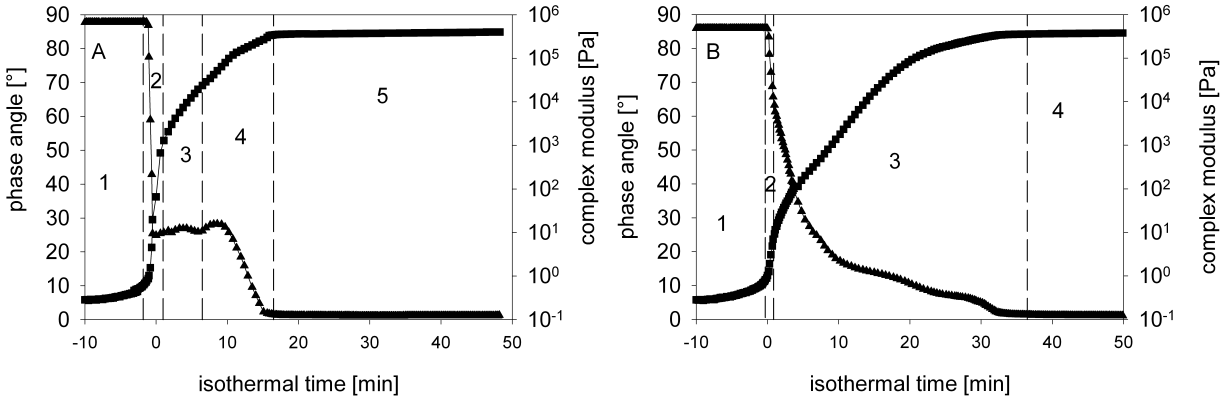

Figure 7.3: Phase angle (▲) and complex modulus (■) of (A) NTF-3 and (B) NTF-1 as a function of isothermal time at 10°C obtained with oscillatory rheology (NTF=no trans fat)

- Section 5: δ remains at 1°, indicating a completely crystallized sample.

Also shown in Figure 7.3A is the complex modulus. The changes in complex modulus correspond with the timescale of events in the phase angle. In section 1 the low values illustrate the liquid state of the sample, in section 2 the fat gains structure as α crystals are formed, in section 3 and 4 this increasing trend is maintained due to the polymorphic transition of α to β' crystals and the subsequent formation of β' crystals from the melt. In section 5 the complex modulus reaches an equilibrium value which can be used to evaluate the macroscopic properties of the sample. The increase in complex modulus and the decrease in phase angle are not only due to the primary crystallization, but also to development of the microstructure by aggregation. These two processes cannot be completely separated. Walstra (1987) already pointed out that ongoing crystallization and particularly recrystallization cause a growing together or sintering of the flocculated crystals, thereby greatly enhancing the strength of the bonds in the network, which can be seen as an increase in complex modulus. Sintering can already occur in a very early stage (Johansson 1995).

For NTF-1, phase angle and complex modulus behave quite differently, as presented in Figure 7.3B. As discussed earlier, NTF-1 has a different primary crystallization mechanism than NTF-2 and NTF-3: NTF-1 crystallizes into two fractions, both assumed to be in the β' polymorph. This difference in primary crystallization mechanism can also be found in

the rheological data:

- Section 1: δ is close to 90° indicating a completely melted sample
- Section 2: δ decreases to about 65°, due to the crystallization of the higher melting fraction and aggregation of the crystals.
- Section 3: δ further decreases to 1° due to crystallization of the lower melting triacylglycerols and network formation
- Section 4: δ is close to 0°, indicating a fully crystallized sample.

The complex modulus of NTF-1 is similar to that of NTF-3 as can be deduced from Figure 7.4B: thus the difference in primary crystallization mechanism can not be assessed based on the complex modulus. When evaluating the complex moduli of the NTF-series presented, it can be seen that the differences between these fats are mainly situated in the rate of increase of the complex modulus. In other words, the NTF-fats develop a rather similar network strength, but the time scale in which this happens differs. Polarized light microscopy (data not shown) revealed that aggregation was preceded by a period of nucleation and crystal growth (primary crystallization). The aggregates grew for some time before network formation occurred. For NTF-1 this network developed slowly, which agrees with the long and gradual decrease of the phase angle and increase in complex modulus. For NTF-2 network formation occurred slightly sooner, but the gradual increase in complex modulus is very similar to the one seen for NTF-1. On the other hand, network formation happened very quickly for NTF-3, which is in agreement with the rapid increase of the complex modulus in section 2 (Figure 7.3A). For all the NTF-fats, the complex modulus reached an equilibrium value. NTF-3 attained an equilibrium value of $3.52 * 10^5 \pm 2.64 * 10^3$ Pa at 16 minutes isothermal time, while NTF-1 and NTF-2 reached their equilibrium values of $3.44 * 10^5 \pm 5.03 * 10^3$ Pa and $3.45 * 10^5 \pm 1.73 * 10^3$ Pa respectively at 34 and 28 minutes isothermal time. The equilibrium value of NTF-3 was significantly (p=0.05) higher compared to NTF-1 and NTF-2, which did not significantly differ (p=0.05).

For the HTF-fats, the complex modulus increased rapidly as is illustrated in Figure 7.4D, indicating a rapid crystallization process. As has been discussed earlier, the HTF-fats showed a rapid single step primary crystallization. Based on the complex moduli, it can be assumed that the microstructural development is also very rapid and very similar

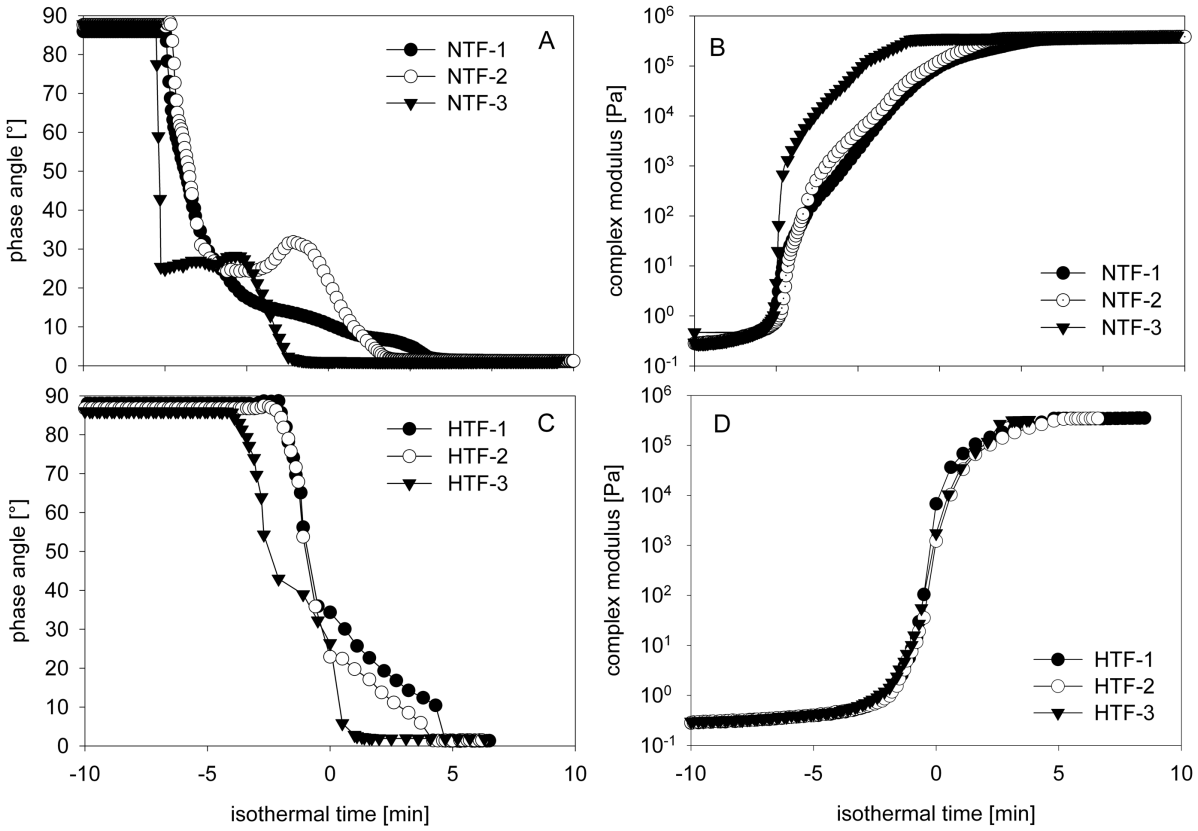

Figure 7.4: Phase angle (A and C) and complex modulus (B and D) of the NTF-series and the HTF-series respectively as a function of isothermal time at 10°C (NTF=no trans fat; HTF=high trans fat)

for all HTF-fats. The phase angle (Figure 7.4C) shows an earlier onset of crystallization for HTF-3 and a rapid crystallization for all samples. Polarized light microscopy (data not shown) revealed that during primary crystallization small crystals were formed which subsequently aggregated to a network structure. The strong increase in complex modulus coincided with this network formation. The similarity of the complex modulus indicates a similar microstructure for the HTF-fats, based on which a similar hardness can be expected.

As for the NTF-fats, the complex modulus of the HTF-fats attained an equilibrium value: $3.44 * 10^5 \pm 4.58 * 10^3$ Pa for HTF-1, $3.34 * 10^5 \pm 8.08 * 10^3$ Pa for HTF-2 and $3.20 * 10^5 \pm 3.78 * 10^3$ Pa. No significant (p=0.05) differences in equilibrium value were

found between HTF-1 and HTF-2, but the one of HTF-3 was significantly (p=0.05) lower than those of HTF-1 and HTF-2, which agrees with the ratio of (saturated fatty acids + C18:1t) to unsaturated fatty acids for the HTF-fats. This significant difference might be due to the fact that structure breakdown occurred when the equilibrium value was just reached. This structure breakdown would be due to the test conditions no longer being within the linear viscoelastic region after less than 5 minutes isothermal time. For HTF-1 and HTF-2 this structure breakdown occurred some minutes later, which also indicated the similarity of the microstructure. When comparing the rheological data of the HTF- and NTF-series, the main difference can be found in the timescale of events. Based on pNMR and DSC-results, it was already clear that the HTF-series crystallized much faster than the NTF-series. This observation is confirmed by the rheological data. Comparing the end values of the complex modulus between the different fat series led to this result: HTF-3<HTF-2=HTF-1=NTF-1=NTF-2<NTF-3 (p=0.05). This result might also be influenced by the fact that the HTF-sample could not be measured for the complete period due to structure breakdown.

7.3.4 Hardness as a function of time at 10°C

Figure 7.5A shows the hardness of the HTF-series. At 30 and 90 min storage time no significant (p=0.05) differences were detected between the three HTF-fats, while at 60 min the hardness of HTF-1 was significantly lower. It appears that differences in chemical composition were not translated into general differences in hardness. Based on the fatty acid profile (Table 7.1) an increasing hardness going from HTF-3 to HTF-1 could be expected as HTF-3 has the lowest ratio of (saturated + C18:1t) to unsaturated and HTF-1 the highest. Furthermore, HTF-3 reached the highest equilibrium SFC-value and HTF-1 the lowest. Although the HTF reached their plateau SFC-value before 30 min isothermal time (Figure 7.1A), hardness continued to increase beyond this point, indicating SFC is not the sole factor to determine hardness (Narine and Marangoni 1999c; Narine and Marangoni 1999e). However, it must be kept in mind that, when using different equipment to follow crystallization, comparison between results must be done with caution. Differences in sample weight or volume, equipment design and its impact on the thermodynamics of the system and, heat and mass transfer conditions existing in each measurement device, may affect the process to a different extent. Other factors than SFC influencing mechanical

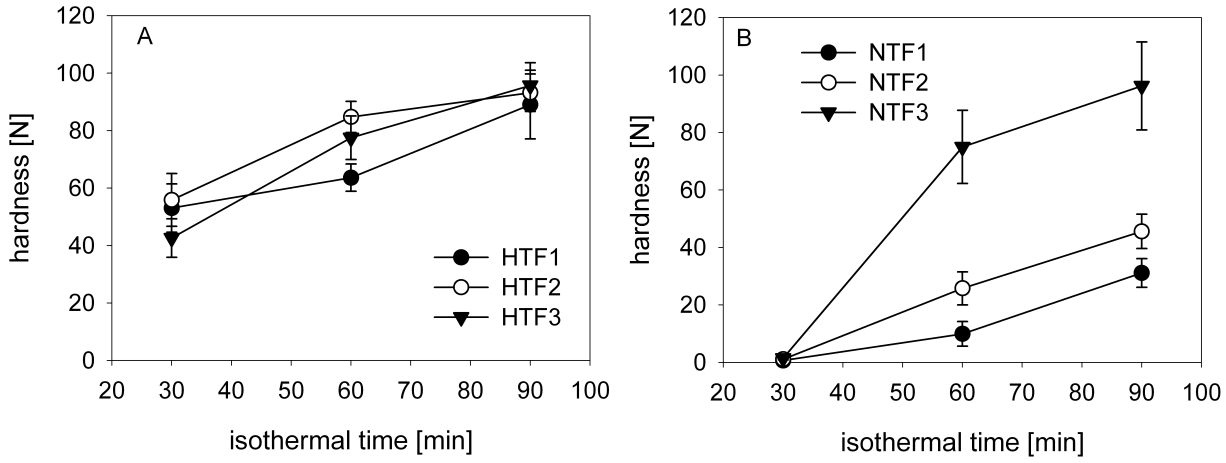

Figure 7.5: Hardness of (A) HTF and (B) NTF as a function of isothermal time at 10°C obtained with penetrometry (NTF=no trans fat; HTF=high trans fat)

properties of edible fats include the polymorphism of the solid state as well as the microstructure of the crystal network (Marangoni and Narine 2002; Braipson-Danthine and Deroanne 2004). As the peak maximum in the melting profiles did not change as a function of time, polymorphism can not be an explanation. A very plausible explanation for the change in hardness is sintering of the crystals. This leads to a further strengthening of the crystal network, and subsequently an increase in hardness, without an increase in SFC (Kloek 1998).

The hardness of the NTF-fats is presented in Figure 7.5B. At 60 and 90 minutes the hardness of the NTF-fats was significantly (p=0.05) different, being at both storage times the highest for NTF-3 and the lowest for NTF-1. This agrees with the ratios (saturated fatty acids + C18:1) to unsaturated fatty acids which increased form NTF-1 over NTF-2 to NTF-3. Thus, in the case of NTF-fats, differences in composition were reflected by differences in hardness. At 30 minutes isothermal time, all three NTF displayed very low hardness values. No significant differences were found, which is in contrast to the significant differences found in SFC. This observation indicates again that SFC is not the sole factor determining the hardness. Within the next 30 min, hardness increased significantly, especially for NTF-3. For NTF-1 and NTF-2 the increase was less pronounced. For NTF-2 and NTF-3, the increase in hardness between 30 and 60 minutes isothermal time can not be explained by the SFC as an equilibrium value was reached before or around 30 minutes

(Figure 7.1B). Because the peak maximum in the melting profiles did not shift, changes in polymorphism could not be the cause of this changing hardness. This change is likely to be due to phenomena like sintering (Kloek 1998). For NTF-1 on the other hand, the hardness increase between 30 and 60 min is linked with a significant increase in SFC, while this is not the case for the change in hardness from 60 to 90 minutes.

At 30 min storage time, the hardness of the NTF-series was significantly (p=0.05) lower than those of the HTF-series, and HTF-3 was significantly (p=0.05) lower than HTF-1 and HTF-2. At 60 min storage time this order has changed: NTF-1, NTF-2 and HTF-1 were significantly lower than HTF-3 which itself was significantly (p=0.05) lower than NTF-3, HTF-1 and HTF-2. At 90 min storage time NTF-3 was not significantly (p=0.05) different from the HTF-fats, which had a significantly (p=0.05) higher hardness than NTF 1 and NTF-2. NTF-1 was significantly (p=0.05) lower in hardness than NTF-2. So, from all the fats studied, the HTF-series plus NTF-3 displayed the highest hardness after 90 min storage time, while the lowest values were found for NTF-1. The difference between the NTF-fats can be explained based on the chemical composition (Table 7.2 and Table 7.3): NTF-3 has the highest percentages of PPP, POP, POS, SOS, which are all rather high melting triacylglycerols, while these percentages are much lower in NTF-1. It appears that compositional differences in the HTF-series do not cause major variations in hardness, while this is clearly the case for the NTF-series. The presence of trans fat seems to flatten the compositional variations between the HTF-series, possibly due to the presence of a greater number of triacylglycerols.

7.4 Conclusions

In summary, trans containing palm oil based confectionery fats all crystallized much faster than their trans free equivalents. Based on the stop-and-return DSC experiments, it could be concluded that the HTF-series crystallized directly into a more stable polymorph, most likely β'. Although the HTF-series differed in chemical composition, this difference was not reflected in major variations in SFC, or in network formation, as expressed by the complex modulus, or in hardness. The presence of trans fat seems to reduce the influence of compositional variations to some degree.

The trans free palm oil based confectionery fats showed more differences. The stop-and-return experiments revealed different mechanisms of primary crystallization: NTF-2 and NTF-3 showed a two-step primary crystallization of polymorphic nature, while for NTF-1 the two-step process was due to crystallization in a high-melting and a low-melting fraction. For the NTF-series, differences in chemical composition led to differences in SFC, network formation and hardness. NTF-3, which has the highest ratio saturated to unsaturated fatty acid, showed the highest SFC value, the fastest network formation (increase in complex modulus) and the highest hardness values. Based on these results, NTF-3 behaved similar to the HTF-fats. For the NTF-series, differences in chemical composition had a major influence on the crystallization process.

Manufacturers have to be aware that, when replacing trans containing fats with their trans free alternatives, differences in chemical composition between these alternatives can have a tremendous effect on the final product quality. The formulation of a suitable alternative is, therefore, not straightforward. In addition, some modification of processing conditions might be anticipated.

General Conclusions

The fat crystal network plays an important role in fat rich products as it determines many of their macroscopic properties. In this research, a wide range of experimental techniques was applied to study the microstructural properties of isothermally crystallizing palm oil, resulting in a more profound understanding of this important structure level.

The usefulness of oscillatory rheology to monitor fat crystallization was demonstrated. Similar to the more classically used techniques DSC and pNMR, oscillatory rheology was capable of differentiation between a single step and a two-step primary crystallization process. However, where DSC and pNMR are limited to evaluate primary crystallization, oscillatory rheology also provides information on microstructural development and the final macroscopic properties. The major advantage of oscillatory rheology is that it can record all three stages of crystallization (primary crystallization, microstructural development and macroscopic properties) with one single analysis.

Palm oil proved to follow an α mediated β' crystallization with additional β' formation from the melt at 18, 20 and 22°C. This in contrast to at 25°C where only β' crystals were formed. In addition, it was shown that a higher crystallization temperature resulted in a lower solid fat content and a lower network stiffness. The differences in network stiffness were traced back to microstructural differences. At lower crystallization temperatures, more crystals were present, which was reflected in the higher solid fat content. Furthermore, significantly more interactions between the crystal aggregates were observed, resulting in a more uniform network structure and thus higher network stiffness. At 25°C, larger crystal structures were suspended in the liquid fat matrix with few interactions between the aggregates.

Industrial production processes often involve agitation of the crystallizing mass. In order to gain more insight into the effect of shear, a rheological method was developed capable of monitoring primary crystallization and microstructural development under shear. It was revealed that during crystallization under continuous shear a preliminary network structure was formed. This preliminary network was subsequently destroyed due to ongoing shear and the constituting aggregates remained suspended in the liquid fat matrix, providing some structure to the sample.

Continuous shear also effected the polymorphism of crystallizing palm oil. Applying shear during crystallization did not affect the onset of the α formation, but the transition from α to β crystals was enhanced. The direct formation of β' crystals at 25°C, however, was not affected by the low shear rates used in this study.

Furthermore, the influence of a shear step on subsequent static crystallization was studied. It has been shown that a shear step influences the microstructural organization during the subsequent static crystallization. The extent of the effect of the shear step is determined by both the duration and the applied shear rate but also by the crystallization temperature. Rheological analysis showed an earlier increase of the complex modulus provided that the applied shear rate was high enough and applied during a sufficiently long period. In addition, different microstructures were visualized depending on the applied shear rate and duration of the shear step. Generally, increasing shear rates and shear times resulted in larger aggregates and lower network stiffness. This change in microstructural properties will also affect the macroscopic properties (for instance hardness) of the final product. Furthermore, the effect of crystallization temperature on the microstructural development should thus also be kept in mind as lower final complex moduli and different microstructures were found at 25°C compared to 18°C.

The fat crystal network and consequently the macroscopic properties are not only influenced by processing conditions such as crystallization temperature and shear rate, but also by the chemical composition of the crystallizing fat. It has been shown that in trans containing fats the effect of compositional variations are reduced to some degree. Trans free fats on the other hand, are largely affected by compositional variations. Replacing trans containing fats by their trans free equivalents is thus not an easy task as differences

in chemical composition between the trans free alternatives can have a tremendous effect on the final product quality.

This research has shed light on the microstructure of palm oil and the influence of shear and temperature thereon. In addition, the comparison has been made between trans containing and trans free palm oil-based confectionery fats. However, much is left to be unraveled. A major challenge will be to characterize the microstructural development of fat blends in industrial manufacturing. To adapt an industrial process in such a way that the desired product quality and functionality is guaranteed, more insight and understanding into the fat crystal network is needed. Nowadays, the microstructural development on an industrial scale, starting with nucleation and crystal growth and leading toward final macroscopic properties, remains mainly a 'black box' process. The research presented here provides a first step in understanding the hidden processes.

References

Anderson, A. and P. Williams (1965). *Margarine*. Oxford (UK).

AOCS Official Method Ce 1-62 (1997). Fatty acid profile. Champaign, AOCS press.

Aquilano, D. and G. Sgualdino (2001). Fundamental aspects of equilibrium and crystallization kinetics. In N. Garti and K. Sato (Eds.), *Crystallization processes in fats and lipid systems*, pp. 1–51. New York (USA): Marcel Dekker Inc.

Asta, M., F. Spaepen, and J. van der Veen (2004). Solid-liquid interfaces: molecular structure, thermodynamics, and crystallization. MRS Bulletin.

Autio, K. and M. Salmenkallio-Marttila (2001). Light microscopic investigations of cereal grains, doughs and breads. *Lebensmittel-Wissenschaft Und-Technologie-Food Science and Technology 34*, 18–22.

Awad, T. S., M. A. Rogers, and A. G. Marangoni (2004). Scaling behavior of the elastic modulus in colloidal networks of fat crystals. *Journal of Physical Chemistry B 108*, 171–179.

Bell, A., M. H. Gordon, W. Jirasubkunakorn, and K. W. Smith (2007). Effects of composition on fat rheology and crystallisation. *Food Chemistry 101*, 799–805.

Berger, K. (1981). Food uses of palm oil. *PORIM occasional paper 2*, 1–27.

Berger, K. (2001). Palm oil. In F. Gunstone (Ed.), *Structured and modified lipids*, pp. 119–154. New York (USA): Marcel Dekker Inc.

Berger, K. G. and W. Wright (1986). Crystallization behavior of palm oil. *PORIM Occasional Paper 17*, 1–10.

Biliaderis, C. (1983). Differential scanning calorimetry in food reserach - a review. *Food Chemistry 10*, 239–265.

Blonk, J. C. G. and H. van Aalst (1993). Confocal scanning light-microscopy in food research. *Food Research International 26*, 297–311.

Boistelle, R. (1988). Fundamentals of nucleation and crystal growth. In N. Garti and K. Sato (Eds.), *Crystallization and polymorphism of fats and fatty acids. Surfactant science series. Volume 31*, pp. 189–276. New York (USA): Marcel Dekker Inc.

Braipson-Danthine, S. and C. Deroanne (2004). Influence of sfc, microstructure and polymorphism on texture (hardness) of binary blends of fats involved in the preparation of industrial shortenings. *Food Research International 37*, 941–948.

Braipson-Danthine, S. and V. Gibon (2007). Comparative analysis of triacylglycerol composition, melting properties and polymorphic behavior of palm oil and fractions. *European Journal of Lipid Science and Technology 109*, 359–372.

Breitschuh, B. and E. J. Windhab (1998). Parameters influencing cocrystallization and polymorphism in milk fat. *Journal of the American Oil Chemists' Society 75*, 897–904.

Brosio, E., F. Conti, A. Dinola, and S. Sykora (1980). Pulsed low resolution NMR-study on crystallization and melting processes of cocoa butter. *Journal of the American Oil Chemists' Society 57*, 78–82.

Brunello, N., S. E. McGauley, and A. Marangoni (2003). Mechanical properties of cocoa butter in relation to its crystallization behavior and microstructure. *Lebensmittel-Wissenschaft Und-Technologie-Food Science and Technology 36*, 525–532.

Busfield, W. K. and P. N. Proschogo (1990). Thermal-analysis of palm stearine by DSC. *Journal of the American Oil Chemists' Society 67*, 171–175.

Campos, R., S. S. Narine, and A. G. Marangoni (2002). Effect of cooling rate on the structure and mechanical properties of milk fat and lard. *Food Research International 35*, 971–981.

Carter, C., W. Finley, J. Fry, D. Jackson, and L. Willis (2007). Palm oil markets and future supply. *European Journal of Lipid Science and Technology 109*, 30314.

Che Man, Y. B., T. Haryati, H. M. Ghazali, and B. A. Asbi (1999). Composition and thermal profile of crude palm oil and its products. *Journal of the American Oil Chemists' Society 76*, 237–242.

Che Man, Y. B. and P. Z. Swe (1995). Thermal analysis of failed-batch palm oil by differential scanning calorimetry. *Journal of the American Oil Chemists' Society 72*, 1529–1532.

Chen, C. W., O. M. Lai, H. M. Ghazali, and C. L. Chong (2002). Isothermal crystallization kinetics of refined palm oil. *Journal of the American Oil Chemists' Society 79*, 403–410.

Chong, C., Z. Kamarudin, P. Lesieur, A. G. Marangoni, C. Bourgaux, and M. Ollivon (2007). Thermal and structural behavior of crude palm oil: crystallization at very slow cooling rates. *European Journal of Clinical Investigation 109*, 410–421.

Cmolik, J. and J. Pokorny (2000). Physical refining of edible oils. *European Journal of Lipid Science and Technology 102*, 472–486.

De Graef, V., K. Dewettinck, D. Verbeken, and I. Foubert (2006). Rheological behaviour of crystallizing palm oil. *European Journal of Lipid Science and Technology 108*, 864–870.

De Greyt, W. and M. Kellens (2000). Refining practice. In W. Hamm and R. Hamilton (Eds.), *Edible oil processing*, pp. 79–128. Sheffield (UK): Sheffield Academic Press.

DeCostello, B. (1997). Parallel superposition rheology of polyethylene as a function of temperature. *Journal of Non-Newtonian Fluid Mechanics 68*, 303–309.

deMan, J. (1964). Effect of cooling procedures on consistency, crystal structure and solid fat content of milk fat. *Dairy Industries 29*, 244–246.

deMan, J. (1998). Functionality of palm oil in food products. *Journal of food lipids 5*, 159–170.

Deman, J. M. and A. Beers (1987). Fat crystal networks: structure and rheological properties. *Journal of Texture studies 18*, 303–318.

deMan, L. and J. deMan (1994). Functionality of palm oil and palm kernel oil in margarine and shortening. *PORIM occasional papers 32*, 1–16.

deMan, L., J. M. deMan, and B. Blackman (1989). Physical and textural evaluation of some shortenings and margarines. *Journal of the American Oil Chemists' Society 66*, 128–132.

Depypere, F. (2005). *Characterisation of fluidised bed coating and microcapsule quality: a generic approach*. Ph. D. thesis, Ghent University, Belgium.

Deroanne, C., J.-M. Marcoen, J.-P. Wathelet, and M. Severin (1977). La double crystallisation de l'huile de palme mise en evidence par diffraction des rayons-x et analyses calorimétrique différentielle. *Journal of Thermal Analysis 11*, 109–119.

Dhonsi, D. and A. G. F. Stapley (2006). The effect of shear rate, temperature, sugar and emulsifier on the tempering of cocoa butter. *Journal of Food Engineering 77*, 936–942.

Durrenberger, M. B., S. Handschin, B. Conde-Petit, and F. Escher (2001). Visualization of food structure by confocal laser scanning microscopy (clsm). *Lebensmittel-Wissenschaft Und-Technologie-Food Science and Technology 34*, 11–17.

Ferrando, M. and W. Spiess (2000). Review: Confocal scanning laser microscopy. a powerful tool in food science. *Food Science and Technology International 6*, 267–284.

Fils, J. (2000). The production of oils. In W. Hamm and R. Hamilton (Eds.), *Edible oil processing*, pp. 47–78. Sheffield (UK): Sheffield Academic Press.

Foubert, I. (2003). *Modelling isothermal cocoa butter crystallization: influence of temperature and chemical composition.* Ph. D. thesis, Ghent University, Belgium.

Foubert, I., K. Dewettinck, D. Van de Walle, A. Dijkstra, and P. Quinn (2007). Physical properties: structural and physical characteristics. In F. Gunstone, J. Harwood, and A. Dijkstra (Eds.), *The Lipid Handbook*, pp. 471–534. New York (USA): CRC press.

Foubert, I., E. Fredrick, J. Vereecken, M. Sichien, and K. Dewettinck (2008). Stop-and-return DSC method to study fat crystallization. *Thermochimica Acta 471*, 7–13.

Foubert, I., J. Vereecken, K. Smith, and D. K. (2006). Relationship between crystallization behavior, microstructure and macroscopic properties in trans containing and trans free coating fats and coatings. *Journal of Agricultural and Food Chemistry 54*, 7256–7262.

Gapor, M. (1990). Content of vitamin e in palm oil and its antioxidant activity. *Palm Oil Devision, Palm Oil Research Institute of Malaysia 12*, 25–27.

Garbolino, C., G. R. Ziegler, and J. N. Coupland (2000). Ultrasonic determination of the effect of shear on lipid crystallization. *Journal of the American Oil Chemists'*

Society 77, 157–162.

Garside, J. (1987). General principles of crystallization. In V. M. V. Blanshard and P. Lillford (Eds.), *Food structure and behaviour*, pp. 35–49. London (UK): Academic Press.

Gee, P. T. (2007). Analytical characteristics of crude and refined palm oil and fractions. *European Journal of Lipid Science and Technology 109*, 373–379.

Ghotra, B., S. Dyal, and S. Narine (2002). Lipid shortenings: a review. *Food Research International 35*, 1015–1048.

Gibon, V., W. De Greyt, and M. Kellens (2007). Palm oil refining. *European Journal of Lipid Science and Technology 109*, 315–335.

Goderis, B. and H. Reynaers (2002). Haal meer uit uw thermische analyse experimenten! synchrotron WAXD en SAXS gecombineerd met DSC en nog zoveel meer. *Chemie Magazine 2*, 46.

Goh, E. (2002). Applications and uses of palm and palm kernel oils on specialty products. *Malaysian Oil Science and Technology 11*, 46–50.

Goh, E. M. and R. E. Timms (1985). Determination of mono- and diglycerides in palm oil, olein and stearin. *Journal of the American Oil Chemists' Society 62*, 730–734.

Goh, S., Y. Choo, and A. Ong (1985). Minor components of palm oil. *Journal of the American Oil Chemists' Society 62*, 237–240.

Gunasekaran, S. and M. Ak (2000). Dynamic oscillatory shear testing of foods- selected applications. *Trends in Food Science and Technology 11*, 115–127.

Gunstone, F. and J. Harwood (2007). Occurence and characterisation of oils and fats. In F. Gunstone, J. Harwood, and A. Dijkstra (Eds.), *The Lipid Handbook*, pp. 37–142. New York (USA): CRC press.

Hagemann, J. (1988). Thermal behavior and polymorphism of acylglycerides. In N. Garti and K. Sato (Eds.), *Crystallization and polymorphism of fats and fatty acids. Surfactant science series. Volume 31*, pp. 9–95. New York (USA): Marcel Dekker Inc.

Haighton, A. (1976). Blending, chilling and tempering of margarine. *Journal of the American Oil Chemists'Society 53*, 397–399.

Hamm, W. (1995). Trends in edible oil fractionation. *Trends in Food Science and Technology 6*, 121–126.

Hartel, R. (1992). Solid-liquid equilibrium: crystallization in foods. In H. Schwartzber and R. Hartel (Eds.), *Physical chemistry of foods*, pp. 47–81. New York: Marcel Dekker Inc.

Heertje, I. (1993). Microstructural studies in fat research. *Food Structure 12*, 77–94.

Heertje, I., M. Leunis, W. Van Zeyl, and E. Berends (1988). Product microscopy of fatty products. *Food Microstructure 6*, 1–8.

Heertje, I., H. Nederlof, H. Hendrickx, and E. Lucassenreynders (1990). The observation of the displacement of emulsifiers by confocal laser scanning microscopy. *Journal of the American Oil Chemists' society 9*, 305–319.

Heertje, I., J. van Eendenburg, J. Cornelissen, and A. Juriaanse (1988). The effect of processing on some microstructural characteristics of fat spreads. *Food Microstructure 7*, 189–193.

Herrera, M. L. and R. W. Hartel (2000a). Effect of processing conditions on physical properties of a milk fat model system: Microstructure. *Journal of the American Oil Chemists' Society 77*, 1197–1204.

Herrera, M. L. and R. W. Hartel (2000b). Effect of processing conditions on physical properties of a milk fat model system: Rheology. *Journal of the American Oil Chemists' Society 77*, 1189–1195.

Himawan, C., V. M. Starov, and A. G. F. Stapley (2006). Thermodynamic and kinetic aspects of fat crystallization. *Advances in Colloid and Interface Science 122*, 3–33.

Illingworth, D. (2002). Fractionation of fats. In A. Marangoni and S. Narine (Eds.), *Physical properties of lipids*, pp. 411–477. New York(USA): Marcel Dekker.

Jacobsberg, B., P. Deldime, and M. Gapor (1978). Tocopherols and tocotrienols in palm oil. *Oleagineux 33*, 239–247.

Jacobsberg, B. and C. Oh (1976). Studies in palm oil crystallization. *Journal of the American Oil Chemists' Society 53*, 609–617.

Johansson, D. (1994). *Colloids in fats.* Ph. D. thesis, Lund University, Sweden.

Johansson, D. (1995). The influence of temperature on interactions and structures in semisolid fats. *Journal of the American Oil Chemists' Society 72*, 1091–1099.

Juriaanse, A. C. and I. Heertje (1988). Microstructure of shortenings, margarine and butter - a review. *Food Microstructure 7*, 181–188.

Kalab, M., P. Allanwojtas, and S. S. Miller (1995). Microscopy and other imaging techniques in food structure-analysis. *Trends in Food Science and Technology 6*, 177–186.

Kawamura, K. (1979). Dsc thermal-analysis of crystallization behavior in palm oil. *Journal of the American Oil Chemists' Society 56*, 753–758.

Kawamura, K. (1980). Dsc thermal-analysis of crystallization behavior in palm oil .2. *Journal of the American Oil Chemists' Society 57*, 48–51.

Kellens, M. (1991). *Polymorphism of saturated monoacid traicylglycerols.* Ph. D. thesis, Catholic University of Leuven, Belgium.

Kellens, M. (2000). Oil modification prcatices. In W. Hamm and R. Hamilton (Eds.), *Edible oil processing*, pp. 129–173. Sheffield(Great Britain): Sheffield Academic Press.

Kellens, M., V. Gibon, M. Hendrix, and W. De Greyt (2007). Palm oil fractionation. *European Journal of Lipid Science and Technology 109*, 336–349.

Kloek, W. (1998). *Properties of fats in relation to their crystallization.* Ph. D. thesis, Wageningen (The Netherlands).

Kloek, W., T. van Vliet, and P. Walstra (2005). Mechanical properties of fat dispersions prepared in a mechanical crystallizer. *Journal of Texture Studies 36*, 544–568.

Larsson, K. (1966). Classification of glyceride crystal forms. *Acta Chemica Scandinavica 20*, 2255–2260.

Larsson, K. (1994). *Lipids-Molecular organization, physical functions and technical applications.* Scotland: The Oily Press.

LeBotlan, D. and I. Heliefourel (1995). Assessment of the intermediate phase in milk-fat by low-resolution nuclear-magnetic-resonance. *Analytica Chimica Acta 311*, 217–223.

LeBotlan, D. J. and L. Ouguerram (1997). Spin-spin relaxation time determination of intermediate states in heterogeneous products from free induction decay NMR signals. *Analytica Chimica Acta 349*, 339–347.

Litwinenko, J. W., A. M. Rojas, L. N. Gerschenson, and A. G. Marangoni (2002). Relationship between crystallization behavior, microstructure, and mechanical properties in a palm oil-based shortening. *Journal of the American Oil Chemists' Society 79*, 647–654.

Loisel, C., G. Lecq, G. Keller, and M. Ollivon (1998). Dynamic crystallization of dark chocolate as affected by temperature and lipid additives. *Journal of Food Science 63*, 73–79.

Long, K., M. A. Jamari, A. Ishak, L. J. Yeok, R. Abd Latif, Ahmadilfitri, and O. M. Lai (2005). Physico-chemical properties of palm olein fractions as a function of diglyceride content in the starting material. *European Journal of Lipid Science and Technology 107*, 754–761.

Lucas, T., D. Le Ray, P. Barey, and F. Mariette (2005). NMR assessment of ice cream: Effect of formulation on liquid and solid fat. *International Dairy Journal 15*, 1225–1233.

MacMillan, S. D., K. J. Roberts, A. Rossi, M. A. Wells, M. C. Polgreen, and I. H. Smith (2002). In situ small angle x-ray scattering (saxs) studies of polymorphism with the associated crystallization of cocoa butter fat using shearing conditions. *Crystal Growth and Design 2*, 221–226.

Mandelbrot, B. (1965). *The fractal geometry of nature*. New York (USA): Freeman Press.

Marangoni, A. (2002a). Special issue of fri: Crystallization, structure and functionality of fats. *Food Research International 35*, 907–908.

Marangoni, A. (2005). Dynamic methods. In A. Marangoni (Ed.), *Fat crystal networks*, pp. 161–177. New York (USA): Marcel Dekker.

Marangoni, A. G. (2000). Elasticity of high-volume-fraction fractal aggregate networks: A thermodynamic approach. *Physical Review B 62*, 13951–13955.

Marangoni, A. G. (2002b). The nature of fractality in fat crystal networks. *Trends in Food Science and Technology 13*, 37–47.

Marangoni, A. G. and R. W. Hartel (1998). Visualization and structural analysis of fat crystal networks. *Food Technology 52*, 46–51.

Marangoni, A. G. and S. S. Narine (2002). Identifying key structural indicators of mechanical strength in networks of fat crystals. *Food Research International 35*, 957–969.

Marangoni, A. G. and D. Rousseau (1996). Is plastic fat rheology governed by the fractal nature of the fat crystal network? *Journal of the American Oil Chemists' Society 73*, 991–994.

Marangoni, A. G. and D. Rousseau (1998a). The influence of chemical interesterification on the physicochemical properties of complex fat systems. 1. melting and crystallization. *Journal of the American Oil Chemists' Society 75*, 1265–1271.

Marangoni, A. G. and D. Rousseau (1998b). The influence of chemical interesterification on the physicochemical properties of complex fat systems. 3. rheology and fractality of the crystal network. *Journal of the American Oil Chemists' Society 75*, 1633–1636.

Mariette, F. and T. Lucas (2005). NMR signal analysis to attribute the components to the solid/liquid phases present in mixes and ice creams. *Journal of Agricultural and Food Chemistry 53*, 1317–1327.

Materials Research Laboratory (2008). Introduction to x-ray diffraction. http://www.mrl.ucsb.edu/mrl/centralfacilities/xray/xray-basics/index.html.

Mazzanti, G., S. E. Guthrie, E. B. Sirota, A. G. Marangoni, and S. H. J. Idziak (2003). Orientation and phase transitions of fat crystals under shear. *Crystal Growth and Design 3*, 721–725.

Mazzanti, G., S. E. Guthrie, E. B. Sirota, A. G. Marangoni, and S. H. J. Idziak (2004a). Effect of minor components and temperature profiles on polymorphism in milk fat. *Crystal Growth and Design 4*, 1303–1309.

Mazzanti, G., S. E. Guthrie, E. B. Sirota, A. G. Marangoni, and S. H. J. Idziak (2004b). Novel shear-induced phases in cocoa butter. *Crystal Growth and Design 4*, 409–411.

Mazzanti, G., A. G. Marangoni, and S. H. J. Idziak (2005). Modeling phase transitions during the crystallization of a multicomponent fat under shear. *Physical Review E 71*, 041607.

Narine, S. and A. Marangoni (2005). Microstructure. In A. Marangoni (Ed.), *Fat crystal networks*, pp. 179–254. New York (USA): Marcel Dekker.

Narine, S. S. and K. L. Humphrey (2004). A comparison of lipid shortening functionality as a function of molecular ensemble and shear: microstructure, polymorphism, solid fat content and texture. *Food Research International 37*, 28–38.

Narine, S. S. and A. G. Marangoni (1999a). The difference between cocoa butter and salatrim (r) lies in the microstructure of the fat crystal network. *Journal of the American Oil Chemists' Society 76*, 7–13.

Narine, S. S. and A. G. Marangoni (1999b). Fractal nature of fat crystal networks. *Physical Review E 59*, 1908–1920.

Narine, S. S. and A. G. Marangoni (1999c). Mechanical and structural model of fractal networks of fat crystals at low deformations. *Physical Review E 60*, 6991–7000.

Narine, S. S. and A. G. Marangoni (1999d). Microscopic and rheological studies of fat crystal networks. *Journal of Crystal Growth 199*, 1315–1319.

Narine, S. S. and A. G. Marangoni (1999e). Relating structure of fat crystal networks to mechanical properties: a review. *Food Research International 32*, 227–248.

Nawar, W. (1996). Lipids. In O. Fennema (Ed.), *Food Chemistry*, pp. 239–319. New York: Marcel Dekker.

Ng, W. (1990). A study of the kinetics of nucleation in a palm oil melt. *Journal of the American Oil Chemists' Society 67*, 879–882.

Ng, W. L. and C. H. Oh (1994). A kinetic-study on isothermal crystallization of palm oil by solid fat-content measurements. *Journal of the American Oil Chemists' Society 71*, 1135–1139.

Noor Lida, H., M. Suria, and I. Razali (1997). Trans fatty acids free food formulations based on palm oil and its products: a review. *PORIM occasional paper 36*, 1–21.

Nor Aini, I. and M. Miskandar (2000). Utilization of palm oil and palm products in shortenings and margarines. *Trends in Food Science and Technology 11*, 115–127.

O'Brien, R. (1996). Shortenings: types and formulations. In Y. Hui (Ed.), *Bailey's industrial oil and fat products. Vol.3. 5^{th} edition*, pp. 161–192. New York (USA): John Wiley and sons.

Ojijo, N. K., I. Neeman, S. Eger, and E. Shimoni (2004). Effects of monoglyceride content, cooling rate and shear on the rheological properties of olive oil/monoglyceride

gel networks. *Journal of the Science of Food and Agriculture 84*, 1585–1593.

Okiy, D. A. (1978). Interaction of triglycerides and diglycerides of palm oil. *Oleagineux 33*, 625–628.

Okiy, D. A., W. B. Wright, K. G. Berger, and I. D. Morton (1978). Physical-properties of modified palm oil. *Journal of the Science of Food and Agriculture 29*, 1061–1068.

Persmark, U., K. Melin, and P. Stahl (1976). Palm oil, its polymorphism and solidification properties. *Rivista Italiana delle Sostanze Grasse 53*, 301–306.

Pople, J. A., I. W. Hamley, and G. P. Diakun (1998). An integrated couette system for in situ shearing of polymer and surfactant solutions and gels with simultaneous small angle x-ray scattering. *Review of Scientific Instruments 69*, 3015–3021.

Rha, C. K. (1979). Viscoelastic properties of food as related to micro-structures and molecular-structures. *Food Technology 33*(10), 71–76.

Riiner, U. (1970). Polymorphism of fats and oils investigated by temperature programmed x-ray diffraction. *Lebensmittel-Wissenschaft und Technologie 3*, 101–106.

Roman-Gutierrez, A. D., S. Guilbert, and B. Cuq (2002). Description of microstructural changes in wheat flour and flour components during hydration by using environmental scanning electron microscopy. *Lebensmittel-Wissenschaft Und-Technologie-Food Science and Technology 35*, 730–740.

Rombaut, R., N. Declercq, I. Foubert, and K. Dewettinck (2008). Triacylglycerol analysis of fats and oils by evaporative light scattering detection. *Journal of the American Oil Chemists' society in press*.

Rossell, J. (1985). Fractionation of lauric oils. *Journal of the American Oil Chemists' Society 62*, 385–390.

Sato, K. (1999). Solidification and phase transformation behaviour of food fats - a review. *Fett-Lipid 101*, 467–474.

Sato, K., S. Ueno, and J. Yano (1999). Molecular interactions and kinetic properties of fats. *Progress in Lipid Research 38*, 91–116.

Shellhammer, T. H., T. R. Rumsey, and J. M. Krochta (1997). Viscoelastic properties of edible lipids. *Journal of Food Engineering 33*, 305–320.

Shi, Y. P., B. M. Liang, and R. W. Hartel (2005). Crystal morphology, microstructure, and textural properties of model lipid systems. *Journal of the American Oil Chemists' Society 82*, 399–408.

Shih, W.-H., W. Shih, S.-I. Kim, J. Liu, and I. Aksay (1990). Scaling behavior of the elastic properties on colloidal gels. *Physical Review A 42*, 4772–4779.

Shukla, A. and S. Rizvi (1988). Relationship among chemical composition, microstructure and rheological properties of butter. *Milchwissenshaft 51*, 144–148.

Siew, W. (2001). Understanding the interactions of diacylglycerols with oils for better product performance. *Palm Oil Development 36*, 6–12.

Siew, W. (2002). Palm oil. In Gunstone (Ed.), *Vegetable oils in food technology: composition, properties and uses*, pp. 59–97. New York (USA): CRC press.

Siew, W. and W. L. Ng (2000). Differential scanning thermograms of palm oil triglycerides in the presence of diglycerides. *Journal of Oil Palm Research 12*, 1–7.

Siew, W. L. and W. L. Ng (1995a). Diglyceride content and composition as indicators of palm oil quality. *Journal of the Science of Food and Agriculture 69*, 73–79.

Siew, W. L. and W. L. Ng (1995b). Partition-coefficient of diglycerides in crystallization of palm oil. *Journal of the American Oil Chemists' Society 72*, 591–595.

Siew, W. L. and W. L. Ng (1996). Effect of diglycerides on the crystallisation of palm oleins. *Journal of the Science of Food and Agriculture 71*, 496–500.

Siew, W. L. and W. L. Ng (1999). Influence of diglycerides on crystallisation of palm oil. *Journal of the Science of Food and Agriculture 79*, 722–726.

Singh, A. P., C. Bertoli, P. R. Rousset, and A. G. Marangoni (2004). Matching avrami indices achieves similar hardnesses in palm oil-based fats. *Journal of Agricultural and Food Chemistry 52*, 1551–1557.

Sonwai, S. and M. R. Mackley (2006). The effect of shear on the crystallization of cocoa butter. *Journal of the American Oil Chemists' Society 83*, 583–596.

Steffe, J. (1996). *Rheological methods in food process engineering*. East Lansing, Freeman Press.

Strasburger, M. and R. Ludescher (1995). Theory and applications of fluorescent microscopy in food research. *Trends in Food Science and Technology 6*, 69–75.

Tan, C. and Y. Che Man (2000). Differential scanning calorimetric analysis of edible oils: comparison of the thermal properties and chemical composition. *Journal of the American Oil Chemists' Society 77*, 143–155.

Tan, C. P. and Y. B. C. Man (2002). Comparative differential scanning calorimetric analysis of vegetable oils: I. effects of heating rate variation. *Phytochemical Analysis 13*, 129–141.

Tan, Y.-A., R. Sambanthamurthi, K. Sundram, and M. Wahid (2007). Valorization of palm by-products as functional components. *European Journal of Lipid Science and Technology 109*, 380–393.

Tang, D. M. and A. G. Marangoni (2006). Computer simulation of fractal dimensions of fat crystal networks. *Journal of the American Oil Chemists' Society 83*, 309–314.

Tietz, R. A. and R. W. Hartel (2000). Effects of minor lipids on crystallization of milk fat-cocoa butter blends and bloom formation in chocolate. *Journal of the American Oil Chemists' Society 77*, 763–771.

Timms, R. E. (1984). Phase-behavior of fats and their mixtures. *Progress in Lipid Research 23*, 1–38.

Toro-Vazquez, J., E. Dilbildox-Alvarado, H. Herrera-Coronado, and M. Charo-Alonso (2001). Triacylglycerol crystalliation in vegetable oils: application of models, measurements and limitations. In N. Widlak, R. Hartel, and S. Narine (Eds.), *Crystallization and solidification properties of lipids*, pp. 53–78. New York (USA): Champaign, IL, USA: AOCS press.

Toro-Vazquez, J., V. Herrera-Coronado, E. Dibildox-Alvarado, M. Charo-Alonso, and C. Gomez-Aldapa (2002). Induction time of crystallization in vegetable oils, comparative measurements by differential scanning calorimetry and diffusive light scattering. *Journal of Food Science 67*, 1057–1065.

Toro-Vazquez, J. F., M. Briceno-Montelongo, E. Dibildox-Alvarado, M. Charo-Alonso, and J. Reyes-Hernandez (2000). Crystallization kinetics of palm stearin in blends with sesame seed oil. *Journal of the American Oil Chemists' Society 77*, 297–310.

Toro-Vazquez, J. F., D. Perez-Martinez, E. Dibildox-Alvarado, M. Charo-Alonso, and J. Reyes-Hernandez (2004). Rheometry and polymorphism of cocoa butter during

crystallization under static and stirring conditions. *Journal of the American Oil Chemists' Society 81*, 195–202.

Toro-Vazquez, J. F., E. Rangel-Vargas, E. Dibildox-Alvarado, and M. A. Charo-Alonso (2005). Crystallization of cocoa butter with and without polar lipids evaluated by rheometry, calorimetry and polarized light microscopy. *European Journal of Lipid Science and Technology 107*, 641–655.

Traitler, H. and A. Dieffenbacher (1985). Palm oil and palm kernel oil in food products. *Journal of the American Oil Chemists' Society 62*, 417–421.

Trezza, E., A. M. Haiduc, G. J. W. Goudappel, and J. P. M. van Duynhoven (2006). Rapid phase-compositional assessment of lipid-based food products by time domain NMR. *Magnetic Resonance in Chemistry 44*, 1023–1030.

van den Tempel, M. (1961). Mechanical properties of plastic-disperse systems at very small deformations. *Journal of Colloid Science 16*, 284–296.

Vereecken, J., I. Foubert, K. W. Smith, and K. Dewettinck (2007). Relationship between crystallization behavior, microstructure, and macroscopic properties in trans-containing and trans-free filling fats and fillings. *Journal of Agricultural and Food Chemistry 55*, 7793–7801.

Vodovotz, Y., E. Vittadini, J. Coupland, D. J. McClements, and P. Chinachoti (1996). Bridging the gap: Use of confocal microscopy in food research. *Food Technology 50*, 74–82.

Vreeker, R., L. L. Hoekstra, D. C. Denboer, and W. G. M. Agterof (1992). The fractal nature of fat crystal networks. *Colloids and Surfaces 65*, 185–189.

Walstra, P. (1987). Fat crystallization. In J. Blanshard and P. Lillford (Eds.), *Food Structure and Behaviour*, pp. 67–85. London (UK): Academic Press.

Walstra, P. (2003). *Physical chemistry of foods*. New-York (USA): Marcel Dekker Inc.

Walstra, P., W. Kloek, and T. van Vliet (2001). Fat crystal networks. In S. K. Garti N. (Ed.), *Crystallization processes in fats and lipid systems*, pp. 289–321. New York (USA): Marcel Dekker Inc.

Wesdorp, L. (1990). *Liquid-multiple solid phase equilibria in fat - theory and experiments*. Ph. D. thesis, TU Delft, The Netherlands.

Whorlow, R. (1992). *Rheological techniques, second edition.* New York (USA), Ellis Horwood Ltd.

Wright, A. J. and A. G. Marangoni (2003). The effect of minor components on milk fat microstructure and mechanical properties. *Journal of Food Science 68*, 182–186.

Wright, A. J., S. E. McGauley, S. S. Narine, W. M. Willis, R. W. Lencki, and A. G. Marangoni (2000). Solvent effects on the crystallization behavior of milk fat fractions. *Journal of Agricultural and Food Chemistry 48*, 1033–1040.

Wright, A. J., S. S. Narine, and A. G. Marangoni (2000). Comparison of experimental techniques used in lipid crystallization studies. *Journal of the American Oil Chemists' Society 77*, 1239–1242.

Yap, P. H., J. M. deMan, and L. deMan (1989). Polymorphism of palm oil and palm oil products. *Journal of the American Oil Chemists' Society 66*, 693–697.

Zaliha, O., C. L. Chong, C. S. Cheow, and A. R. Norizzah (2005). Crystallization and rheological properties of hydrogenated palm oil and palm oil blends in relation to crystal networking. *Eiropean Journal of Lipid Science and Technology 107*, 634–640.

Zaliha, O., C. L. Chong, C. S. Cheow, A. R. Norizzah, and M. J. Kellens (2004). Crystallization properties of palm oil by dry fractionation. *Food Chemistry 86*, 245–250.

Ziegleder, G. (1985). Improved crystallization behavior of cocoa butter under shearing. *International Zeitschrift fur Lebensmittl Technologie und Verffarenstechnik 36*, 412–416.

Ziegleder, G. (1990). DSC-thermal analysis and kinetics of cocoa butter crystallization. *Fett Wissenschaft Technologie-Fat Science Technology 92*, 481–485.

List of symbols

a	particle diameter [m]
a_a	average primary particle diamete [m]
A	Hamaker's constant [N]
A_J	global kinetic coefficient [s^{-1} m^{-3}]
C	concentration [m^{-3} or equivalent]
C_s	concentration at saturation [m^{-3}]
d_a	the average diameter of an aggregate [m]
d	distance between reflecting entities [Å]
	fractal dimension [-]
D	Eucledian (integer) dimension [-]
e	Euler number = 2.718281... [-]
F	relative amount of crystallized material at given time t [-]
G'	elastic or storage modulus [Pa]
G''	viscous or loss modulus [Pa]
$\|G^*\|$	complex modulus [Pa]
G	Gibbs free energy [J]
	shear modulus [Pa]
ΔG^*	critical activation free energy for nucleation [J]
ΔG^*_{het}	critical free energy for heterogeneous nucleation [J]
ΔG^*_{vd}	critical free energy for volume diffusion [J]
ΔG_{vd}	Gibbs free energy change for volume diffusion [J]
ΔG_s	surface free energy change [J]
ΔG_v	volume free energy change [J]
ΔH_m	molar enthalpy change [J $mole^{-1}$]

H_0	inter particle distance [m]
J	nucleation rate [s^{-1} m^{-3}]
k	Boltzmann constant [1.380×10^{-23} J K^{-1}]
N	number of molecules per volume unit [m^{-3}]
	number of primary particles in an aggregate [-]
n	number of connecting chains between two neighboring aggregates [-]
r	radius [m]
r^*	critical radius [m]
R_g	universal gas constant [8.314 J $mole^{-1}$ K^{-1}]
s	reciprocal distance [$Å^{-1}$]
T_K	absolute temperature [K]
T_{Km}	absolute melting temperature [K]
ΔT	supercooling ($=T_{Km} - T_K$) [K]
V_m	molar volume [m^3 $mole^{-1}$]
δ	phase angle [°]
γ	surface free energy per unit surface area [J m^{-2}]
	strain or deformation [-]
γ°	shear rate or rate of deformation [s^{-1}]
γ_0	maximum strain or strain amplitude [-]
$\Delta\mu$	chemical potential [J $mole^{-1}$]
λ_{em}	wavelength of the emitted light [nm]
λ	wavelength of the X-rays [Å]
σ	supersaturation ratio ($=\frac{C}{C_s}$)
	shear stress [Pa]
σ_0	maximum stress or stress amplitude [Pa]
$ln\sigma$	supersaturation ($=\ln(\frac{C}{C_s})$) [-]
ω	contact angle [°]
θ	scattering angle or wetting angle [°]
η	viscosity [Pa s]
	refractive index [-]
η^*	apparent viscosity [Pa s]
Φ	volume fraction solids [-]

List of abbreviations

CSLM	confocal scanning laser microscopy
DSC	differential scanning calorimetry
EM	electron microscopy
ESEM	environmental electron microscopy
F face	flat face
FID	free induction decay
HTF	high-trans fat
K face	kinked face
L	lauric acid
M	myristic acid
NA	numerical aperture
NTF	non-trans fat
O	oleic acid
P	palmitic acid
PLM	polarized light microscopy
pNMR	pulsed nuclear magnetic resonance
RBD	refined bleached and deodorized
S	stearic acid
S face	stepped face
SAXS	small angle x-ray diffraction
SEM	scanning electron microscopy
TEM	transmission electron microscopy
WAXD	wide angle x-ray diffraction
XRD	x-ray diffraction

Curriculum vitae

Veerle De Graef werd geboren te Beveren (Waas) op 28 januari 1980 en behaalde in 1998 het diploma Hoger Secundair Onderwijs, richting Latijn-Wiskunde aan het Sint-Annacollege te Linkeroever. In juli 2003 studeerde zij met onderscheiding af als Bio-ingenieur in de Scheikunde aan de Universiteit Gent.

Vanaf november 2003 startte zij als wetenschappelijk medewerker in het Laboratorium voor Levensmiddelentechnologie en -proceskunde (Vakgroep Voedselveiligheid en Voedselkwaliteit, Faculteit Bio-ingenieurswetenschappen, Universiteit Gent). Tot eind december 2004 onderzocht zij het fenomeen migratievetbloem in het kader van een IWT O& O onderzoeksproject in samenwerking met Barry-Callebaut en onder leiding van prof. dr. ir. Koen Dewettinck. Na het behalen van een IWT-specialisatiebeurs, schakelde zij op 1 januari 2005 over van chocolade naar palmolie, eveneens onder promotorschap van prof. dr. ir. Koen Dewettinck.

Tijdens deze periode stond zij in voor de scriptiebegeleiding van binnen-en buitenlandse studenten. In het kader van haar onderzoek werkte zij samen met prof. dr. Bart Goderis (Departement Chemie, afdeling Moleculaire en Nanomaterialen) en prof. dr. ir. Peter Van Puyvelde (Departement Chemische Ingenieurstechnieken, afdeling Toegepaste Reologie en Polymeer Verwerking) van de Katholieke Universiteit Leuven en verbleef zij in februari 2008 aan de Faculteit Landbouwwetenschappen van de Universiteit van Aarhus (Tjele, Denemarken). Haar onderzoek op gebied van de microstructurele eigenschappen van isotherm gekristalliseerde palmolie heeft geleid tot meerdere publicaties in internationale peer-reviewed wetenschappelijke tijdschriften en verscheidene bijdragen aan internationale wetenschappelijke conferenties.

In juli 2005 behaalde zij met onderscheiding het diploma Geaggregeerde voor het Secundair onderwijs (AILO toegepaste biologische wetenschappen). In 2008 behaalde zij tevens het getuigschrift van de postgraduaatsopleiding: doctoraatsopleiding in de toegepaste biologische wetenschappen.

Relevant publications in international peer-reviewed journals

De Graef, V., P. Van Puyvelde, B. Goderis and K. Dewettinck. Influence of shear flow during and prior to isothermal static crystallization of palm oil. European Journal of Lipid Science and Technology (in press)

De Graef, V., B. Goderis, P. Van Puyvelde, I. Foubert and K. Dewettinck (2008). Development of a rheological method to characterize palm oil crystallizing under shear. European Journal of Lipid Science and Technology 110, 521-529.

De Graef, V., I. Foubert, K.W. Smith, F.W. Cain and K. Dewettinck (2007). Crystallization behavior and texture of trans containing and trans free palm oil based confectionery fats. Journal of Agricultural and Food Chemistry 55, 10258-10265.

De Graef, V., K. Dewettinck, D. Verbeken, and I. Foubert (2006). Rheological behaviour of crystallizing palm oil. European Journal of Lipid Science and Technology 108, 864870.

Other publications in international peer reviewed journals

Wiking, L., De Graef, V., Rasmussen, M. and Dewettinck, K. Relations between crystallization mechanisms and microstructure of milk fat. International Dairy. Journal (submitted).

Nopens, I., I. Foubert, V. De Graef, D. Van Laere, K. Dewettinck, and P.A. Vanrolleghem (2008) Automated image analysis tool for migration fat bloom evaluation of chocolate coated food products. LWT - Food Science and Technology, 41, 1884-1891.

De Graef, V., I. Foubert, E. Agache, H. Bernaert, A. Landuyt, P.A. Vanrolleghem, and K. Dewettinck (2005). Prediction of migration fat bloom on chocolate. European Journal of Lipid Science and Technology 107, 297-306.

Vermeiren, L., F. Devlieghere, V. De Graef, and J. Debevere (2005). In vitro and in situ

growth characteristics and behaviour of spoilage organisms associated with anaerobically stored cooked meat products. Journal of Applied Microbiology 98, 33-42.

Presentations at international conferences

Similarities between the crystallization of fats and polymers, CABUS, S., DE GRAEF, V., VAN PUYVELDE, P., DEWETTINCK, K.and GODERIS, B., Belgian Polymer Group Annual Meeting, De Haan, Belgium, 22-23 May 2008

Similarities between the crystallization of fats and polymers, CABUS, S., DE GRAEF, V., VAN PUYVELDE, P., DEWETTINCK, K.and GODERIS, B., Seventh International Conference on X-Ray Investigations of Polymer Structure (XIPS), Cracow, Poland, 5-7 December 2007

The effects of fat crystal morphology on the rheological properties of milk fat, WIKING, L., FOUBERT, I., DE GRAEF, V., RASMUSSEN, M., and DEWETTINCK, K., European Congress of Chemical Engineering (ECCE-6), Copenhagen, Denmark, 16-20 September 2007

Crystallization behavior and texture of trans containing and trans free palm oil based on confectionery fats, DE GRAEF, V., DEWETTINCK, K., SMITH, K., CAIN, F. and FOUBERT, I., 98th AOCS Annual Meeting and Expo, Quebec, Canada, 13-16 May 2007

Rheological analysis of the influence of pre-shearing on the static crystallization of palm oil, DE GRAEF, V., FOUBERT, I. and DEWETTINCK, K., 98th AOCS Annual Meeting and Expo, Quebec, Canada, 13-16 May 2007

Rheological behaviour of crystallizing palm oil, DE GRAEF, V., VERBEKEN, D., FOUBERT, I. and DEWETTINCK, K., 4th EuroFedLipid Congress, Madrid, Spain, 1-4 October 2006